

Passively Mode-locked Diode-pumped Yb:CaF₂ Oscillator

by

Yang Yu

A thesis submitted in partial fulfillment of the requirements for the degree of

Master of Science

in

Photonics and Plasmas

Department of Electrical and Computer Engineering
University of Alberta

© Yang Yu, 2014

Abstract

Ultrafast (UF) mode-locked lasers are powerful tools in scientific research and industrial applications including material processing, nonlinear optics, attosecond science, metrology, etc. For the last 20 years, there has been a growing demand for reliable, compact, high power UF lasers. Passively modelocked diode-pumped solid-state lasers (DPSSL) based on semiconductor saturable absorber mirrors (SESAM's) and Kerr lens mode-locking (KLM) which have demonstrated good performance in terms of pulse duration, peak power, pulse repetition rates and maintainability. $\text{Yb}^{3+}:\text{CaF}_2$ has been recognized as a good candidate for a highly efficient high power femtosecond laser, because of its simple energy-level scheme, high quantum efficiency (~ 1), very small quantum defect ($< 10\%$), long upper-state lifetime (2.4 ms), broad emission spectrum (> 70 nm), high thermal conductivity and compatibility with high power InGaAs diode pumping. In this thesis, a passively mode-locked diode-pumped $\text{Yb}^{3+}:\text{CaF}_2$ oscillator has been developed. In the case of the SESAM mode-locking cavity, energetic Q-switched modelocked laser pulses were generated. A Kerr-lens mode-locked oscillator was constructed for continuous-wave modelocking operations by incorporating an additional optical element with an enhanced nonlinear Kerr coefficient, which represents the first such investigation for an $\text{Yb}^{3+}:\text{CaF}_2$ oscillator to our best knowledge. A 2-pulse per round trip KLM operation was obtained with output power is 970 mW at 10 W pump and 164 MHz repetition rate. The output spectrum had a FWHM of 3 nm and centered at 1053 nm.

Acknowledgements

It is impossible for me to finish the work presented in this thesis without the support of many people. First of all I wish to express my sincere gratitude to my supervisor, Prof. Robert Fedosejevs, for his guidance, encouragement, so many valuable suggestions and financial support for the past 3 years. I am so grateful to be his student and regard him as my lifetime role model. At the same time, I also wish to express my sincere appreciation for Dr. Henry Tiedje and Dr. Ilya Utkin for their friendly and patient help in my research work. I would like to thank my labmates Travis Schoepp, Raj Masud, Mianzhen Mo, and Zhijiang Chen for spending their valuable time discussing the experimental results with me. I would like to thank Prof. Ursula Keller, Prof. Stefan Nolte and Dr. Jörg Körner for their citation permissions.

I am in life debt to my Mom who gave up her 24-year career and came to Edmonton to take care of the whole family for 10 months after my baby boy was born. And I am truly grateful for my wife who unconditionally takes care of the baby most of the time, so I could focus on my work. This thesis is dedicated to my family, the most important part of my life.

Yang Yu

Edmonton, 2014

Table of Contents

1	Introduction.....	1
1.1	Ultrashort laser pulses characteristics and applications	1
1.1.1	Ultrashort pulse duration.....	1
1.1.2	Broad Spectrum.....	2
1.1.3	High peak intensity.....	3
1.2	Current ultrafast laser system and motivations	5
1.3	Overview of thesis.....	8
2	The Development of ultrashort pulse lasers and Yb ³⁺ femtosecond lasers	10
2.1	Ultrafast laser development history.....	10
2.2	Ultrafast ytterbium-doped bulk lasers	15
3	Laser oscillation theory.....	22
3.1	Laser system overview	22
3.2	Laser Modeling	23
3.2.1	Population inversion.....	23

3.2.2 Transition cross sections	25
3.3 Relaxation Oscillation	26
3.4 Quasi-three-level system	27
3.5 Yb ³⁺ : CaF ₂ Crystal Properties	29
3.6 Laser resonator Design.....	34
3.6.1 Laser Pumping.....	34
3.6.2 Laser beam propagation	35
3.6.3 Astigmatism compensation	39
4 Nonlinear optics and Kerr effect.....	42
4.1 Nonlinear optics introduction.....	42
4.2 Kerr Effect.....	44
4.2.1 Nonlinear refractive index.....	44
4.2.2 Transverse Kerr effect	46
4.2.3 Longitudinal Kerr effect and Self Phase Modulation.....	48
4.3 Kerr Medium nonlinear ABCD matrix	50

5	Modelocking Technology and KLM	53
	5.1 Laser pulses generation through mode locking.....	53
	5.2 Multiple longitudinal modes operation	56
	5.2.1 Homogeneous gain media	56
	5.2.2 Inhomogeneous gain media.....	57
	5.3 Master equation for modelocking	58
	5.3.1 Complex envelop for optical field.....	58
	5.3.2 Modelocking master equation	59
	5.4 Active Modelocking	62
	5.5 Passive Modelocking.....	64
	5.6 SESAM mode-locking	67
	5.7 Kerr Modelocking	71
	5.8 Soliton mode-locking	75
	5.9 Other Modelocking technology.....	78
6	Experiment Design and Result.....	80

6.1 Oscillator pump design and CW performance	80
6.2 Passive mode-locking with SESAM	88
6.3 KLM experiment with ZnS	93
6.3.1 High nonlinearity crystal ZnS	93
6.3.2 ZnS KLM Laser cavity design	94
6.3.3 ZnS KLM experiment results	99
6.4 KLM experiment with 10mm SF57 nonlinear glass	102
6.4.1 High nonlinearity glass SF57	102
6.4.2 SF57 Z-cavity KLM design and result.....	103
6.4.3 SF57 W-cavity KML design and result.....	109
6.5 Conclusion.....	116
7 Discussion of experimental results	117
7.1 CW operation stability.....	117
7.2 SESAM damage analysis	120
7.3 ZnS KLM experiment	123

7.4 SF57 multiple pulse ML operation.....	126
7.4.1 Multiple-pulse ML operation with a few ns pulse separation	127
7.4.2 Multiple-pulse ML operation with 1 ns pulse separation.....	132
7.5 SF57 KLM cavity analysis	134
7.5.1 Cavity misalignment evaluation.....	134
7.5.2 Lens effect	138
7.5.3 Minimizing degradation at the stability limit.....	139
7.6 KLM self-starting mechanism.....	139
7.7 Symmetric cavity experiment and spectral analysis.....	141
7.8 Conclusion.....	144
8 Comparison to previous results.....	145
8.1 Comparison with previous Yb:CaF ₂ modelocked systems	145
8.2 Comparison with other modelocked lasers using extra medium elements ..	147
9 Summary and future work	150
9.1 Thesis summary.....	150

9.2 Future work	152
-----------------------	-----

List of Tables

Table 1-1 Extreme experimental conditions provided by UF laser	5
Table 2-1 Comparison of Yb ³⁺ -doped UF laser and Ti ³⁺ :sapphire UF lasers.....	16
Table 2-2 Yb ³⁺ doped femtosecond laser performance	18
Table 3-1 Yb: YAG laser and Yb: CaF ₂ laser performance comparison.....	33
Table 3-2 ABCD matrices for usually used optical elements [29].....	38
Table 6-1 Pump laser diode specification [1] [2].....	81
Table 6-2 SESAM specifications [4]	89

List of Figures

Figure 1-1 The scale of things [1], courtesy of U. Keller, used by permission	1
Figure 1-2 Typical laser pulse energy vs Repetition rate [10].....	4
Figure 1-3 UF laser ablation, courtesy of Stefan Nolte used by permission [13].....	5
Figure 2-1 Optical pulse duration development compared to electronic switching speeds [64]	15
Figure 2-2 Yb ³⁺ doped femtosecond laser performance for different host materials ..	19
Figure 2-3 Thermal properties versus spectroscopic properties for different undoped host crystals at room temperature [86].....	20
Figure 3-1 Laser oscillator theory diagram.....	22
Figure 3-2 Laser resonator diagram.....	23
Figure 3-3 Two, three, four-level systems [91]	24
Figure 3-4 Optical intensity I_{total} vs ΔN for two-, three-, four-level system	25
Figure 3-5 Quasi-3-level laser system energy level.....	28
Figure 3-6 Yb ³⁺ energy level diagram in Yb:CaF ₂ crystal.....	29
Figure 3-7 Yb:CaF ₂ absorption cross sections for 20 °C and 200 °C [112]	31
Figure 3-8 Yb:CaF ₂ emission cross sections for 20 °C and 200 °C [112].....	32
Figure 3-9 (a) Relative change in the peak absorption cross sections (940 nm) and (b) peak emission cross sections (1030 nm) in different materials [112].....	33
Figure 3-10 Laser oscillator schematic diagram.....	36
Figure 3-11 Laser beam propagation	37
Figure 3-12 Folding mirror and Brewster-angle plate geometry. Coordinate and parameters are used as shown	40

Figure 4-1 Second Harmonic generation	44
Figure 4-2 Transverse Kerr effect.....	46
Figure 4-3 Laser beam self-trapping.....	47
Figure 4-4 SPM effects and spectrum broadening.....	49
Figure 4-5 Laser beam focused inside Kerr medium.....	51
Figure 5-1 Laser pulses generation through modelocking principle	54
Figure 5-2 Homogeneous broadened medium.....	56
Figure 5-3 Inhomogeneously broadened laser medium.....	57
Figure 5-4 Laser pulse envelope and electric field	58
Figure 5-5 Slow saturable absorber modelockig with dynamic gain saturation.....	66
Figure 5-6 Slow saturable absorber modelocking with constant gain [158]	66
Figure 5-7 Fast Saturable absorber modelocking	66
Figure 5-8 Loss modulation of active modelocking and passive modelocking [148].	67
Figure 5-9 Typical layout of a SESAM (top) and a plot of typical reflectivity vs incident fluence (bottom) [161]	68
Figure 5-10 Time-dependent reflectivity for a SESAM with 0.78 ps recovery time ..	69
Figure 5-11 Q-Switching modelocking and burned SESAM	71
Figure 5-12 Hard Aperture Kerr lens modelocking [2]	72
Figure 5-13 TEM ₀₀ mode aperture transmission ratio	73
Figure 5-14 Soft aperture Kerr Modelocking [140].....	74
Figure 5-15 Negative dispersion prism pairs	77
Figure 6-1 LU0975 diode drive diagram	81
Figure 6-2 MOSFET output characteristics and diode current protect diagram.....	82
Figure 6-3 Lumic diode output power versus operating current.....	82

Figure 6-4 LIMO Diode performance and Yb:CaF ₂ absorption without lasing	83
Figure 6-5 Yb:CaF ₂ CW cavity configuration	84
Figure 6-6 Pump and lasing beam divergence	86
Figure 6-7 Pump absorption in Yb:CaF ₂ crystal.....	86
Figure 6-8 SESAM modelocking theoretical design	89
Figure 6-9 SESAM modelocking cavity design	90
Figure 6-10 SESAM QML operations.....	91
Figure 6-11 SESAM burn spot and surface crack	91
Figure 6-12 ZnS, CaF ₂ and ZnSe transmitting windows [188]	94
Figure 6-13 ZnS KML cavity	95
Figure 6-14 Kerr strength variation with cavity design	96
Figure 6-15 Beam radius as a function of position in the cavity	96
Figure 6-16 OC laser beam radius variation vs intracavity power	97
Figure 6-17 Regions of geometrical stability (in white) for cavity as a function of folding mirrors distance and the equivalent curved mirror focal length....	98
Figure 6-18 ZnS KLM mode beating.....	100
Figure 6-19 ZnS multiple-pulse KLM operation.....	100
Figure 6-20 ZnS KLM Q-switching envelope	101
Figure 6-21 ZnS KLM spectrum.....	102
Figure 6-22 ZnS surface frequency generation.....	102
Figure 6-23 SF57 KLM cavity design	103
Figure 6-24 SF57 Kerr lens strength vs cavity design.....	104
Figure 6-25 SF57 KLM laser cavity thermal stability	105
Figure 6-26 SF57 3-pulse per round trip KLM.....	105

Figure 6-27 SF57 KLM 3-pulse per round trip spectrum.....	106
Figure 6-28 Laser performance at threshold.....	107
Figure 6-29 SF 57 ML and CW beam radius inside laser cavity.....	108
Figure 6-30 M4 and Yb:CaF ₂ beam waist change vs intracavity power	109
Figure 6-31 SF57 W-cavity KLM.....	109
Figure 6-32 SF57 2-pulse per round trip KLM.....	110
Figure 6-33 SF57 2-pulse KLM spectrum.....	111
Figure 6-34 SF57 twin pulses KLM operation	111
Figure 6-35 SF57 KLM W-cavity with GVD compensation.....	112
Figure 6-36 SF57 KLM with GVD compensation with 100μm radius diode pump .	113
Figure 6-37 SF57 KLM with GVD compensation at 50μm radius diode pumping ..	114
Figure 6-38 Spectrum of SF57 KLM 6 pulses per round trip.....	115
Figure 6-39 Other higher oscillating modes during KLM operation.....	115
Figure 7-1 Yb:CaF ₂ CW mode output spikes	117
Figure 7-2 Yb:CaF ₂ self-amplitude modulation	117
Figure 7-3 Yb:CaF ₂ CW cavity configuration	118
Figure 7-4 Yb:CaF ₂ random QS and QML operation for the laser cavity configuration shown in Fig.7-3.	119
Figure 7-5 Modified SESAM ML Cavities	121
Figure 7-6 SESAM ML pulse trains and Q-switching envelop.....	122
Figure 7-7 KLM experiment with 3mm ZnS.....	123
Figure 7-8 ZnS surface SFG	124
Figure 7-9 SF57 multiple pulse ML operation for the cases of (a) a few nanoseconds pulse separation and (b) ~1ns pulse separation.....	126

Figure 7-10 Pulses collide cavity configurations and scheme	127
Figure 7-11 KLM strength variation with SF57 pulse collision position	130
Figure 7-12 Spectrum width comparisons for gain, single and multiple pulses.....	131
Figure 7-13 Matrix description of the resonator	134
Figure 7-14 SF57 KLM cavity design	136
Figure 7-15 OC beam radius change vs intracavity power with different cavity design	136
Figure 7-16 Beam radius affect by different folding mirror incidence angle	137
Figure 7-17 SF57 Z-shaped symmetric cavity.....	142
Figure 7-18 Spectrum of a symmetric cavity.....	142

List of Abbreviation

APM	Additive-pulse mode-locking
CPA	Chirped pulse amplification
CPM	Colliding pulse modelocking
CW	Continuous wave
DFG	Difference-frequency generation
DPSSL	Diode pump solid state lasers
EM	Electricity and Magnetism
FSR	Free spectral range
FWHM	Full width at half-maximum
GDD	Group delay dispersion
GVD	Group velocity dispersion
HHG	High harmonic generation
HWHM	Half width at half-maximum
InGaAs	Indium, Gallium and Arsenic
KLM	Kerr lens modelocking
ML	Mode locking
NIR	Near infrared
OC	Output coupler
OCT	Optical coherence tomography

OPCPA	Optical parametric chirped-pulse amplification
OR	Optical rectification
QED	Quantum electrodynamics
QML	Q-switching mode locking
SAM	Self-amplitude modulation
SESAM	Semiconductor saturable absorber mirror
SFG	Sum frequency generation
SHG	Second harmonic generation
SPM	Self-phase modulation
UF	Ultra-fast
VUV	Vacuum ultraviolet
XUV	Extreme ultraviolet

1 Introduction

1.1 Ultrashort laser pulses characteristics and applications

Ultrashort laser pulses generated by passively mode-locked ultrafast lasers have extended the capability of mankind to explore phenomena in the picosecond to attosecond time domain and opened up many new applications areas. A brief introduction to characteristics and applications of ultrashort laser pulses is given in this chapter

1.1.1 Ultrashort pulse duration

Since the very beginning of human history, people have never stopped extending our boundaries in the space and time domain.

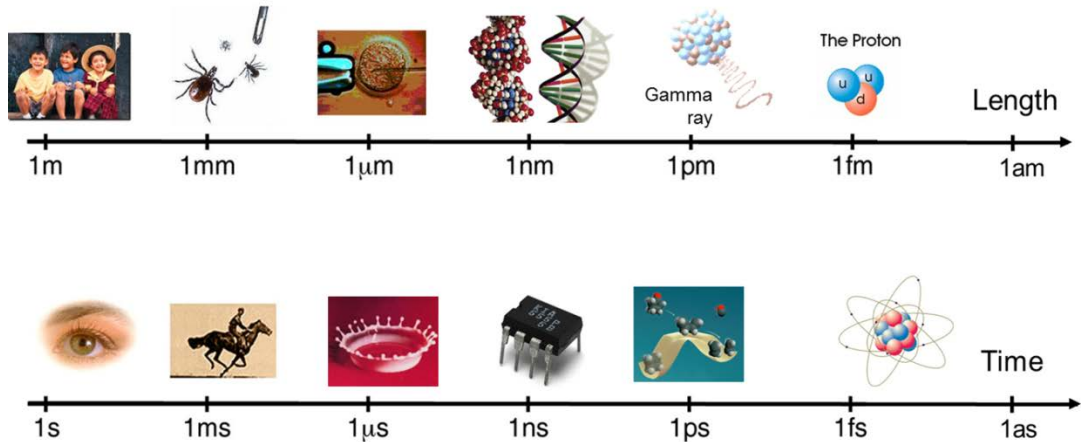


Figure 1-1 The scale of things [1], courtesy of U. Keller, used by permission

As illustrated in Fig. 1-1 our spatial probe resolution has improved continually from the scale size of an insect's body (millimeter), to a cell diameter (micrometer), to the

scale length of DNA pieces (nanometer), to the wavelength of Gamma radiation (picometer) to the diameter of a proton (femtometer) [2] and our ability to resolve temporal phenomena has significantly evolved from that of a camera mechanical shutter (millisecond), to camera flash lamps (microsecond), to integrated circuit clock cycle times (nanosecond), to chemical process time scales (picosecond) and to the electron cloud distortion times (femtosecond) [3].

Lasers and specifically ultrafast (UF) pulse laser techniques allow people to observe and manipulate matter on a femtosecond time scale so we are now able to resolve fundamental physical phenomena like: electrons transferring between atoms, and the breaking and formation of molecular bonds, which occur on the timescale of hundreds of femtoseconds or less. A new discipline “femto-chemistry” based on femtosecond laser technology has been established to study fundamental chemical reaction dynamics. A.H.Zewail was awarded the 1999 Chemistry Nobel prize for his pioneering work and contribution to observing molecular dynamics on an atomic scale resolution by using a femtosecond laser probe [4] [5].

1.1.2 Broad Spectrum

From the nature of Fourier transforms, the product of pulse-duration and its spectral bandwidth must be of order unity (or larger). So as the pulse duration decreases, the bandwidth increases correspondingly. Pulses of 100 fs have bandwidths on the order of 10 terahertz (THz), and the shortest visible laser pulses extend over much of the

visible spectrum appearing white. Optical coherence tomography (OCT), a non-invasive cross-sectional imaging technology for biological systems, needs a broad optical spectrum source to provide ultrahigh spatial resolution. Compared with other broadband sources, a femto-second laser will offer much higher average power and as a result a few micrometer 2D spatial resolution can be achieved [6].

UF broad spectrum pulse trains are also worked as stable multi-wavelength sources, they possess stable comb-shaped optical spectra and the spacing of the individual longitudinal modes exactly equals the pulse repetition rate [7]. These frequency combs have greatly simplified high precision optical frequency measurements, and provide the most reliable experimental means for measuring absolute frequencies and fundamental physics constants (Rydberg constant). In quantum electrodynamics (QED) experiments, it allows people to calculate hydrogen atom energy levels with 12 digits of accuracy [8]. John L. Hall and Theodor W. Hänsch were awarded the Nobel Physics Prize in 2005, for their development of the UF laser-based optical frequency comb technique [9].

1.1.3 High peak intensity

A typical high power UF laser system contains two parts: a laser oscillator and a laser amplifier section. For oscillators, the output pulse energy is typically at the nanojoules level with 100 MHz order repetition rate. The amplifier pulse energies range is from millijoules to joules with 1 Hz to 1 kHz pulse repetition rates. Typical laser system pulse energy and repetition rate characteristics are illustrated by Fig 1-2. Even higher terawatt (10^{12} W) and petawatt (10^{15} W) peak powers can be obtained from such systems based on chirped pulse amplification (CPA) and optical parametric

chirped-pulse amplification (OPCPA) techniques. In order to achieve high pulse energy, lower repetition rates must normally be employed.

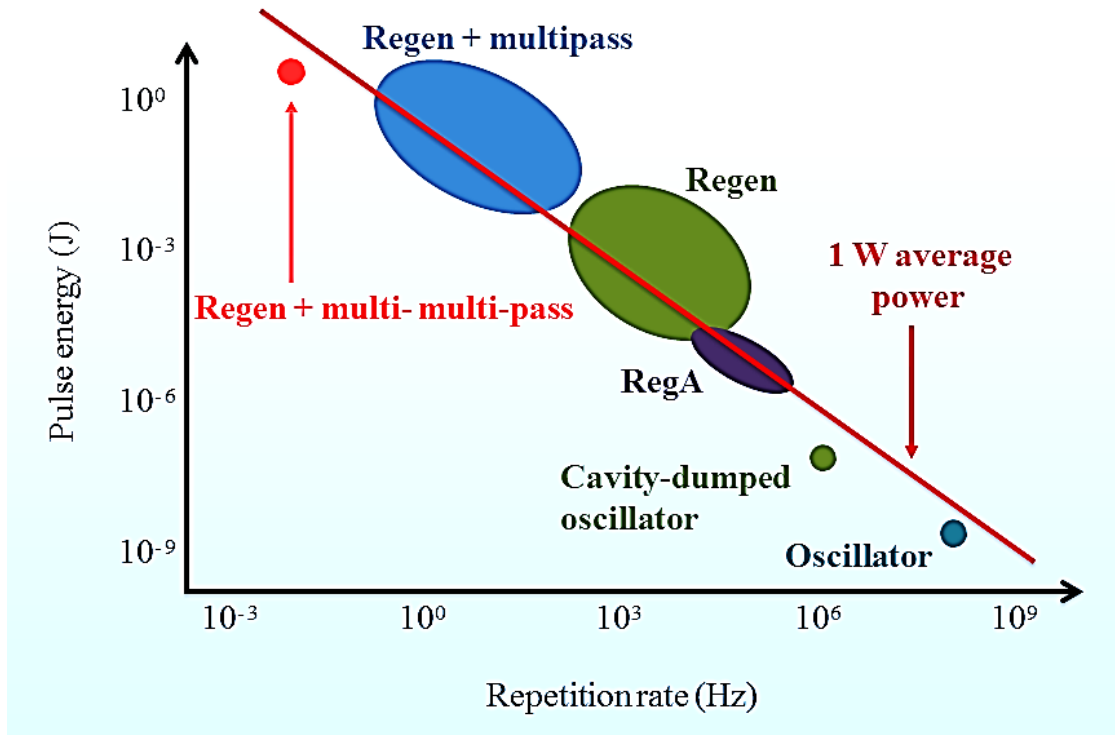


Figure 1-2 Typical laser pulse energy vs Repetition rate [10]

Laser ablation is a representative application for UF lasers. The high peak intensity laser pulse is able to evaporate target material in a non-thermal manner. The material can undergo a transition from solid to liquid or gas on a femtosecond time scale which is faster than carrier–lattice equilibration times (picoseconds) as well as thermal transfer time [11]. As a result, the fabrication of precise microstructures and minimally invasive surgery (e.g. corneal and brain tumor removal) have become possible [12]. Comparative examples of the use of femtosecond laser pulses are shown in Fig 1-3 (left), compared to picosecond (middle) and nanosecond pulses (right) results when

drilling micro holes in stainless steel. Due to the different energy deposition time, quite different mechanical and thermal effects were induced.

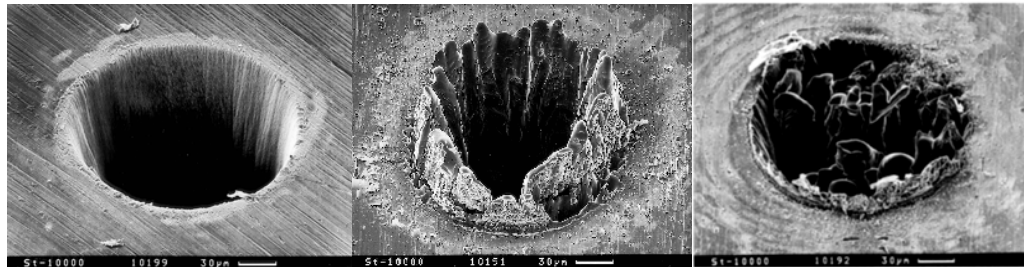


Figure 1-3 UF laser ablation, courtesy of Stefan Nolte used by permission [13]

Last but not least, high power UF lasers also can provide extreme experimental conditions compared to these which are normally experienced on earth.

Table 1-1 Extreme experimental conditions provided by UF laser

	UF laser	Earth
Radiation Intensity [14]	$>10^{22}$ W/m ²	1.368 W/m ²
Radiation Pressure [15]	10^{12} bar	1 bar
Acceleration [16]	10^{21} g	1 g
Magnetic field intensity [17]	10^9 Gauss	0.5 Gauss

1.2 Current ultrafast laser system and motivations

The recent development of semiconductor high power laser technology enables diode pumped solid-state lasers (DPSSL) to be an attractive candidate for high energy

ultrashort laser pulse generation with a compact system size. The choice of gain medium is one of the most important issues in UF DPSS laser systems design. So far the most successful, popular and commercially available UF lasers are the ones based on transition-metal (Cr^{3+} , Ti^{3+} , Ni^{2+} , Co^{2+} , etc) doped crystals. Ti:sapphire femtosecond lasers provide more than 400 nm (around 650 nm-1070 nm) spectral tuning range and as short as 5 fs pulse durations directly output from oscillators. Furthermore they are 4-level energy scheme and do not suffer from ground level thermal population. These properties have established their dominant position [18] [19]. However, there are still some drawbacks for Ti:sapphire lasers, which limit UF laser applications.

1. Ti:sapphire lasers are expensive even though they have been developed for more than 23 years. The main limitation is that they need an expensive pump laser (gaseous ions laser 514 nm or DPSS laser 532 nm) to operate.
2. Electrical-to-optical power transfer efficiency is still very low, so power scalability is limited, and electrical power consumption becomes a concern for industrial applications.
3. They are not “turn-key” systems, so a large number of optical components and precisely controlled cooling system are necessary for normal operation, which not only increases the system complexity but also makes it quite difficult for untrained staff to maintain.

So developing a kind of cost-effective, high-efficiency, simple ultrashort pulse laser system is the key to opening the doors to UF laser applications in industry and new

opportunities in high power femtosecond laser physics. Nowadays the emergence of a new generation of very high efficient (~60%, depending on wavelength) high-power InGaAs laser diodes [20] allow Yb³⁺-doped materials become a new generation laser medium. Yb³⁺-doped crystalline materials have been recognized as an attractive candidate to generate femtosecond laser pulses with high repetition rate, huge pulse energy with high energy transfer efficient. The absorption bands of Yb³⁺ located between 940 nm and 980 nm can be efficiently pumped by InGaAs laser diodes. With the rapidly improving InGaAs laser diode technology, the whole ultrafast laser system cost can be greatly reduced with high efficiency performance.

Nowadays ultrafast Yb fiber systems are mature industrial products. Such fiber based systems are limited by the small mode areas of single-mode fibers. The net dispersive effects and nonlinear effects (Kerr effect, etc.) per round trip in fiber oscillators are much stronger than bulk lasers [27], and these strong nonlinear effects allow modelocking at low powers but also require operation at low power levels to avoid strong nonlinear pulse distortion effects. Such fiber oscillators typically are limited to an average power of a few tens of mW and the pulse energies typically are well below a nanojoule [28], which are generally significantly lower than bulk lasers due to the scalability of laser beam aperture size in DPSS laser systems [29]. Furthermore mode-locked fiber lasers usually generate longer pulse durations than bulk lasers [30]. Recently heavily doped Yb:CaF₂ has attracted considerable interest because of its capability for high power broadband amplification and sub-100 fs pulses generation

[21]. At high dopant concentrations (>0.5%), due to valence mismatch between Ca^{2+} and Yb^{3+} , the Yb^{3+} ions inside the crystal matrix create hexameric clusters [22]. As a result Yb^{3+} ions will exhibit a broader emission spectrum than single isolated ions. In addition, Yb:CaF_2 has a high thermal conductivity, making them a preferable candidate for high average power scaling [23]. Another advantage for CaF_2 over many other materials is that it can be easily grown up to 200mm diameter wafers with ultra-high quality by temperature gradient technique [24].

Limited by the Yb:CaF_2 small nonlinear refractive-index (n_2), it is tricky but possible to initialize and sustain self-modelocked operation (Kerr lens modelocking, KLM) without additional modelocking mechanism assist [25]. However the self-starting modelocking difficulty can be effectively reduced by employing an additional highly nonlinear self-focusing element or semiconductor saturable absorber mirror (SESAM) [21] [26]. The all solid-state simple structure laser cavities are easy to maintain with much lower budget cost than Ti:sapphire laser.

1.3 Overview of thesis

In this thesis a passively mode-locked diode-pumped $\text{Yb}^{3+}:\text{CaF}_2$ oscillator based on SESAM and KLM in a passive nonlinear element is presented. In chapter 2, the development of UF lasers and Yb^{3+} femtosecond laser is briefly reviewed. In chapter 3, background on quasi-3 level continuous wave (CW) laser operation, properties of $\text{Yb}^{3+}:\text{CaF}_2$ and the assessment of laser dynamics are provided. In chapter 4, the nonlinear optical response and Kerr medium modeling are introduced. In chapter 5,

laser modelocking theory especially that for passive modelocking is presented. In chapter 6, experimental results for a KLM system based on a passive nonlinear element are given. In chapter 7, the experimental results are compared with theory. In chapter 8, the experimental results are compared with previous result. Chapter 9 gives a summary and suggestions for the future work.

2 The Development of ultrashort pulse lasers and Yb³⁺ femtosecond lasers

2.1 Ultrafast laser development history

Ultrafast laser science and technology has experienced tremendous progress since the mid-1960s, and among the techniques developed modelocking (ML) is the most powerful and practical approach to achieve ultrashort laser pulse trains. By forcing longitudinal modes to operate in a phase-locked coherent manner, the mixing of these initial “noise” signals yield a short pulse after many round trips. The pulse duration becomes shorter and shorter and the spectrum becomes wider and wider on every pass through the resonator until the balance between the shortening mechanism introduced by loss modulation and lengthening mechanism induced by finite bandwidth of the gain, optical dispersion and nonlinear effects is achieved. The overall goal of laser mode-locking is to develop more efficient and robust technology to generate ever shorter pulses with ever higher peak power.

Modelocking technology is divided two broad areas: “active” modelocking and “passive” modelocking. In 1964 Hargrove demonstrated the first “active” mode-locked laser by using a fused quartz block as an optical transducer to achieve synchronous intra-cavity loss modulation [31]. Although active modelocking technology was initially developed for short laser pulse generation, it does not lead to ultrashort pulses as the cavity loss modulation frequency is fixed at a harmonic of $1/T_R$, where T_R is cavity round time in the nanosecond range. In addition, the electro-optical modulators

which are the frequently used in active modelocking of lasers have a limited bandwidth.

Passive modelocking using passive modulators (for example, saturable absorbers) is much more effective in loss modulation and pulse shaping, and acts as a modelocking mechanism while the pulse builds up. Mocker and Collins reported the first passively mode-locked laser in 1965 [32], when they utilized a saturable dye cell as an intracavity loss modulator for ruby lasers and generated a modelocked pulses train. The pulses train was modulated by a Q-switching envelope, so this phenomenon was called Q-switched modelocking. The first continuous wave (CW) passive ML laser was demonstrated by Ippen, Shank, and Dienes in 1972. They employed a saturable dye cell in a Rhodamine 6G laser and achieved stable continuous output of picosecond pulses [33]. They also have generated the first sub-picosecond pulses from a mode-locked CW dye laser in 1974 [34].

Although a dye laser is very powerful in ultrashort pulses generation, it has a few drawbacks. The gain medium sometimes is toxic and decays rapidly, the dye jets and resonator cavity requires careful alignment. Solid state lasers can overcome some of these issues. However, due to much smaller gain cross-sections such systems would lead to lasing in a Q-switching modelocking (QML) regime which is not ideal for many applications. It had been a challenge for most passively mode-locked solid-state laser until the first low-loss intracavity saturable absorber was designed properly to prevent

Q-switching in 1992 [35]. For the past two decades, passive modelocking technology based on semiconductor saturable absorber mirrors (SESAM's) and nonlinear refractive effects (Kerr lens effect) enabled diode pumped solid-state lasers (DPSSL) to overcome Q-switching instability and generate laser pulses with excellent pulse duration, pulse energy and pulse repetition rates.[36]

Since the Kerr-lens-induced mode locking (KLM) was successfully achieved for the first time in a Ti:sapphire laser [37], this operation mode has been attempted in almost every type of solid state laser [38]. In a KLM laser, one utilizes the power-dependent beam profile shaping induced by the Kerr lens effect together with appropriate apertures (soft aperture or hard aperture) to create an effective saturable absorber with femtosecond (fs) response time. In a carefully controlled cavity, laser pulses experience lower loss at higher peak power (short pulses) and higher loss at lower peak power (CW). As a result, this mechanism prefers the short pulse generation to CW lasing and leads to a stable mode locking operation. The KLM effect is almost insensitive to laser wavelength and has extremely fast response time (on the order of a few femtosecond). It can be applied to femtosecond and picosecond pulses generation in various kinds of solid state lasers. Moreover, the simple cavity configuration makes it one of the most widely used mode-locking techniques to generate ever shorter and more powerful laser pulses.

A brief history for the development of ultrafast (UF) lasers can be summarized as

following:

- In the 1960s, extensive research was conducted to generate microsecond (μ s) and nanosecond (ns) laser pulses. Q-switching and modelocking theories were established and achieved in ruby, He-Ne laser and others [39] [40] [41].
- In the 1970s, active mode-locking, passive mode-locking and synchronous pumping technologies were developed to generate picosecond and sub-picosecond laser pulses, which is the real beginning of the ultrafast laser era [42] [43] [44] [45].
- In the 1980s with extensive introduction of femtosecond techniques and tremendous success of ultrashort dye lasers, sub-100 fs laser pulses were achieved in colliding pulse mode-locked (CPM) dye lasers in 1981[46]. In 1985, 27 fs pulses were achieved from self-phase modulation, group-velocity dispersion, saturable absorption, and saturable gain balancing in a CPM dye laser [47]. In 1987 a 6 fs pulse was achieved in a dye laser by additional amplification together with external fiber-grating pulse compression [48].
- In the 1990s, significant development of semiconductor saturable absorber mirrors (SESAM), Kerr-lens modelocking technology as well as short pulse semiconductor diode lasers were achieved. The self-starting, stable and reliable ultrafast solid state laser ended the domination of dye lasers in the UF region [49] [50] [51] [52]. After 12 years the world's shortest laser pulse duration record (dye laser 6fs [48]) was broken by a KLM Ti:sapphire laser (5.4 fs) without any external pulse compression in 1999 [53] [54].
- In the 2000s, slightly shorter pulses which are close to 5 fs had been obtained by using

KLM Ti:Sapphire lasers and chirped mirrors in 2001[55]. Further research showed that shorter pulse can only be achieved by using an external compression method. Sub-4 femtosecond Ti:sapphire laser pulses (3.8 fs) were demonstrated with internal spatial light modulator (SLM) and external pulse compression by using cascaded hollow fiber in 2003 [56]. By coherent control of four-wave mixing and fix phase locking within the pulse envelope with a Xe cell, trains of single-cycle optical pulses with 1.6 fs pulse width were realized by Harris' group in 2005 [57]. Although in theory, it is difficult to generate less than one optical cycle pulse, their pulse center wavelength was 650 nm giving a pulse that is less than 0.8 optical cycles long. Great developments in femtosecond pulse technology since 2001 have opened the gates to attosecond science and in the same year a 250 attosecond (as) extreme ultraviolet (XUV) pulse was achieved by Krausz using the high-harmonic generation method [58]. In 2008, 80 attosecond ultrashort optical pulses were reported by Professor Kleineberg [59].

- In the 2010s, a 67 attosecond XUV pulse was generated by HHG with a double optical gating technique in 2012. The HHG system was pumped by a Ti:sapphire amplifier (750 nm, 7 fs and 1.4 mJ) and a Ne-filled hollow fiber spectral broadening gas cell and chirped-mirror were used for optical pulses compression [60].

There is no doubt that attosecond technology and science will be the next stage in the evolution of ultrashort pulses. However so far the attosecond pulses generated by high harmonic generation (HHG) are not traditional laser pulses and the pulse energy is strongly dependent on femtosecond laser intensity with very low power conversion

efficiency ($<10^{-6}$) [61]. Another approach to generating high peak power laser pulses is to generate much higher pulse energies with longer pulse durations. Nowadays, several high-energy-class diode-pumped solid-state lasers (HEC-DPSSLs) are being constructed worldwide to produce pulses with energy more than 100 J [62] and Lawrence Livermore National Laboratory has already generated 1.7 megajoules (MJ or million joules) of ultraviolet light at 350 terawatts peak power in nanosecond pulses [63].

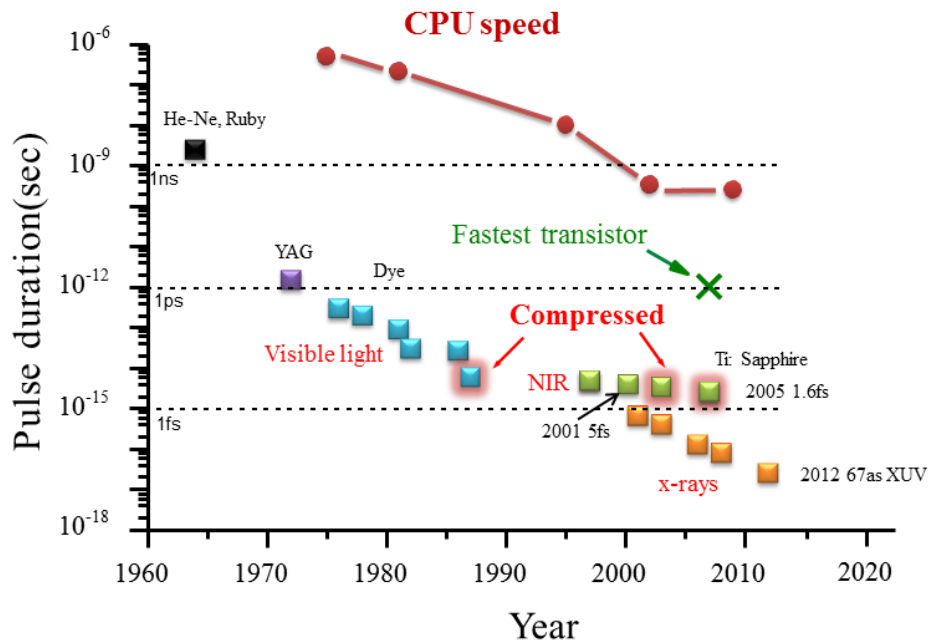


Figure 2-1 Optical pulse duration development compared to electronic switching speeds [64]

2.2 Ultrafast ytterbium-doped bulk lasers

As a result of high power InGaAs diodes development [65] and pumping schemes [66], ytterbium (Yb)-doped bulk lasers become ideal candidates for ultrashort laser pulses

generation in the 1 μm region as well as high power lasers. The trivalent Yb^{3+} ions have electronic-levels in two manifolds resulting in a quasi-three level laser with a low quantum defect between pump and lasing photons. Low quantum defect leads very high pumping efficiencies and low thermal loading for high power operation. Several factors are vital to achieve high power efficiency: small quantum defect, low parasitic losses and a high gain coefficient. In the high power regime, excellent thermal conductivity with a refractive index with weak temperature dependence and a weak tendency for thermally induced stress fracture are also desirable. Yb^{3+} doped materials have long fluorescence lifetimes (several hundred μs to a few ms), high quantum efficiency, and a broad emission spectrum in the 1 μm rage (1010 nm to 1100 nm). Due to these properties they show great potential for the development of directly diode pumped high power and ultrafast lasers. A comparison of Yb^{3+} lasers and Ti^{3+} : Sapphire lasers is given in table 2.1[67].

Table 2-1 Comparison of Yb^{3+} -doped UF laser and Ti^{3+} :sapphire UF lasers

Gain material	Yb^{3+} -doped laser	Ti^{3+} :sapphire laser
Pulse duration	Sub 100 fs	Sub 10 fs
Optical-to-optical conversion efficiency	$\sim 50\%$ (sub ps) $>80\%$ possible (CW)	$<20\%$
Available wavelength range	1010~1100 nm	650~1050 nm
Quantum defect	<10%	$\sim 30\%$

Pump power required for 100 W output power	≥ 200 W	>500 W
Electro-optical efficiency	$>30\%$ possible (fs)	$<5\%$
Commercially available pump power from single module	>1 KW	>100 W
Heat loads for 100W output	>12 W	>150 W
System Cost	High	Very High

The performance of Yb-doped crystal lasers is strongly affected by crystal-host properties. The influences of host crystal include ion lattice vibronic interaction, electron-phonon coupling and electric field stark effect. A number of materials have been studied to date. YAG (Yttrium Aluminum Garnet) is an ideal host material for its high thermal conductivity, large emission cross sections and strong mechanical toughness. It is one of the most developed and commercially available ones. The first femtosecond regime Yb:YAG laser was reported in 1995 by using SEASM modelocking producing 540 fs pulses [68]. The subsequent research showed that some Yb^{3+} doped material gain bandwidths are broad enough to support sub-100 fs pulse generation, and the first sub-100 fs diode-pumped Yb^{3+} doped solid-state laser materials were phosphate glass (65 mW, 58 fs) and silicate glass (53 mw, 61 fs) [69]. Nowadays several kinds of Yb^{3+} crystalline material are able to generate 100 fs regime pulses. However the drawbacks include poor mechanical toughness compared with YAG, lower thermal conductivity and anisotropic structure. The problems become more severe in high power operation. Furthermore, due to Yb^{3+} reabsorption losses and

high-Q cavity designs to favor ultrashort pulses operation, the optical-to-optical efficiency is typically limited to less than 10%. Recent Yb³⁺doped femtosecond laser performance is summarized in Table 2-2 and Figure 2-2.

Table 2-2 Yb³⁺ doped femtosecond laser performance

Material	Δt (fs)	P _{out} (mW)	P _{pump} (W)	Pump Source	ML Technique	Year	Ref
Yb:KYW	71	120	3.2	Two LD	KLM	2001	70
Yb:BOYS	69	80	1.6	LD	SESAM	2002	71
Yb:SYS	70	156	4	LD	SESAM	2004	72
Yb:YVO ₄	61	54	0.4	FCLD	KLM	2005	73
Yb:KLuW	70	81	3	Ti:sapphire	SESAM	2005	74
Yb:LuVO ₄	58	85	1.8	Ti:sapphire	SESAM	2006	75
Yb:CALGO	68	520	15	FCLD	SESAM	2007	76
Yb:LSB	67	39	2	LD	SESAM	2007	77
Yb:NaYW	53	91	1.35	Ti:sapphire	SESAM	2007	78
Yb:YAG	100	151	4.7	FCLD	KLM	2008	79
Yb:YVO ₄	80	1000	3.5	TLD	KLM	2008	80
Yb:CaF ₂	99	380	4.5	FCLD	SESAM	2009	81
Yb:Sc ₂ O ₃	66	1500	8	LD	KLM	2009	82
Yb:Y ₂ O ₃	56	380	5	LD	KLM	2009	82
Yb:YAG	35	107	4.7	FCLD	KLM	2011	83
Yb:CaF ₂	68	2300	7	SMFL	KLM	2013	84
Yb:KGW	67	3000	30	FCLD	KLM	2013	85

Note: LD-Laser diode, FCLD-Fiber coupled laser diode, TLD-Tapered laser diode, SMFL-Single mode fiber laser.

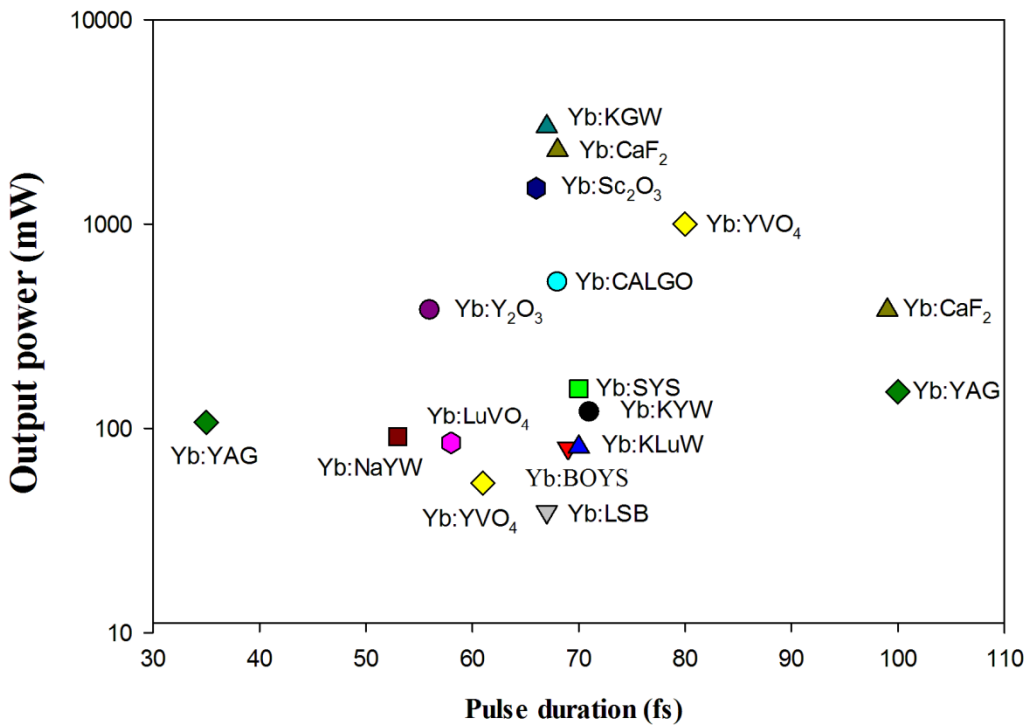


Figure 2-2 Yb³⁺ doped femtosecond laser performance for different host materials
(The data is taken from the references given in Table 2.2)

Recently heavily doped Yb:CaF₂ has attracted considerable interest because of its capability for high power broadband amplification and sub-100 fs pulse generation [81][84]. At high dopant concentrations (>0.5%), due to mismatch between Ca²⁺ and Yb³⁺, the Yb³⁺ ions inside the crystal matrix creates hexameric clusters. As a result the Yb³⁺ ion will exhibit a broader emission spectrum than single isolated ions. In addition Yb:CaF₂ also has high thermal conductivity as well, making it a preferable candidate for high average power scaling as shown in Figure 2.3 [86]. Another advantage for CaF₂ crystals over other materials is that it can be easily grown up to diameters of about 200 mm in ultra-high-quality by Bridgman–Stockbarger technique, Czochralski

process or temperature-gradient methods [87].

However, the dopant concentration cannot be made too high and the high Yb-doped compounds exhibit significantly reduced thermal conductivity. For example, undoped CaF₂ thermal conductivity value is 9.7W/m/K and it is reduced to 6 W/m/K with 2.6 % Yb³⁺ doping [88]. Cryogenic cooling generally has a positive effect on Yb³⁺ laser performance, for example when cooling down from room temperature to liquid nitrogen temperature the peak emission and absorption cross section of 2.5% doped YbCaF₂ crystal are improved by a factor of 3 and thermal conductivity slightly reduced from 5.4 Wm⁻¹K⁻¹ to 4.9 Wm⁻¹K⁻¹[89]. As emission peaks become stronger they also become narrower which is detrimental for ultrashort pulse generation and amplification. However the spectrum can still be sufficiently broad to support ultrashort laser pulses production.

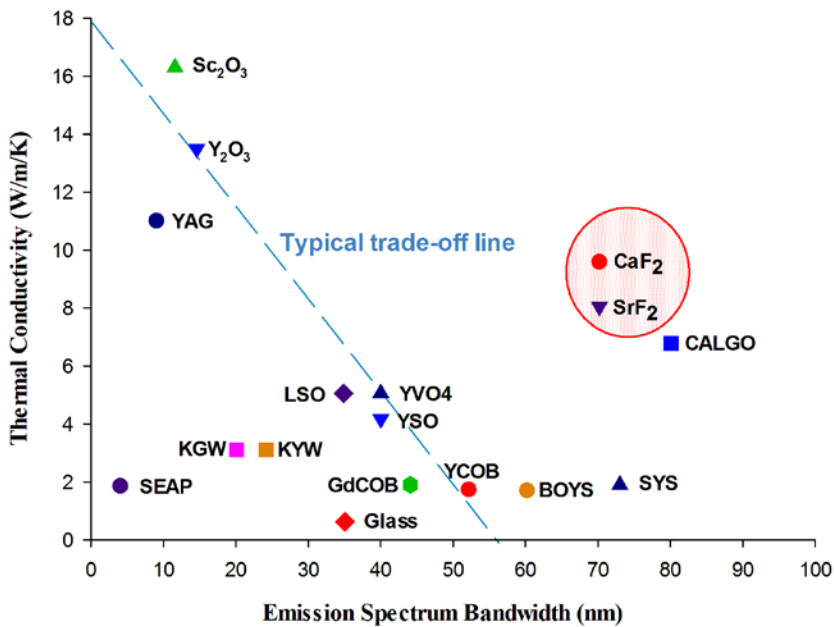


Figure 2-3 Thermal properties versus spectroscopic properties for different undoped host crystals at room temperature [86]

Friebel et al. demonstrated the first sub-100 fs mode-locked Yb:CaF₂ laser oscillator, with 380 mw average power output and 13nm bandwidth spectrum centered at 1053nm in 2009 [81]. In 2013 a 68 fs-2.3W Kerr-lens mode-locked Yb:CaF₂ oscillator was demonstrated by Machinet et al., the wavelength was centered at 1049 nm with a 19 nm bandwidth. The first Yb³⁺:CaF₂ based TW peak power amplifier system (seed pulses were generated by a Ti:sapphire oscillator, Mira 900 Coherent Inc.) was reported by Mathias Siebold et al. in 2009, with 197 mJ output pulse energy and 192 fs duration, at a low repetition(~1Hz) rate at a center wavelength of 1031 nm with a bandwidth of 11 nm[90].

3 Laser oscillation theory

3.1 Laser system overview

It is well known that laser is the abbreviation for “Light Amplification by Stimulated Emission of Radiation”, however in addition to light amplification one needs a feedback resonator to allow the laser mode to build up and a pump source to energize the gain medium. As shown in Fig 3-1, an oscillator is an amplifier with positive feedback.

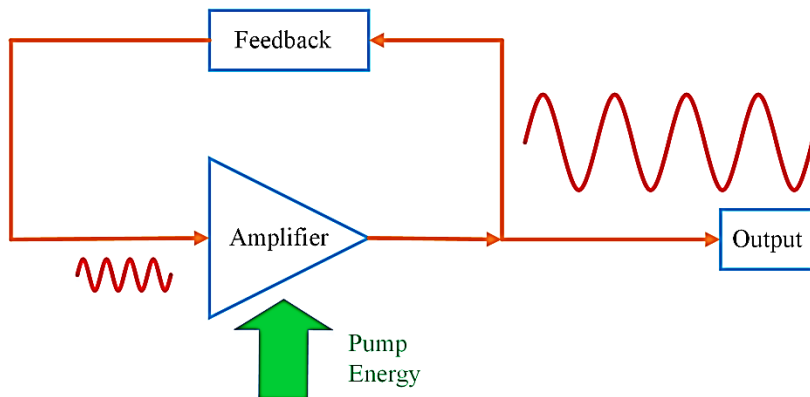


Figure 3-1 Laser oscillator theory diagram

There are a wide variety of lasers, covering the spectral range from the soft X-ray region (a few nm wavelength) to the far infrared region (hundreds of μm wavelength), delivering optical power from microwatts (or lower) to petawatts and pulse energies from nanojoules to megajoules, operating from continuous wave mode (CW) to femtosecond pulse durations, and having spectral line widths from just a few hertz to 100 terahertz. The working gain material utilized includes free electrons, ions, atoms, molecules, plasma, gases, liquids and solids [91]. The essential elements of a laser system are shown in Figure 3-2:

- [1] Laser gain medium to provide optical amplification, total roundtrip gain must be greater than or equal the roundtrip loss.
- [2] Excitation source, a pumping process to excite the atoms of gain medium into higher quantum-mechanical energy level.
- [3] Optical feedback elements, including a high reflectivity mirror and partial reflectivity mirror (OC, output coupler), allow the laser beam to oscillate back and forth inside the optical oscillator with output emission from the output coupler. The cavity also works as a Fabry–Pérot interferometer with distinct longitudinal and transverse modes.

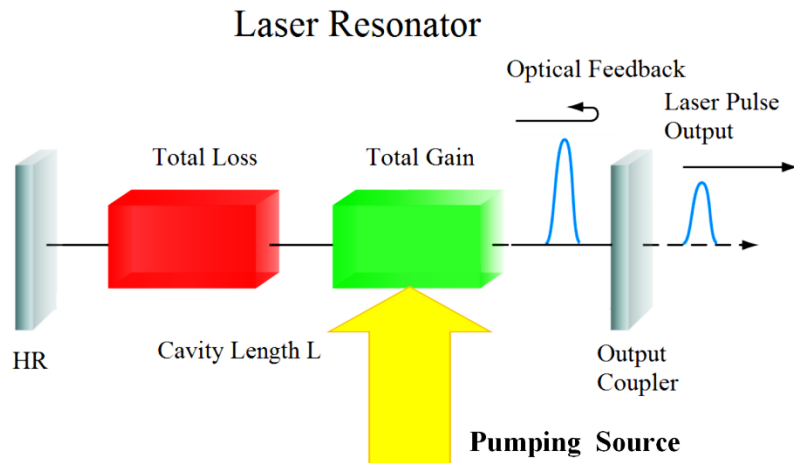


Figure 3-2 Laser resonator diagram

Obviously, the laser signal cannot be amplified indefinitely, and the gain is limited by amplifier gain saturation. When the system reaches a steady state, it means that the total gain and loss (mirror, diffraction, etc.) are balanced with each, and the system works in an equilibrium mode.

3.2 Laser Modeling

3.2.1 Population inversion

The simplest models of laser systems are two, three and four-level systems as illustrated in Figure 3-3

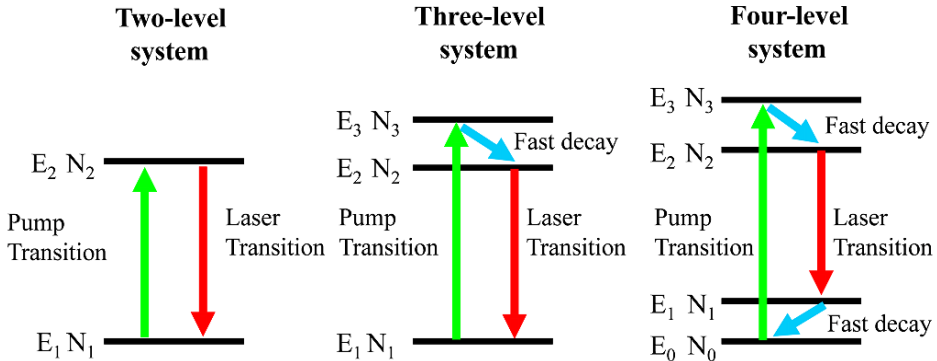


Figure 3-3 Two, three, four-level systems [91]

At room temperature according to the Boltzmann distribution the population density in level 1 (N_1) is much larger than level 2 (N_2), however if we introduce some pumping mechanism the system can be put into a nonthermal equilibrium state and in some special cases we can obtain $\Delta N = N_2 - N_1 > 0$. This is a non-equilibrium state of population inversion with upper energy level more populated than the lower level. In this case the system will begin to emit energy and worked as an amplifier for incoming optical signals that are resonant with the transition.

There are three fundamental processes during laser operation: spontaneous emission, stimulated emission and absorption. Each of them is associated an Einstein coefficient which is used to describe the probability of the process occurring: spontaneous emission probability A_{21} with unit s^{-1} , stimulated emission probability B_{21} with unit $cm^3 s^{-2} J^{-1}$ and absorption probability B_{12} with unit $cm^3 s^{-2} J^{-1}$. The detailed proof can be found from quantum mechanics that $B_{12} = B_{21}$. We can define laser saturation intensity

$I_{\text{sat}} \propto A_{21}/B_{21}$. The total intracavity optical intensity is given by $I_{\text{total}} = I_{\text{ASE}} + I_{\text{laser}}$ where I_{ASE} is the amplified spontaneous emission intensity and I_{laser} is the laser intensity. Given a population inversion threshold $N_{\text{threshold}}$ to overcome cavity loss, we are able to show the relationship between ΔN and I_{total} for different systems as shown in Fig 3-4 [92].

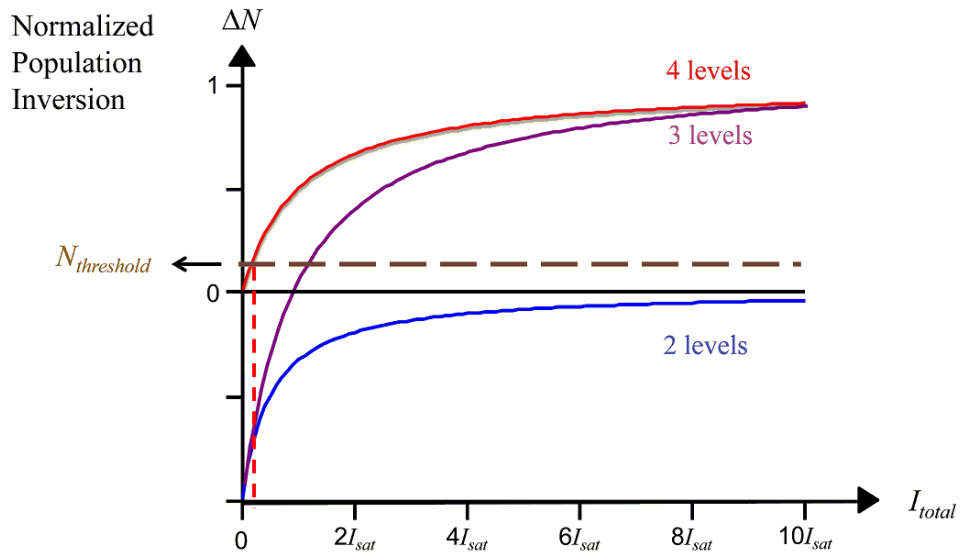


Figure 3-4 Optical intensity I_{total} vs ΔN for two-, three-, four-level system

As illustrated in Figure 3-4, a two-level system can never achieve lasing, a three-level system can achieve lasing only if the pump strength is fairly high while a four-level system lasing can achieve lasing much easier.

3.2.2 Transition cross sections

Only identifying the lasing threshold is not enough to fully describe laser system operation. Three gain material parameters are important in order to determine laser behavior which are the absorption cross section $\sigma_{\text{abs}}(\lambda)$, emission cross section $\sigma_{\text{em}}(\lambda)$,

and upper-state lifetime τ . The two transition cross sections are used to quantify the possibilities of optically induced transitions, which are given by the product of corresponding cross-sections and photon flux [93].

$$R_{\text{transition}} = \sigma \frac{I}{h\nu} \quad 3.1$$

Where $R_{\text{transition}}$ is how many transition events per atom happen per second (in the unit of s^{-1}), σ is the transition cross section dependent on wavelength, I is the optical intensity and $h\nu$ is the photon energy. In the majority of cases, only the absorption cross section for the pump wavelength and the emission cross section for the lasing wavelength are important. Laser pump saturation intensity I_{Psat} is inversely proportional to the product of transition cross sections at pump wavelength and upper-state lifetime τ , which can be calculated by [94]

$$I_{\text{Psat}} = \frac{hc}{\lambda_p [\sigma_{\text{abs}}(\lambda_p) + \sigma_{\text{em}}(\lambda_p)] \tau} \quad 3.2$$

And laser gain saturation fluence F_{sat} can be expressed by [95]

$$F_{\text{sat}} = \frac{hc}{\lambda_l [\sigma_{\text{abs}}(\lambda_l) + \sigma_{\text{em}}(\lambda_l)]} \quad 3.3$$

3.3 Relaxation Oscillation

At the beginning of laser operation most laser systems undergo relaxation oscillations before settling down to steady state operation. It takes hundreds of microseconds to a few milliseconds to achieve the stable state. For DPSS, where the upper-state lifetime is far greater than resonator round-trip time, the relaxation oscillation frequency is determined as following [96]:

$$f_{ro} \approx \frac{1}{2\pi} \sqrt{\frac{2(g_0 - l)}{\tau_L T_R}} \quad 3.4$$

Where g_0 is the small signal gain coefficient, l is the total cavity round-trip loss, τ_L is upper-state lifetime and T_R is the resonator round-trip time.

3.4 Quasi-three-level system

A quasi-three-level laser medium is an intermediate situation between three-level system and four-level system, its lower level is quite close to ground state and partially populated with a thermal distribution. During laser operating, the gain material will re-absorb some lasing power, exciting lower level ions to the upper level. However this effect will be reduced and minimized if the pump intensity is high enough to excite most ions from the ground level to the higher level and thus the lower level of ions will become depopulated [96].

For quasi three level systems, the spectral shape of the overall optical gain depends on the excitation level of the ions as the contribution from absorption will decrease with higher population inversion. As a consequence, the output wavelength can be tuned by resonator losses. Higher cavity losses require higher gain, thus a higher excitation level, and consequently allow a shorter wavelength. Re-absorption is stronger at shorter lasing wavelengths as there are more ions locate at ground level compared with lower level. The re-absorption process does not contribute to a complete loss of pump or lasing energy, as the excited ions can contribute to stimulated emission again after they go into the upper level. Cryogenic cooling can be used to reduce absorption in quasi 3-level systems and in some cases improve the thermo-mechanical properties and thermal conductivity. However it is impossible to avoid laser material heating issues for high power operation even when aggressive cooling technology is applied

[97]. All Ytterbium doped gain media are examples of quasi-three-level medium as shown in Fig. 3.5. Typical absorption and emission cross-sections for Yb laser system are will be shown in section 3.5.

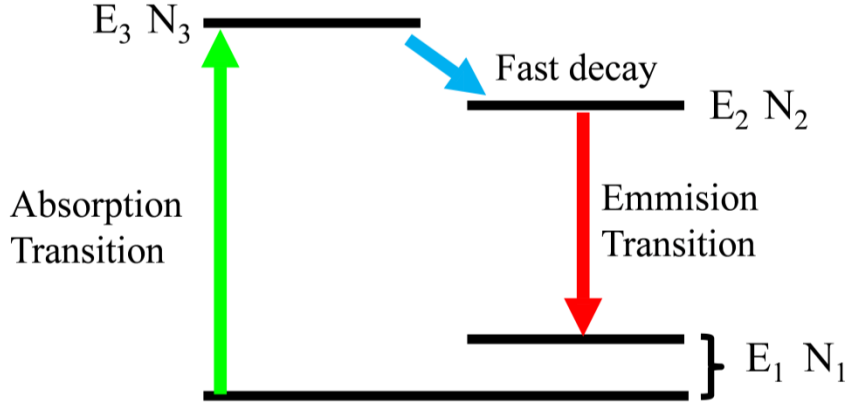


Figure 3-5 Quasi-3-level laser system energy level

In most general case, the rate equation for a quasi-three-level system is [94]:

$$\frac{dN_1}{dt} = \frac{N_2}{\tau} + \sigma_{em}(\lambda_l) \frac{\lambda_l I_l}{hc} N_2 + \sigma_{em}(\lambda_p) \frac{\lambda_p I_p}{hc} N_2 - \sigma_{abs}(\lambda_l) \frac{\lambda_l I_l}{hc} N_1 - \sigma_{abs}(\lambda_p) \frac{\lambda_p I_p}{hc} N_1 \quad 3.5$$

Where I_l is the intracavity laser intensity ($\text{W}\cdot\text{cm}^{-2}$), I_p is the pump intensity. The medium linear gain at λ_l is defined by [94]:

$$g(\lambda_l) = \sigma_{em}(\lambda_l) N_2 - \sigma_{abs}(\lambda_l) N_1 \quad 3.6$$

In Ytterbium lasers the un-pumped or weakly pumped medium is absorbing energy at the laser wavelength. Consequently, a minimum pump intensity $I_{transp}(\lambda_l, \lambda_p)$ is needed to achieve gain medium transparent at λ_l , which is also called transparency intensity. By combining equation 3.5 and 3.6, the expression of transparency intensity is

$$I_{transp}(\lambda_l, \lambda_p) = \frac{hc}{\lambda_p \left[\sigma_{abs}(\lambda_p) \times \frac{\sigma_{em}(\lambda_l)}{\sigma_{abs}(\lambda_l)} - \sigma_{em}(\lambda_p) \right] \tau} \quad 3.7$$

3.5 Yb³⁺: CaF₂ Crystal Properties

The choice of the gain material is one of the most important issues when designing a diode-pumped high peak power laser system. The trivalent ion rare-earth element Ytterbium (Yb³⁺) is a prominent high-power lasers gain medium, its quantum defect of 10% is much smaller compared with 25% for neodymium. It can also be doped in a variety of host materials including glasses, ceramics and crystals. The Yb³⁺ ion is ideally suited for diode pumped laser systems as it has absorption bands in the 900-1000nm region where efficient diode pump lasers exist [98].

Yb³⁺ only has two main energy level manifolds, the ground level $^2F_{7/2}$ and the excited level $^2F_{5/2}$. The band gap between the two manifolds is approximately 10000 cm⁻¹, and the next higher level is in 5d configuration beginning near 100000 cm⁻¹ which is far from pump wavelength [99]. The Ytterbium ion ground manifold is split over approximately 700 cm⁻¹ by the crystal fields, which is then thermally populated by the ambient temperature. This simple electronic structure reduces the possibility of unwanted competitive processes such as excited-state absorption and up-conversion. At room temperature people categorize Yb³⁺ lasers as a quasi-three level laser system [10].

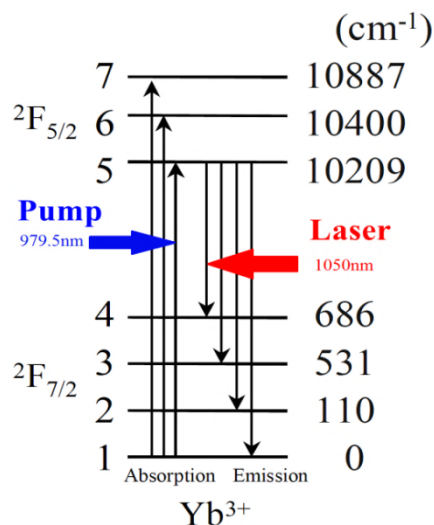


Figure 3-6 Yb³⁺ energy level diagram in Yb:CaF₂ crystal

The achievement of efficient laser performance is determined not only by the properties of active ions but also by the physical-chemical interaction of the ions with the host material lattice as well. The host material plays an important role in two different aspects [100]:

- First of all, it modifies the intrinsic properties of doping ions including the lifetime of the upper state and the Stark shift which are important factors in laser operation.
- Secondly, the host material thermal properties dominate the thermal dissipation process and the appearance of the thermal gradients during the pumping process. Strong temperature gradients induce internal thermal stress and strain, which modify the optical properties of medium including refractive index, thermal lens effect and absorption. As a result several problems such as depolarization of the laser, a change of resonator stability condition, a degradation of laser beam quality and higher losses would arise and complicate the whole system [101].

Among host crystals, fluoride materials show promising characteristics such as a low refractive index which minimizes undesirable non-linear optical effects when the lasing media is pumped by high-intensity sources. They have high transparency over a wide range of the electromagnetic spectrum, i.e. from VUV to IR, and consequently, can be used in many optical components [102]. Calcium fluoride (CaF_2) has been considered as one of the first generation of solid-state laser hosts, and the first $\text{Yb}^{3+}:\text{CaF}_2$ laser was reported in 1967 [103]. Other divalent as well as trivalent rare-earth ions such as Sm^{2+} , Dy^{2+} or Nd^{3+} ions doping lasers were also reported at 1960s [104][105] [106] [107] [108] [109].

However subsequent work showed that CaWO₄, YAG, and other oxide and fluoride glasses had better performance compared with CaF₂. One of the main reasons is that in order to keep material electrically neutral, charge compensation is required during doping process. When the divalent Ca²⁺ ion is substituted by a trivalent rare earth ion it leads to a complex ion structure site: pairs of adjacent rare earth ions, trimers and clusters which are depended on the nature of the substituted rare-earth dopant cation and of the dopant concentration. The second main reason is that adding supplementary co-dopants generally degrades crystal optical quality and thermo-optical properties. This issue is much more severe for the high power laser application [110]. The third main reason was an effective laser pumping source fluence limitation, so the first diode pumped Yb³⁺:CaF₂ laser was only demonstrated in 2004 [111].

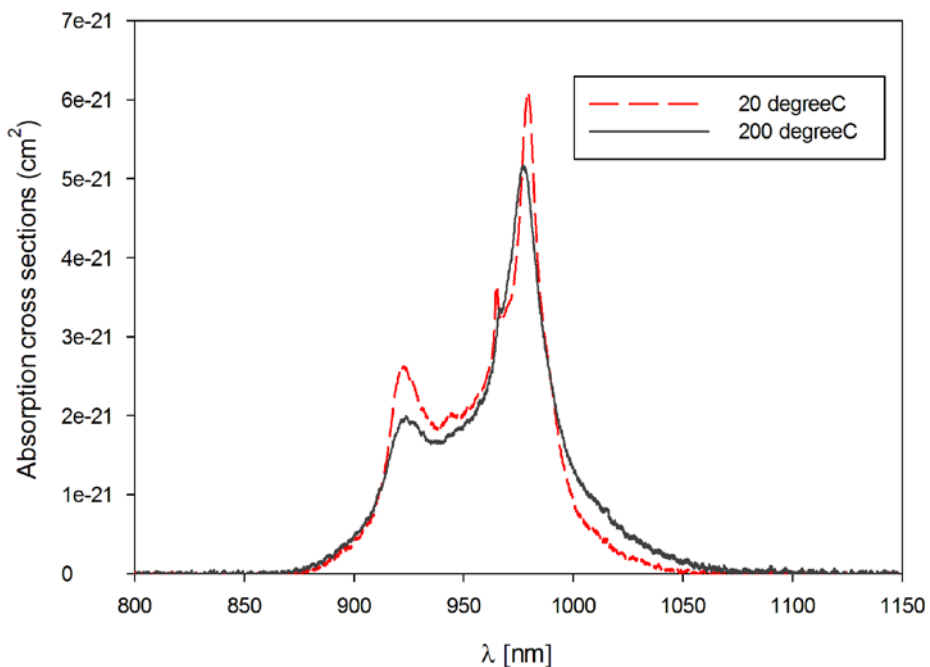


Figure 3-7 Yb:CaF₂ absorption cross sections for 20 °C and 200 °C [112]

YAG is one of the most important and most investigated Ytterbium-doped host materials. Its favorable properties include robustness, long fluorescence life time, and large absorption and emission cross sections. Recent research has showed that Yb:

CaF_2 has better absorption and emission stability performance than Yb: YAG [22], i.e. cross section variations with temperature are less pronounced than YAG, which is an important property for high power laser applications.

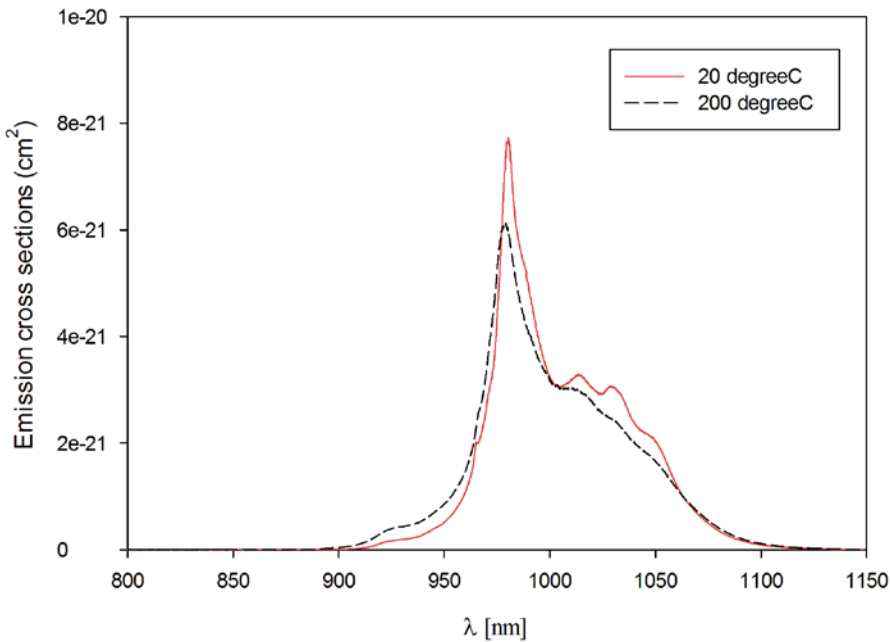


Figure 3-8 Yb:CaF₂ emission cross sections for 20 °C and 200 °C [112]

Yb:CaF₂ absorption and emission cross sections experimental results for 20 °C and 200 °C are shown in Figure 3-7 and Figure 3-8. In general, laser has a worse overall performance at higher temperatures. Direct comparisons of normalized absorption (940 nm) and emission cross sections (1030 nm) thermal stabilities for Yb:YAG, Yb:LuAG and Yb:CaF₂ (3 at .% Yb³⁺ for all) are shown in Fig 3-9. The values for different temperatures are normalized to 20 degreesC. Yb:CaF₂ is less sensitive to temperature changes, the peak emission cross sections reduced by a rate of ~10% per 100 K temperature rise, while 1030 nm emission line of Yb:YAG is reduced ~20% per 50K temperature increase.

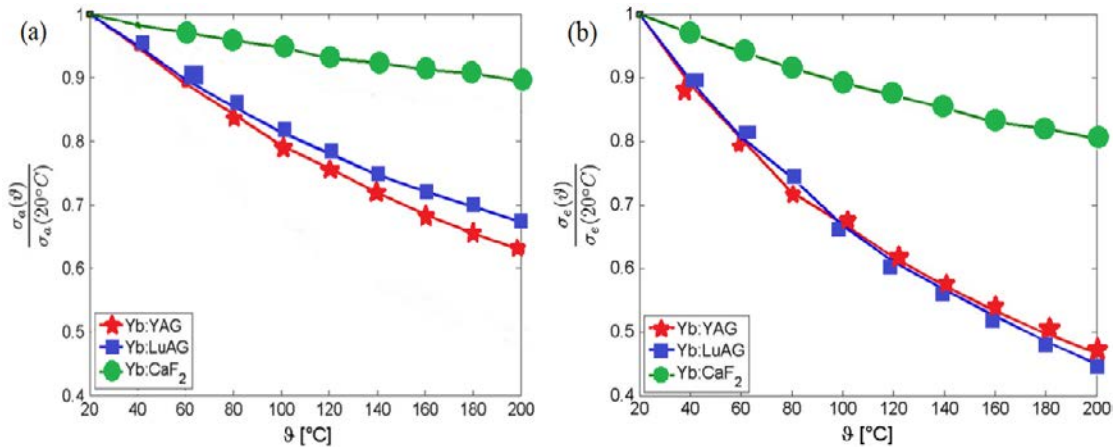


Figure 3-9 (a) Relative change in the peak absorption cross sections (940 nm) and (b) peak emission cross sections (1030 nm) in different materials [112], courtesy of Jörg Körner, used by permission

A long upper-state lifetime means that a significant population inversion can be maintained with relatively low injected power. The Yb³⁺ upper state lifetime in CaF₂ is twice longer than in YAG and spectral line-width is also broader than YAG. The nonlinear refractive index of CaF₂ is about five times smaller than that of YAG. A brief comparison of spectroscopic and laser parameters for Yb:YAG and Yb:CaF₂ is given in Table 3-1[113].

Table 3-1 Yb: YAG laser and Yb: CaF₂ laser performance comparison

Laser host	Yb: YAG	Yb:CaF ₂
Wavelength λ_a [nm] at absorption peak	942	979.8
Room-temperature laser wavelength λ_l [nm]	1029	1050
σ_{abs} [10^{-21} cm^2]	8.0	5.4
σ_{em} [10^{-21} cm^2]	20	1.7

Lifetime [ms]	0.95	2.4
Tuning range [nm]	1020–1083	1000–1072
Shortest ML pulse duration [fs]	35[114]	68[115]
Refractive index	1.815	1.429
Nonlinear refractive index [10^{-13} esu] [116]	2.7	0.43

For Yb:CaF₂ crystal as used in this thesis, at room temperature the transition cross sections [118] are:

$$\lambda_l=1053 \text{ nm}, \sigma_{em}(\lambda_l)=1.6 \times 10^{-21} \text{ cm}^2 \text{ and } \sigma_{abs}(\lambda_l)=0.029 \times 10^{-21} \text{ cm}^2$$

$$\lambda_p=979.6 \text{ nm}, \sigma_{abs}(\lambda_p)=5.4 \times 10^{-21} \text{ cm}^2 \text{ and } \sigma_{em}(\lambda_p)=4.8 \times 10^{-21} \text{ cm}^2$$

According to equation 3.2, 3.3 and 3.7, we are able to calculate the Yb:CaF₂ gain saturation fluence $F_{\text{sat}} \approx 116 \text{ J/cm}^2$, the pump saturation intensity $I_{\text{Psat}}=8.3 \text{ kW/cm}^2$, and the pump transparency intensity $I_{\text{min}} \approx 288 \text{ W/cm}^2$.

3.6 Laser resonator Design

3.6.1 Laser Pumping

Laser systems require an external pump source and an InGaAs diode is the ideal candidate to excite Yb³⁺ ions between 900 nm and 1000 nm in a DPSSL. InGaAs is a family of chemical compounds of the three chemical elements: indium, gallium and arsenic. Indium and gallium are both "group III" elements, and arsenic is a "group V" element. In semiconductor physics, compounds of elements in these groups are called "III-V" compounds. Diode pumping has significant advantages over flash lamp

pumping of solid-state lasers and advantages over the use of direct diode lasers due to improved efficiency and mode quality [116].

- [1] A diode laser is the most efficient pump source for DPSS, a high electrical to optical efficiency of the pump source (~60% or higher) leads to a high overall efficiency.
- [2] The spectral bandwidth of a diode laser is much narrower than flash lamps, which is able to pump target active ions directly to the designated pump levels. It reduces quantum defects and improves pump power efficiency.
- [3] When used in end pumping design, it allows extraordinary mode overlapping between the laser beam and the pump source, providing high beam quality and power efficiency.
- [4] Diode lifetimes can be well above 10000 hours, dramatically reducing the longtime maintenance cost and the compact size makes systems easier to maintain.

Diode technology was initially limited by low power output, low packaging density, and extremely high cost until 1980. More recently laser diode arrays with high power (>100 W per strip), high efficiency (>60%) and long lifetime room temperature (300 K) operation are commercially available at ever improving cost per watt

3.6.2 Laser beam propagation

A laser resonator is an arrangement of optical mirrors that forms a standing wave resonator to confine the oscillating laser beam. The optical resonator is a major component of laser systems, which determines the laser spatial properties such as beam

waist size, beam waist location, output divergence angle, transverse mode profile and longitudinal distribution.

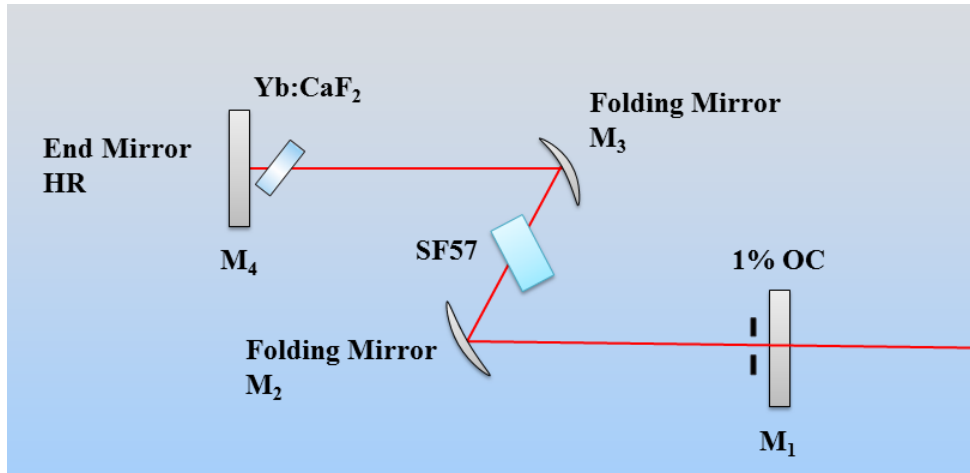


Figure 3-10 Laser oscillator schematic diagram

The cavity design is especially important for Kerr lens modelocking which will be discussed further in Chapter 5. It is important to analyze beam propagation behavior within the cavity in detail. Laser beams are strictly confined along the resonator optical axis, so they can be described by paraxial wave equation [118].

$$\frac{\partial^2 u}{\partial x^2} + \frac{\partial^2 u}{\partial y^2} - 2ik \frac{\partial u}{\partial z} = 0 \quad 3.8$$

Where $u(x, y, z)$ is related to the electric field, z is the resonator longitudinal axis and x , y are the transverse axes. The corresponding solution is

$$u(x, y, z) = \frac{1}{q(z)} \exp(-ik \frac{x^2 + y^2}{2R(z)}) \exp\left(-\frac{x^2 + y^2}{w^2(z)}\right) \quad 3.9$$

Where

$$\frac{1}{q(z)} = \frac{1}{R(z)} - i \frac{\lambda}{\pi w^2(z)} \quad 3.10$$

The solution corresponds a spherical wave originating from a real source point with a complex radius of curvature $q(z)$. $R(z)$ is the radius of curvature of the wavefront which

increases linearly with increasing propagation distance far from the source, and $w(z)$ is the beam waist. The laser beam transverse electric field and intensity distribution are well approximated by 1st order Gaussian functions, so people refer these laser beam modes as Gaussian beams.

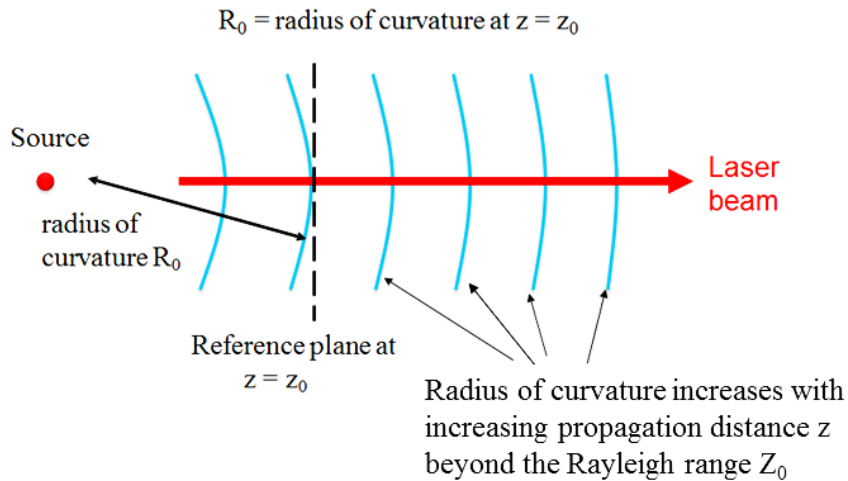


Figure 3-11 Laser beam propagation

For simplicity we only consider the fundamental mode of the Gaussian beam, centered at the origin position ($z=0$) with infinite radius of curvature at its beam waist, $R(0)=\infty$, $w(0)=w_0$. At this point $q(0)$ is a pure imaginary number given by.

$$q(0) = i \frac{\pi w_0^2}{\lambda} = i \cdot Z_R \quad 3.11$$

The quantity Z_R is defined as Rayleigh range which plays a key role in describing the Gaussian beam propagation. The Gaussian ray propagation can be calculated quantitatively by the using of ABCD-Law [119]. Any given paraxial optical system

can be described by a 2*2 matrix $M_{\text{system}} = \begin{pmatrix} A & B \\ C & D \end{pmatrix}$ and if the q parameter q_{in} at the

optical system entrance is given, we can determine the q parameter at the output q_{out} by

$$q_{out} = \frac{Aq_{in} + B}{Cq_{in} + D} \quad 3.12$$

The ABCD matrices of some typical optical elements are summarized in Table 3.2. In these more general cases the mode propagation can be different in the two orthogonal (vertical and horizontal) directions

Table 3-2 ABCD matrices for usually used optical elements [119]

Optical Elements	ABCD-Matrix
Free space propagation L with index n_0	$\begin{pmatrix} 1 & L/n_0 \\ 0 & 1 \end{pmatrix}$
Thin lens with focal length f	$\begin{pmatrix} 1 & 0 \\ -1/f & 1 \end{pmatrix}$
Sagittal plane for curve mirror (radius R) with incident angle θ to axis	$\begin{pmatrix} 1 & 0 \\ -2\cos\theta/R & 1 \end{pmatrix}$
Tangential plane for curve mirror (radius R) with incident angle θ to axis	$\begin{pmatrix} 1 & 0 \\ -2/R\cos\theta & 1 \end{pmatrix}$
Sagittal Plane for Brewster plate with incident angle θ to axis and thickness t	$\begin{pmatrix} 1 & t\sqrt{n^2+1}/n^2 \\ 0 & 1 \end{pmatrix}$
Tangential Plane for Brewster Plate with incident angle θ to axis and thickness t	$\begin{pmatrix} 1 & t\sqrt{n^2+1}/n^4 \\ 0 & 1 \end{pmatrix}$

Any resonator can be analyzed as periodic sequences of optical elements. Suppose a laser resonator contains N elements, which are labeled 1 to N and the number i element

is assigned a matrix $M_i = \begin{pmatrix} A_i & B_i \\ C_i & D_i \end{pmatrix}$. A periodic sequence of optical elements is schematically indicated by Equation 3.13.

$$q_{in} \Rightarrow \begin{pmatrix} A_1 & B_1 \\ C_1 & D_1 \end{pmatrix} \Rightarrow \begin{pmatrix} A_2 & B_2 \\ C_2 & D_2 \end{pmatrix} \Rightarrow \begin{pmatrix} A_3 & B_3 \\ C_3 & D_3 \end{pmatrix} \dots \dots \Rightarrow \begin{pmatrix} A_N & B_N \\ C_N & D_N \end{pmatrix} \Rightarrow q_{out} \quad 3.13$$

$$M_{system} = \begin{pmatrix} A_N & B_N \\ C_N & D_N \end{pmatrix} \times \begin{pmatrix} A_{N-1} & B_{N-1} \\ C_{N-1} & D_{N-1} \end{pmatrix} \dots \times \begin{pmatrix} A_1 & B_1 \\ C_1 & D_1 \end{pmatrix}$$

The mode of a resonator is defined as a self-consistent field configuration confined within the two resonator end mirrors. In order to reproduce itself while propagating back and forth, the beam parameters must return to the same values after one complete round trip. From this requirement we are able to determine the eigenvalues of the resonator's round-trip matrix given by

$$q_{in} = q_{out} = \frac{Aq_{in} + B}{Cq_{in} + D} \text{ and } \frac{1}{q} = \frac{D - A}{2B} (\mp) \frac{j}{2B} \sqrt{4 - (A + D)^2} \quad 3.14$$

Which yields the corresponding

beam radius:

$$w^2 = \frac{\lambda}{\pi} \frac{2|B|}{\sqrt{4 - (A + D)^2}} \quad 3.15$$

beam waist:

$$w_0^2 = \frac{\lambda}{\pi} \frac{\sqrt{4 - (A + D)^2}}{2|C|} \quad 3.16$$

And the resonator stability condition:

$$-1 < \frac{1}{2}(A + D) < 1 \quad 3.17$$

3.6.3 Astigmatism compensation

Astigmatism means that geometrical ray bundles in the sagittal plane behave differently compared with ray bundles in the tangential plane. For normal incidence cases, the two

bundles behave the same, for oblique incidence we need to treat tangential and sagittal beam separately [120]. A Brewster-angle gain crystal and curved mirror at non-normal incidence angles generate astigmatism, which lead to different beam foci positions, different resonator stability regions, and an elliptical output beam spot shape. The purpose of astigmatism compensation is to produce a maximum overlap between sagittal and tangential stability regimes. Without proper astigmatism compensation, the tangential stable regime may not overlap with sagittal regime which means that there's no available laser operation in this cavity configuration. Astigmatism can be balanced by placing curved mirrors at specific incidence angles.

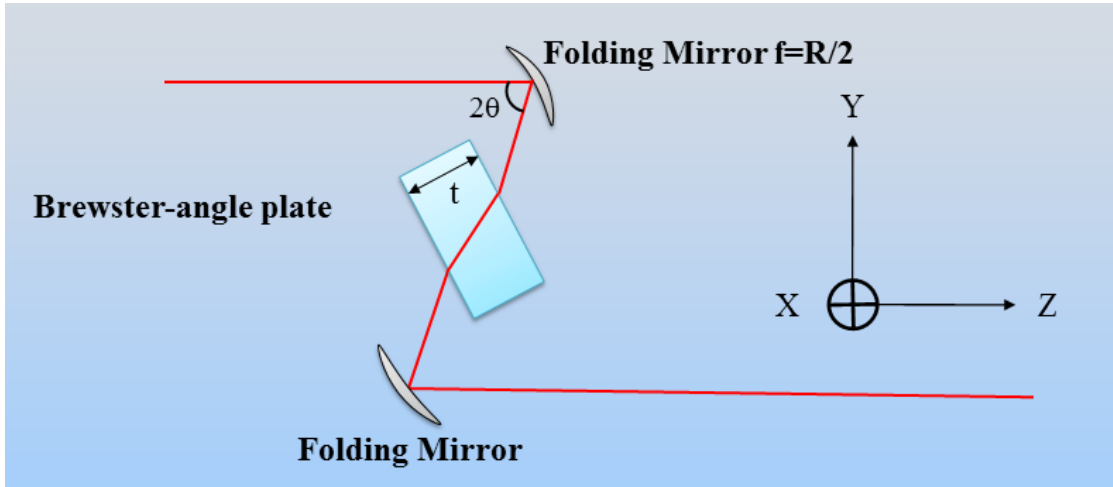


Figure 3-12 Folding mirror and Brewster-angle plate geometry. Coordinate and parameters are used as shown

The focal lengths of the curved mirrors (radius $R, f=R/2$) oblique at incidence angle θ are [121]:

$$\begin{aligned} f_x &= f / \cos \theta \\ f_y &= f \cdot \cos \theta \end{aligned} \quad 3.18$$

The effective paths lengths through a Brewster element with thickness t in sagittal (x axis) and tangential (y axis) planes are [122]:

$$\begin{aligned} d_x &= t\sqrt{n^2 + 1} / n^2 \\ d_y &= t\sqrt{n^2 + 1} / n^4 \end{aligned} \quad 3.19$$

The different distances can compensate for different focal lengths in the sagittal and tangential planes. We can adjust the laser beam incidence angle with folding mirror that the difference in effective path length through Brewster element is equal to the difference in folding mirror focal lengths in the two planes. If two identical curved mirrors $R=R_1=R_2$ are used in astigmatism compensation, it leads to the condition

$$0 = (d_x - d_y) - 2(f_x - f_y) \quad 3.20$$

With $f=R/2$, we get

$$0 = \frac{t\sqrt{n^2 + 1}}{n^4} (n^2 - 1) - 2 \times \frac{R}{2} \left(\frac{1 - \cos^2 \theta}{\cos \theta} \right) \quad 3.21$$

And the corresponding solution for θ is

$$\theta = \arccos \left[\sqrt{1 + \left(\frac{Nt}{2R} \right)^2} - \frac{Nt}{2R} \right] \text{ where } N = \sqrt{n^2 + 1} \frac{n^2 - 1}{n^4} \quad 3.22$$

4 Nonlinear optics and Kerr effect

4.1 Nonlinear optics introduction

Nonlinear optics is the study of the nonlinear optical responses that occur with the interaction of high intensity laser beam with matter. In 1961 Franken et al. first demonstrated the second-harmonic generation effect [123] (transformed ruby laser light at $\lambda=694$ nm to UV blue light $\lambda=347$ nm), which was the first demonstration of optical nonlinearity. Nonlinear effects allow one to change the optical frequency of the light, to change the pulse profile in the spatial and temporal domain, to manufacture ultrafast optical switches for high speed telecommunications and to generate ultrafast pulses to measure some the fastest events probed by humans [124].

Consider the one dimension Maxwell's EM wave equations, the polarization \vec{P} induced in a medium by an external electric field \vec{E} can be expressed as.

$$\vec{P} = \epsilon_0 \chi \vec{E} \quad 4.1$$

Where χ is a unitless proportionality constant called susceptibility and ϵ_0 is the vacuum permittivity. At low intensities situation \vec{P} is linearly proportional to \vec{E} . However when the intensity is strong enough, \vec{P} will have a non-linear dependence on \vec{E} . The non-linear part is very small in CW laser configuration and it is safe to ignore it in most cases. In pulsed laser configurations especially modelocked ultrafast lasers, the nonlinear effect is significantly enhanced and we cannot ignore it anymore. These nonlinearities have proven to be extremely powerful tools for ultrashort laser pulse generation. The one dimension inhomogeneous wave equation is given by

$$\frac{\partial^2 E}{\partial z^2} - \frac{1}{c_0^2} \frac{\partial^2 E}{\partial t^2} = \mu_0 \frac{\partial^2 P}{\partial t^2} \quad 4.2$$

Where μ is called the vacuum permeability, and c_0 is the light speed in vacuum. For the case of linear polarizability the wave equation becomes

$$\frac{\partial^2 E}{\partial z^2} - \frac{(1+\chi)}{c_0^2} \frac{\partial^2 E}{\partial t^2} = 0 \quad 4.3$$

The quantity $\sqrt{1+\chi}$ is defined as the refractive index n and linear refractive index $n_0 = \sqrt{1+\chi^{(1)}}$. Nonlinear optical effects can be described in terms of higher-order terms of the electric field.

$$\vec{P}_{\text{total}} = \epsilon_0 [\chi^{(1)} \vec{E} + \chi^{(2)} \vec{E}^2 + \chi^{(3)} \vec{E}^3 + \dots] = \vec{P}_{\text{linear}} + \vec{P}_{\text{nonlinear}} \quad 4.4$$

The wave equation becomes

$$\frac{\partial^2 E}{\partial z^2} - \frac{n_0^2}{c_0^2} \frac{\partial^2 E}{\partial t^2} = \mu_0 \frac{\partial^2 P_{\text{nonlinear}}}{\partial t^2} = \epsilon_0 \mu_0 \chi^{(2)} \frac{\partial^2}{\partial t^2} (E^2) + \epsilon_0 \mu_0 \chi^{(3)} \frac{\partial^2}{\partial t^2} (E^3) + \dots \quad 4.5$$

The electric field strength for a laser beam can be represented as:

$$E(t) = E_0 \exp(i\omega t) + E_0^* \exp(-i\omega t) \quad 4.6$$

Then

$$E(t)^2 = E_0^2 \exp(2i\omega t) + 2|E_0|^2 + E_0^{*2} \exp(-2i\omega t) \quad 4.7$$

$E_0^2 \exp(2i\omega t)$ and $E_0^{*2} \exp(-2i\omega t)$ introduce new frequency items into the system, which are twice of the original fundamental wave frequency. This phenomenon is called second harmonic generation (SHG) as illustrated in Figure 4.1. More generally, $\chi^{(2)}$ effects include second-harmonic generation (SHG), sum frequency generation (SFG), difference frequency generation (DFG), and optical rectification (OR) producing new frequencies [124]. The widely used green laser pointer is a typical

example of intracavity SHG laser. For most materials $\chi^{(2)}$ is zero, as it only exists in noncentrosymmetric materials.

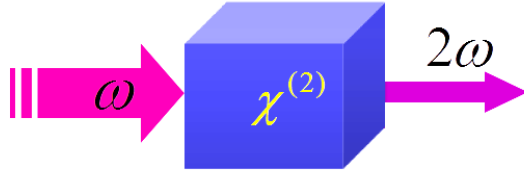


Figure 4-1 Second Harmonic generation

4.2 Kerr Effect

4.2.1 Nonlinear refractive index

$\chi^{(3)}$ effects are initially much weaker than $\chi^{(2)}$ but they can occur in any medium. It was discovered experimentally in 1875 by John Kerr [125]. Third-order nonlinear effects can be explained as following:

$$\begin{aligned} P^{(3)} &= \epsilon_0 \chi^{(3)} E_1(t) E_2(t) E_3(t) \\ &= \epsilon_0 \chi^{(3)} (E_1 e^{-j\omega_1 t} + E_1^* e^{j\omega_1 t})(E_2 e^{-j\omega_2 t} + E_2^* e^{j\omega_2 t})(E_3 e^{-j\omega_3 t} + E_3^* e^{j\omega_3 t}) \end{aligned} \quad 4.8$$

Suppose they all originate from a single laser beam $\omega_1=\omega_2=\omega_3$. The result contains two components: a shifted frequency part and un-shifted frequency part, the former part is very weak without optimum phase matching condition and the latter part is quite important in ultrafast lasers. The resultant polarization can be written in terms of the two frequency terms.

$$P^{(3)} = P^{(3)}(3\omega) + P^{(3)}(\omega) \quad 4.9$$

Considering only the un-shifted polarization component and assuming $\chi^{(2)}=0$, the total polarization is

$$P(\omega) = \varepsilon_0 [\chi^{(1)} E(\omega) + 3\chi^{(3)} |E(\omega)|^2 E(\omega)] = \varepsilon_0 \chi_{\text{eff}} E \quad 4.10$$

where $\chi_{\text{eff}} = \chi^{(1)} + 3\chi^{(3)} |E(\omega)|^2$ and then the effective refractive index

$$n = \sqrt{1 + \chi_{\text{eff}}} = \sqrt{1 + \chi^{(1)} + 3\chi^{(3)} |E(\omega)|^2} = \sqrt{(1 + \chi^{(1)}) \left(1 + \frac{3\chi^{(3)} |E(\omega)|^2}{1 + \chi^{(1)}} \right)} \quad 4.11$$

Recall $n_0 = \sqrt{1 + \chi^{(1)}}$ and nonlinear effect coefficient is usually quite small so with small argument approximation we get

$$n \approx n_0 + \frac{3\chi^{(3)} |E(\omega)|^2}{2n_0} = n_0 + n_2 I \quad 4.12$$

As shown in equation 4.12, the refractive index changes if the incident intensity is large enough. The phenomenon is also known as the optical Kerr effect, with n_2 in units of m^2/W and usually it is quite small. Several typical values for different materials are [126] [127]: air $n_2 = 4 \times 10^{-23} \text{ m}^2/\text{W}$, CaF₂ crystal $n_2 = 1.26 \times 10^{-20} \text{ m}^2/\text{W}$, highly nonlinear lead silicate glass SF57 and ZnS crystal $n_2 = 4.35 \times 10^{-19} \text{ m}^2/\text{W}$ and $n_2 = 1.73 \times 10^{-18} \text{ m}^2/\text{W}$ respectably. In order to make nonlinear refractive index noticeable, the interesting intensity range is $I \approx 1/n_2 \approx 10^{16}\text{--}10^{18} \text{ W/m}^2$. If the laser focused spot is symmetric with a radius of 100 μm and a beam area of $3.14 \times 10^{-8} \text{ m}^2$, then the necessary laser instantaneous power is $\text{area} \times \text{intensity} \approx 3.14 \times 10^{10} \text{ W}$. For 1% refractive index change, we need $3.14 \times 10^8 \text{ W}$ instantaneous power or 0.314 mJ pulse energy for 1 picosecond duration pulses.

This modified refractive index changes the laser profile as its propagation leading to self-induced Kerr effect. If the medium Kerr effect has slow response time, then this result can't be observed. In reality, this effect is fast enough to be regarded as instantaneous and it can have dramatic effects on ultrashort intense light pulses. The

response time can be estimated as follows. The Kerr effect is the result of nonlinear response of bound electrons to incident optical field and the polarization is a result of the distortion of the electron cloud by an applied EM wave. Thus, the time scale is on the order of the orbital period of bound electron around its nucleus [124]:

$$\tau_{\text{response}} = \frac{2\pi a_0}{v} \quad 4.13$$

Where $a_0 \approx 5.29 \times 10^{-11}$ m is the Bohr radius (first orbit), $v \approx 0.007 c_0$ is the typical electron velocity, c_0 is the light speed in vacuum, then $\tau_{\text{response}} \approx 1.5 \times 10^{-16}$ sec or 150 attosecond. So the Kerr effect has a response time which is much shorter than most of the laser pulses and fast enough to generate femtosecond laser pulses.

4.2.2 Transverse Kerr effect

As shown in Figure 4-2, due to an intensity-dependent refractive index, a planar Kerr medium acts as a positive focusing lens dependent on the laser intensity spatial profile.

Self-lensing/ self-focusing

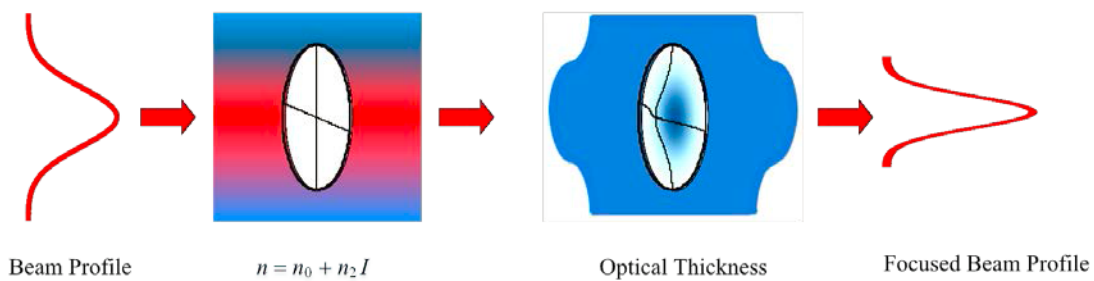


Figure 4-2 Transverse Kerr effect

An intense laser beam propagating in a Kerr medium experiences self-focusing due to the Kerr effect, it leads to an ever increasing intensity at the center of laser beam. A

beam in a homogeneous medium with a power exactly at the self-focusing limit could theoretically exhibit self-propagating or “self-trapping” over a long distance as illustrated in Figure 4-3.

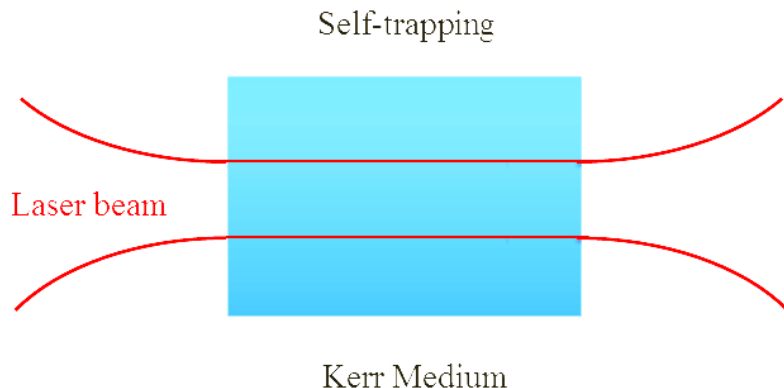


Figure 4-3 Laser beam self-trapping

In this case the beam divergence is exactly compensated by the nonlinear focusing effect, so the beam profile preserves its original shape over a long distance [128]. Obviously the optical intensity cannot be infinitely high, if the intensity is high enough to ionize atoms, one obtains a defocusing effect and refractive index becomes

$$n = n_0 + n_2 I - \Delta n_{\text{plasma}} \quad 4.14$$

Where the Δn_{plasma} is the refractive index change due to ionization defocusing . The nonlinear optical process of self-focusing sets an upper limit on the amount of laser intensity that can be propagated through a medium, above which the beam would experience catastrophic focusing and collapse, as the power is high enough to damage the material [129]. Many studies have investigated the power for catastrophic self-focusing or self-trapping in bulk media, and numerous expressions and values have been derived by use of various arguments or through numerical calculations. Generally,

the distortion of the wavefront can be described in terms of the integrated nonlinear index along the beam path called the B-integral which is given by [130].

$$B \equiv \frac{2\pi}{\lambda} \int_0^L n_2 I(z) dz \quad 4.15$$

To prevent material damage, B should be smaller than 3 to 5. Another important parameter called critical power P_c for self-focusing or self-trapping in bulk medium is given by [131]:

$$P_c = \frac{\alpha \lambda^2}{4\pi n_0 n_2} \quad 4.16$$

For the Gaussian intensity distribution beams $\alpha \approx 1.8$. When $n_2 = 0$, $P_c = \infty$, if the beam power reaches the critical power and the input wavefront curvature is flat, then the beams propagate in a self-guided mode with the same spot size indefinitely. For a CaF₂ crystal $P_{\text{critical}} \approx 9.07$ MW, for a highly nonlinear crystal ZnS $P_{\text{critical}} \approx 82.4$ KW and for SF57 a highly nonlinear lead glass $P_{\text{critical}} \approx 203$ KW.

4.2.3 Longitudinal Kerr effect and Self Phase Modulation

Along the axis of propagation, the longitudinal Kerr effect retards the center of an optical pulse, producing a red shift of the leading part of the pulse, and a blue shift in the trailing part. Consequently, the longitudinal Kerr effect has been named as self-phase modulation (SPM). Due to SPM laser pulses modify their own spectral phase and broaden the spectral profile. This effect is widely used to shorten the pulse duration yielding few-cycle laser pulses [132]. If a high intensity beam $E(z, t) = E_0 e^{i(\omega t - kz)}$ propagates a distance L_k in a Kerr medium, the phase change is

$$\phi(t) = \phi_0(t) + \phi_2(t) = -kn(I)L_k = -k[n + n_2I(t)]L_K \quad 4.17$$

Where $\phi_0(t)$ is the linear phase shift and $\phi_2(t)$ is nonlinear phase shift. For convenience one usually defines $\delta \equiv kn_2L_K$ as SPM coefficient, so the SPM phase shift can be rewritten as:

$$\phi_2(t) = -kn_2L_K I(t) = -\delta I(t) \quad 4.18$$

The time dependent frequency shift can be expressed as:

$$\omega_2(t) = \frac{d\phi_2(t)}{dt} = -\delta \frac{dI(t)}{dt} \quad 4.19$$

As shown in Fig 4-4, the instantaneous frequency is first smaller than and then larger than the central frequency ω_0 .

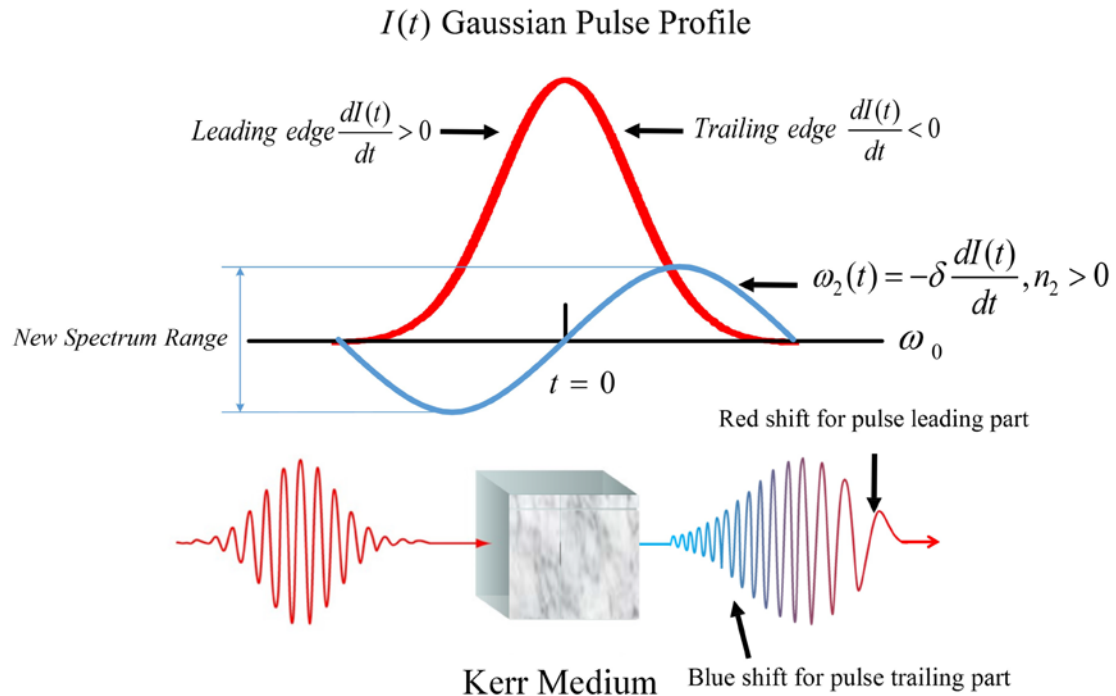


Figure 4-4 SPM effects and spectrum broadening

The SPM can be extremely dramatic, if $I(t)$ changes rapidly with time (for example with femtosecond pulses) which yields a very large time derivative. The frequency shift could be larger than its initial bandwidth, and then the spectrum is broadened.

Supercontinuum generation is a typical SPM application using ultrafast near inferred pulses to generate a white light spectrum (from red, green to blue).

The self-focusing Kerr effects can be applied to Kerr lens modelocking which was a breakthrough in ultrashort pulse generation [133]. In KLM lasers, the Kerr nonlinearity is utilized to produce an ultrafast saturable absorber effect. The phase nonlinearity provided by the Kerr effect and tiny amount of self-focusing is converted into effective amplitude nonlinearity by means of a real or effective aperture and builds a self-amplitude modulator (SAM). A high nonlinearity crystal is necessary for SAM. This could be the laser crystal itself or through a second nonlinear material such as ZnS or SF57 crystal added to the cavity.

4.3 Kerr Medium nonlinear ABCD matrix

In a KLM laser, the intra-cavity high nonlinearity Kerr crystal induces power dependent transverse resonator mode modification. With proper cavity design, a power dependent loss and gain can be responsible for mode-locking. KLM lasers need critical cavity design and alignment to operate effectively, so in order to design a KLM resonator it is useful to model the Kerr medium with a ABCD matrix approximation first. Although the Fresnel diffraction integral and the Fox-Li method are able to provide a more detailed description of the laser field inside the cavity [134] [135] [136], they involve complex calculation methods and are difficult to apply in general design.

A Kerr medium can be described by several nonlinear ABCD matrices and one of them is proposed by Vittorio [137]

$$M = \sqrt{1-\gamma} \begin{pmatrix} 1 & d_e \\ -\gamma/[(1-\gamma)d_e] & 1 \end{pmatrix} \quad 4.20$$

Where d_e is the effective optical length when power $P=0$ and

$$\gamma = \left[1 + \frac{1}{4} \left(\frac{2\pi w_c^2}{\lambda d_e} - \frac{\lambda d_e}{2\pi w_0^2} \right)^2 \right]^{-1} \frac{P}{P_c} \quad 4.21$$

As illustrated in Fig 4.5, w_c is the beam spot size in the center of Kerr medium, w_0 is the beam waist calculated when nonlinearity is zero, and P_c is the self-focusing critical power. If the laser power is fixed, a large Kerr effect is achieved when γ is maximized.

It leads to an optimum focusing condition given by $w_c = w_0 = \sqrt{\lambda d_e / 2\pi}$.

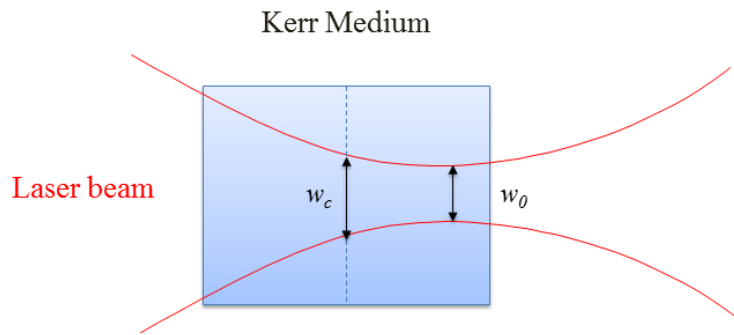


Figure 4-5 Laser beam focused inside Kerr medium

For convenience the matrix can be rewritten as:

$$M = \begin{pmatrix} 1 & d_e/2 \\ 0 & 1 \end{pmatrix} M_k \begin{pmatrix} 1 & d_e/2 \\ 0 & 1 \end{pmatrix}, \quad 4.22$$

$$\text{where } M_k = 1/\sqrt{1-\gamma} \begin{pmatrix} 1-\gamma/2 & -\gamma d_e/4 \\ -\gamma/d_e & 1-\gamma/2 \end{pmatrix} \quad 4.23$$

The Kerr nonlinearity is therefore lumped into the matrix M_k and separated from original CW mode linear propagation. However the model only allows the calculation

of the beam parameters at the output plane, not inside the medium. At relative low power, to the first order M_k could be written as [137]:

$$M_k \approx \begin{pmatrix} 1 & -\gamma d_e / 4 \\ -\gamma / d_e & 1 \end{pmatrix} \quad 4.24$$

Compared with the ABCD matrix $\begin{pmatrix} 1 & z \\ -1/f & 1 \end{pmatrix}$, which stands for a thin lens with focal length f and a free propagation distance of z . M_k can be viewed as a superposition of two effects [137]:

1. Self-focusing effect: a positive lens with focal length f_k : $1/f_k = \gamma/d_e$
2. Self-shortening effect: a propagation through a negative distance $z_k = -\gamma d_e / 4$

Once the beam waist and spot size at the input of the lumped Kerr element K have been determined, the nonlinear matrix M_k can be calculated and applied. The matrix M_k is the same for the beam propagation in the two directions. These concepts can be applied in the design and analysis of Kerr lens modelocked systems as will be discussed in the next chapter.

5 Modelocking Technology and KLM

5.1 Laser pulses generation through mode locking

It is sometimes desirable to operate lasers in pulsed mode other than CW mode, as the peak optical power can be greatly increased when the output pulse has a very short duration. Lasers can be made to emit optical pulses with durations as short as a few femtoseconds and the pulse duration can be further compressed to the attosecond regime by using nonlinear-optical high harmonic generation (HHG) in the deep UV region. For oscillators alone the maximum pulse repetition rates can reach more than 100 GHz, and the maximum pulse energies can reach from tens of millijoules, while the peak powers could extend to more than 10 MW and the peak cavity intensities can reach 10 TW/cm^2 . Four common methods are used for pulsed laser generation: gain switching, Q-switching, cavity dumping and mode locking. Mode-locking is the most widely used technique for periodic ultra-short laser pulses generation, although it is almost impossible to generate single or low repetition rate pulses. The first mode-locking laser was demonstrated in the mid-1960s [138].

The essence of mode-locking is trying to make as many as possible longitudinal modes oscillate together locked in phase and it has been achieved by various techniques, which can be categorized in two groups “active” and “passive” mode-locking. In active mode-locking, an intracavity amplitude or phase modulators is employed to force the cavity modes to oscillate in phase, whereas in passive mode-locking the mechanism is by means of nonlinear optical effects. Kerr lens modelocking (KLM) is a typical passive mode-locking technology. KLM was first successfully demonstrated in a Ti:sapphire laser in 1991 [139] and since then it has created a revolution in ultrashort laser pulse generation.

The transverse Kerr effect generates a positive Kerr lens that focuses the high intensity part of beams to be more strongly focused than the low intensity part. Combined with a properly engineered intracavity aperture, the Kerr lensing produces lower loss for high-intensity propagating pulses and higher loss for low-intensity pulses or CW beams. This combination forms an effective fast saturable absorber and this mechanism is called hard aperture KLM [140]. A similar modelocking mechanism is achieved without a real aperture, if the pump size is slightly smaller than the laser beam size and Kerr lens produces a better overlapping between the pulsed beams and the pump beam than the case of CW beams. The high intensity laser pulses experience higher gain than low intensity ones, and this mechanism also creates an effective fast self-amplitude modulator which is called soft aperture KLM.

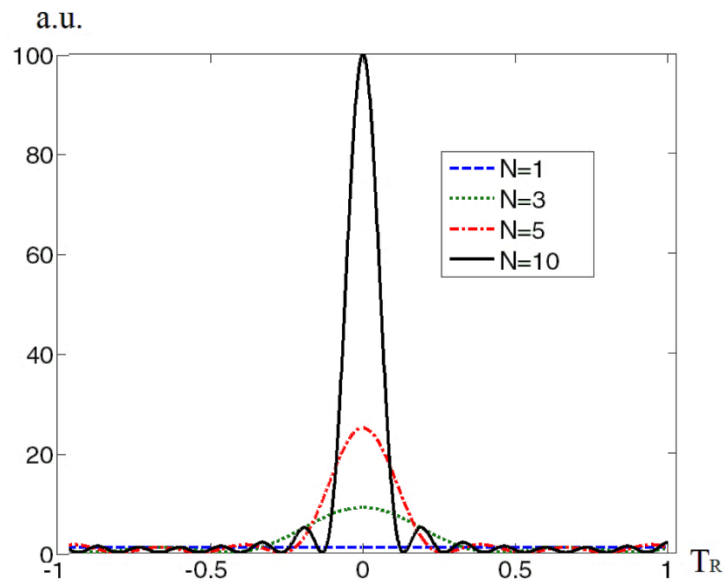


Figure 5-1 Laser pulses generation through modelocking principle

Usually a laser works at multiple longitudinal modes. In the modelocking operation regime these modes oscillate with a maintained fixed phase relationship [141]. These modes constructively interfere with each other's modes, generating a single laser pulse as shown in Fig. 5-1. The figure shows the modelocking result of $N=3, 5, 10$

longitudinal modes whose phases are locked at time $t=0$. Unlike Q-switching technology, which is able to generate nanosecond pulsed laser by changing resonant cavity quality Q with an intracavity variable attenuator, mode-locking forces the modes to oscillate in phase while the quality factor of the resonator is also modulated.

Suppose at steady laser operation $N=2n+1$ modes are available, with centre mode angular frequency ω_0 and adjacent axial mode angular frequency interval $\Omega=2\pi\Delta\nu_q=\pi c/nl$. The centre mode phase is ϕ_0 and phase interval between longitudinal modes is fixed equal to φ . The mode q can be expressed as:

$$E_q(t) = E_0 e^{i(\omega_q t + \varphi_q)} = E_0 e^{i[(\omega_0 + q\Omega)t + (\phi_0 + q\varphi)]} \quad 5.1$$

If all the modes have equal amplitude then the total output is the sum of all the mode field amplitudes:

$$E(t) = \sum_{q=-N}^N E_q(t) = E_0 \frac{\sin[\frac{N}{2}(\Omega t + \varphi)]}{\sin[\frac{1}{2}(\Omega t + \varphi)]} \quad 5.2$$

At phase-locked point $\frac{1}{2}(\Omega t + \varphi)=0, \pi, 2\pi \dots$, the electric field peak amplitude is increased by a factor of N , $E(t)=N \cdot E_0$, and the peak power is increased by a factor of N^2 . The pulse duration is reduced to $\tau \approx 2L/Nc = T_R/N$, where $T_R=2nL/c$ is the cavity round trip time. Obviously a larger N , in other words the more longitudinal modes available, the larger peak power and the shorter the pulse duration. Only standing waves at discrete wavelengths which are resonant in the cavity lead to cavity modes and the frequency interval between these modes is $\Delta\nu_L = c/2nL$. If the cavity length is around 1.5 m then $\Delta\nu_L \approx 10^8$ Hz. For Yb:CaF₂ linewidth with a gain bandwidth

of $\Delta\lambda=72$ nm, the gain bandwidth is calculated as $\Delta\nu_G=(c/\lambda^2)\Delta\lambda \approx 2\times10^{13}$ Hz . Thus $N=\Delta\nu_G/\Delta\nu_L \approx 2\times10^5$ longitudinal modes are available for modelocking which could lead to a short pulse duration down to 50 fs or less.

5.2 Multiple longitudinal modes operation

5.2.1 Homogeneous gain media

In a homogeneously broadened medium all modes are coupled and suffer population loss and gain depletion together. Immediately following laser turn-on a great number of modes have a gain coefficient exceeding the loss threshold and begin to grow. The central mode v_0 experiences the highest gain, and after a transient build-up time the laser gain saturates with the highest mode gain equal to the round trip loss. Since the other modes have lower gain, these modes suffer net round trip loss and eventually vanish. Only a single mode survives as illustrated in Figure 5-2.

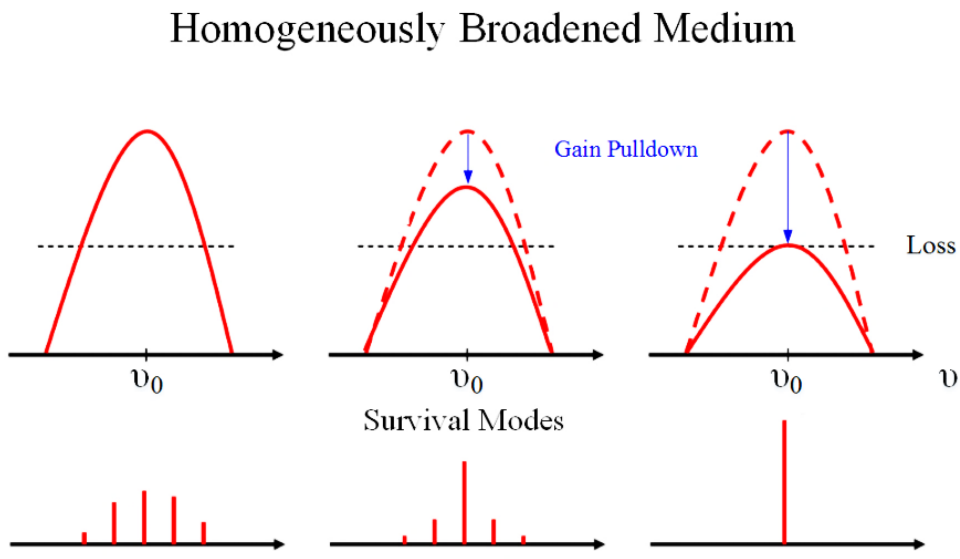


Figure 5-2 Homogeneous broadened medium

So an ideal homogeneously broadened laser oscillates in single mode operation, which cannot be used for modelocking. However in reality due to spatial hole burning effect,

where the gain coefficient is not uniform along the gain material, the laser may oscillate in a few multiple axial modes even for homogeneous line broadening [142].

5.2.2 Inhomogeneous gain media

For an inhomogeneous broadened gain medium, the inversion populations of the various modes are not coupled and the modes can grow independently. These axial modes saturate independently, so that the round trip gain equals the round trip loss for each mode. Thus multiple longitudinal modes can survive in the cavity and the laser oscillates in multiple modes. More precisely, the excited atoms whose frequencies coincide with these modes deplete their inverted population separately. The gain is saturated, and gain profile is pulled down individually by the different longitudinal modes. So a number of “holes” are created in the gain spectral profile, which is usually called spectral hole-burning. In steady state the modes do not compete with each other nor are they related in phase to each. This is illustrated in Fig 5-3.

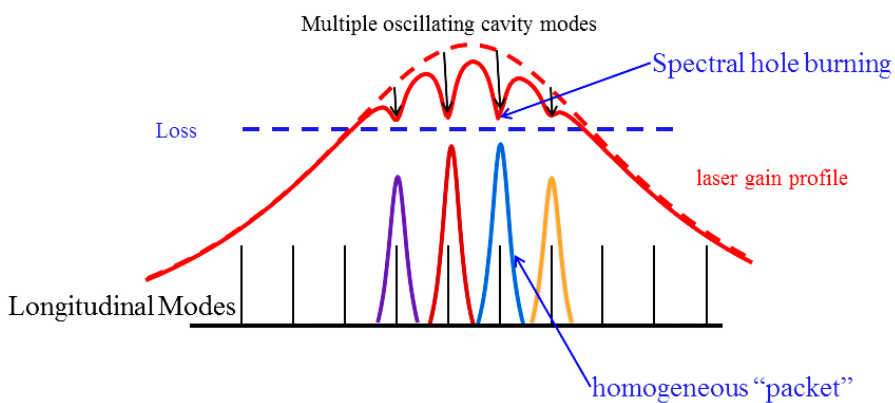


Figure 5-3 Inhomogeneously broadened laser medium

Various high power laser medium can be classified as to their degree of inhomogeneity:
 Nd:YAG weak inhomogeneity, Nd:glass strong inhomogeneity, Ti:sapphire very strong inhomogeneity, Yb: CaF₂ strong inhomogeneity [143] [144].

5.3 Master equation for modelocking

5.3.1 Complex envelop for optical field

In a modelocked laser cavity, multiple longitudinal modes interfere to form a propagating wave packet. This packet is usually described by the pulse envelope $A(t)$, which varies slower than the oscillatory part $E(t)$.

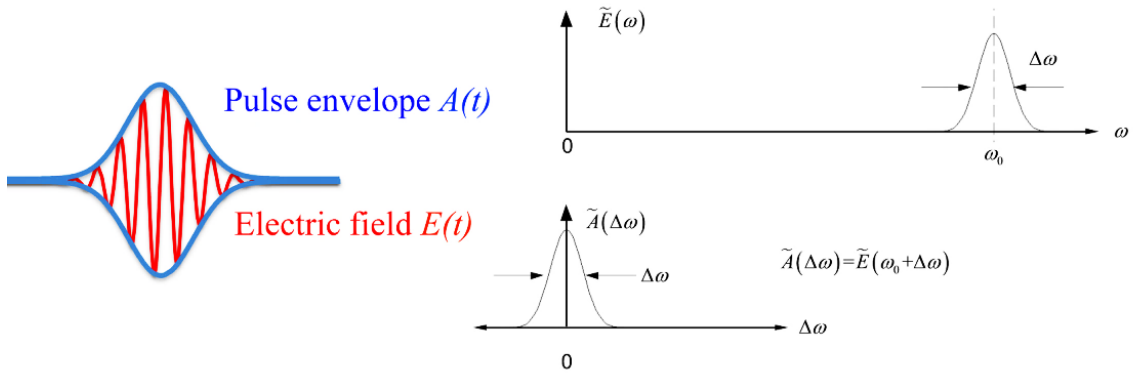


Figure 5-4 Laser pulse envelope and electric field

Based on the slowly varying envelop approximation, any light field $E(z,t)$ can be expressed by two parts: complex amplitude envelope and carrier wave. Any optical pulse can be represented as [145]:

$$E(z,t) = A(z,t) e^{i[\omega_0 t - k_n(\omega_0)z]} \quad \text{with} \quad |A(z,t)|^2 = P(z,t), \quad 5.3$$

For Gaussian pulse $E(t) = e^{-\Gamma t^2} e^{i\omega_0 t}$, the pulse amplitude envelope is $A(t) = e^{-\Gamma t^2}$ and

$\Gamma \equiv \Gamma_1 - i\Gamma_2$, where the pulse duration $\tau_p = \sqrt{2 \ln 2 / \Gamma_1}$ and instantaneous frequency

$$\omega(t) \equiv \frac{d\phi_{tot}(t)}{dt} = \omega_0 + 2\Gamma_2 t. \quad \Gamma_2 \neq 0 \quad \text{means} \quad \omega(t) \quad \text{increases or decreases with time, so}$$

the pulse is chirped. On the contrary $\Gamma_2 = 0$ means $\omega(t)$ does not change with time, and it is an unchirped pulse which is often called a diffraction limited pulse. Due to dispersion effects, the unchirped pulse temporal profile is broadened with time and is stretched into a chirped pulse but its spectrum remains unchanged. Generally an

unchirped pulse is transform-limited yielding minimum time-bandwidth products of $\Delta\nu\Delta t$ FWHM 0.4413 for Gaussian pulses and 0.3148 for hyperbolic secant (soliton) pulses.

5.3.2 Modelocking master equation

The mode-locking mechanism can be well described by the Haus's master equation. Based on the small signal approximation, it combines all the intracavity effects together and forms a partial differential equation as follows [146].

$$T_R \frac{\partial A(T, t)}{\partial T} = \sum_i \Delta A_i = 0 \quad 5.4a$$

Where A is the pulse envelope, T_R is the cavity round-trip time; T is the slowly varying time on a T_R time scale, t is the fast local time describing the pulse envelope on the order of pulse duration, and ΔA_i are the changes in the pulse envelope due to different elements in the cavity. The stable and self-consistent solution for laser operation is when the sum of all the changes in a round-trip equals zero. The effects of the different elements can be described as follows.

1) Gain and gain dispersion

The change of pulse envelope is

$$\Delta A_{gain} = g \left(1 + \frac{1}{\Omega_g^2} \frac{\partial^2}{\partial t^2} \right) A(T, t) = [g + D_g \frac{\partial^2}{\partial t^2}] A(T, t) \quad 5.4b$$

Where g is the saturated gain coefficient for a cavity round trip, $\Omega_g \equiv \Delta\omega_g/2$ is the half width at half maximum (HWHM) of the gain bandwidth and $D_g = g/\Omega_g^2$ is the gain dispersion.

2) Loss Modulator

The change in the pulse envelope is given by

$$\Delta A_{LM} = -M(1 - \cos \omega_m t)A(T, t) \approx -\frac{M\omega_m^2 t^2}{2}A(T, t) = -M_s t^2 A(T, t) \quad 5.4c$$

Where $2M$ is the modulator peak-to-peak modulation depth, ω_m is the modulation frequency equal to the fundamental mode axial mode spacing, $M_s = M\omega_m^2/2$ is loss modulation curvature.

3) Linear loss

$$\Delta A_{LL} = -lA(T, t) \quad 5.4d$$

4) Loss modulation by a fast saturable absorber

$q(t)$ is the saturable amplitude loss coefficient excluding any non-saturable losses is given by

$$q(t) = \frac{q_0}{1 + I_A(t)/I_{sat,A}} \approx q_0 - \gamma_A P(t) \quad 5.4e$$

Where $\gamma_A = \frac{q_0}{I_{sat,A} A_A}$ is the absorber coefficient, q_0 is the unsaturated loss coefficient, $I_{sat,A}$ is the absorber saturation intensity, A_A is the laser mode area on saturable absorber. The pulse envelope change is given by

$$\Delta A_{sat} = A_{in}(t) - A_{out}(t) = (1 - e^{-q(t)} A_{in}(t)) \approx \{1 - [1 - q(t)]\} A_{in}(t) \approx \gamma_A |A|^2 A \quad 5.4f$$

The modulation depth for a saturable absorber typically has a value of a few percent to a fraction of a percent to avoid Q-switching instabilities in passively mode-locked solid-state lasers [147].

5) Group delay dispersion (GDD)

We analyze the effect of group velocity dispersion by taking a Taylor series expansion for the wave vector around the center frequency ω_0 .

$$k_n(\omega) \approx k_n(\omega_0) + k'_n \Delta\omega + \frac{1}{2} k''_n \Delta\omega^2 + \dots \quad 5.4g$$

Where $\Delta\omega = \omega - \omega_0$, $k'_n = \left. \frac{\partial k_n}{\partial \omega} \right|_{\omega=\omega_0}$ and $k''_n = \left. \frac{\partial^2 k_n}{\partial \omega^2} \right|_{\omega=\omega_0}$. The pulse envelope change after

a propagation distance of z in frequency domain with slowly-varying-envelope approximation is given by:

$$\begin{aligned} \tilde{A}(z, \omega) &= e^{-i[k_n(\omega) - k_n(\omega_0)]z} \tilde{A}(0, \omega) \\ &\approx \left\{ 1 - i[k_n(\omega) - k_n(\omega_0)]z \right\} \tilde{A}(0, \omega) \\ &= \left[1 - ik'_n \Delta\omega z - ik''_n \Delta\omega^2 z / 2 \right] \tilde{A}(0, \omega) \end{aligned} \quad 5.4h$$

The linear term in $\Delta\omega$ describes the pulse envelope propagation velocity or group velocity, and the 2nd order term $\Delta\omega^2$ determines the envelope deformation due to dispersion. It is safe to ignore the higher order terms as long as the pulse duration is over 30 fs [148]. In a moving reference system which is travelling at the pulse envelope group velocity, only the second term describing the change in envelop shape during propagation is important. Thus we only need to consider the second order dispersion.

$$A(z, t) \approx \left[1 + iD \frac{\partial^2}{\partial t^2} \right] A(0, t) \quad 5.4i$$

Where $D \equiv \frac{1}{2} k''_n z = \frac{1}{2} \frac{d^2 \phi}{d\omega^2}$ is the dispersion parameter which is equal to half of the total group delay per cavity round trip. Therefore the local pulse envelope change is obtained

$$\Delta A_{GDD} \approx iD \frac{\partial^2}{\partial t^2} A(z, t) \quad 5.4j$$

6) Self- phase modulation (SPM)

The Kerr effect introduces nonlinear refractive index, which produces a nonlinear phase shift during pulse envelop propagation.

$$\phi(z, r, t) = -kn(r, t)z = -k[n + n_2 I(r, t)]z = -knz - \delta_L |A(r, t)|^2 \quad 5.4k$$

Where $\delta_L \equiv kn_2 z / A_L$ is the self-phase modulation (SPM) coefficient, and A_L is the effective laser mode area inside the laser medium, so the local envelop after a propagation of distance z is

$$A(z, t) = e^{-i\delta_L |A(t)|^2} A(0, t) e^{-ik_n(\omega_0)z} \approx \left(1 - i\delta_L |A(t)|^2\right) A(0, t) e^{-ik_n(\omega_0)z} \quad 5.4l$$

After one cavity round trip $e^{-ik_n(\omega_0)z} = 1$, so we obtain

$$\Delta A_{SPM} = -i\delta_L |A|^2 A(T, t) \quad 5.4m$$

7) Carrier-envelope offset (CEO)

The pulse envelope shift after a round cavity trip can be given by

$$\Delta A_{CEO} = i\psi \quad 5.4n$$

This effect is important in the generation of ultrashort few cycle pulse generation (<5fs) [11], when slowly varying envelope approximation begins to fail. In longer pulse duration cases, it is safe to treat $\psi=0$.

5.4 Active Modelocking

In active mode locking lasers, the loss modulator which is typically based on acousto-optic or electro-optic effects produces a sinusoidal loss modulation on the oscillating beams. The period is usually synchronized to cavity round trip time T_R . In frequency domain view, the modulator transfers additional in phase energy to adjacent modes. These modes are separated by the modulation frequency which is adapted to the

cavity round trip frequency. If the gain medium nonlinearity is very small self-phase modulation (SPM) and group-velocity dispersion (GVD) can be ignored. The Haus's master equation for an actively mode-locked laser is simplified to [149]:

$$\sum_i \Delta A_i = T_R \frac{\partial A(T, t)}{\partial T} = \left\{ g + D_g \frac{d^2}{dt^2} - M_s t^2 - l \right\} A(T, t) = 0 \quad 5.5$$

The stable solution is a Gaussian pulse and the pulse duration is:

$$\tau_p = 1.66 \times \sqrt[4]{D_g / M_s} = 1.66 \times \sqrt[4]{\frac{g}{\Omega_g^2} \cdot \frac{2}{M \omega_m^2}} = 0.445 \times \sqrt[4]{\frac{g}{M}} \sqrt{\frac{1}{f_m \Delta f_g}} \quad 5.6$$

Therefore, the pulse duration $\tau_p \propto \sqrt[4]{g}, \sqrt[4]{1/M}, \sqrt{1/f_m}, \sqrt{1/\Delta f_g}$, so a shorter pulse is obtained for a higher modulation frequency and a stronger modulation depth or for a larger gain bandwidth. At steady state the saturated gain is equal to total cavity losses. Therefore a larger output coupler will result in longer pulses and higher average output power is generally obtained at the cost of longer pulses. For example Keller's group used Nd:YLF as a gain medium obtaining 53 ps pulse duration at a wavelength of 1.047 μm with a gain bandwidth of $\Delta\lambda_g = 1.3$ nm [150]. A larger gain bandwidth would result in shorter pulses for a specific gain material. The gain bandwidth can be extended by the SPM effect. Including the SPM effect in the master equation gives:

$$\sum_i \Delta A_i = T_R \frac{\partial A(T, t)}{\partial T} = \left\{ g + D_g \frac{d^2}{dt^2} - M_s t^2 - l - i \delta_L |A(T, t)|^2 \right\} A(T, t) = 0 \quad 5.7$$

The solution is a chirped Gaussian pulse with pulse width:

$$\tau_p = 1.66 \cdot \tau = 1.66 \sqrt{\frac{D_g}{M_s + \phi_{nl}^2 / 4D_g}} \quad 5.8$$

Where $\phi_{nl} = 2kL_g n_2 I_{0,L}$ is the nonlinear phase shift per cavity round trip at peak intensity, L_g is the length of the dispersive material and $I_{0,L}$ is the peak intensity inside SPM medium. Significant SPM effect would shorten the pulse to a few picoseconds regime.

A 12 ps diode-pumped Nd:YAG actively mode-locked laser was reported by G. T. Maker [151] and a sub 10 ps Nd:YLF actively acousto-optic mode-locked laser was demonstrated by the Keller group in 1990 [152]. Further increase in SPM would provide shorter pulses but ultimately would push the laser away from the stable regime of operation. A great amount of negative GVD has to be introduced to balance SPM effect, and the pulse duration could be reduced by a factor of 6. Ultimately a 310 fs pulse was generated from regenerative actively mode-locked Nd:phosphate and silicate lasers [153]. The only method left to further reduce pulse duration is to increase the modulation frequency. However in an actively modelocking laser, the modulation frequency cannot be increased arbitrarily, as the modulator performance is limited to the speed of the electronic signal generators (~ns). In addition the synchronization between modulator and oscillating pulse packet is crucial, and the introduction of complex devices makes system complicated and difficult to maintain. As a result, passive modelocking technology has been developed for generating shorter pulses.

5.5 Passive Modelocking

In passively mode locked lasers, a saturable absorber is engineered to induce self-amplitude-modulation (SAM) effect on the propagating pulses. The ultrashort pulse modulates the gain and loss by itself, thus SAM produces a much larger curvature of loss modulation than in the sinusoidal loss modulation of active mode locking because the modelocked pulse duration can be much shorter than the cavity roundtrip time. Thus the net gain window generated by the pulse can be as short as the pulse itself; the short net gain window shortens the pulses. The mechanism typically starts from random noise fluctuations, once noise spikes are strong enough for the absorber to start working, it will introduce a nonlinear losses to different parts of the pulse profile. The

highest intensity peak in the pulse saturates the absorber more strongly than the lower portions. The peak pulse intensity grows and becomes stronger producing an isolated pulse which then becomes shorter until a stable condition is reached. In general stable pulse generation starts from noise spikes and converts to normal stable operation within 1 ms [148].

The loss modulator performance is determined by the pulse profile and material properties. The saturable absorber is designed to be reliable and self-starting. If the loss modulation becomes too large, it would push the laser away from its stable working condition. The loss modulator changes intra-cavity optical intensity, so the gain needs to adjust itself to balance the changes. In order to keep intra-cavity intensity constant the gain has to respond fast enough, otherwise the increased intensity would bleach the absorber and lead to self Q-switching instabilities or Q-switched mode locking (QML). In QML operation the modelocking train is usually modulated at the relaxation oscillation frequency (a few kHz rate) [154].

Although a large modulation depth of saturable absorber results in shorter pulses, an upper limit is set by the onset of Q-switching instabilities [155]. Q-switching instabilities remained a serious issue for a long time until the first low loss intracavity saturable absorber were designed correctly to prevent self-Q-switching instabilities in solid-state lasers with microsecond or even millisecond upper state lifetimes [156]. The passive mode-locking mechanism can be explained by three fundamental models:

- 1) Slow saturable absorber recovery with dynamic gain saturation. The loss saturates and then recovers faster than the gain, depleting the tail of the laser pulse and causing pulse shortening as shown in Fig 5-5. One can neglect gain recovery within

the pulse duration. For example, a modelocking laser with a dye cell as loss modulator. [157].

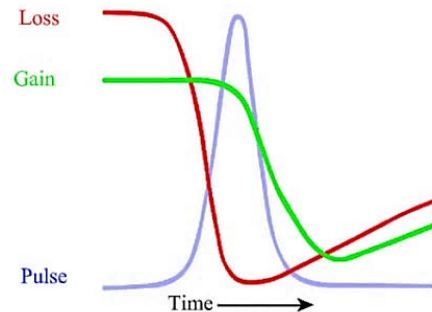


Figure 5-5 Slow saturable absorber modelocking with dynamic gain saturation

- 2) Slow saturable absorber modelocking without dynamic gain saturation, e.g. SESAM and soliton modelocking as shown in Fig 5-6.

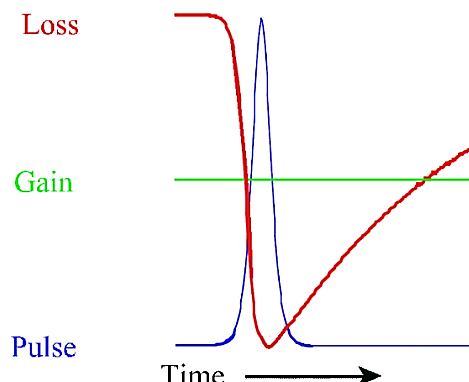


Figure 5-6 Slow saturable absorber modelocking with constant gain [158]

- 3) Fast saturable absorber modelocking as illustrated in Fig 5-7, e.g. KLM

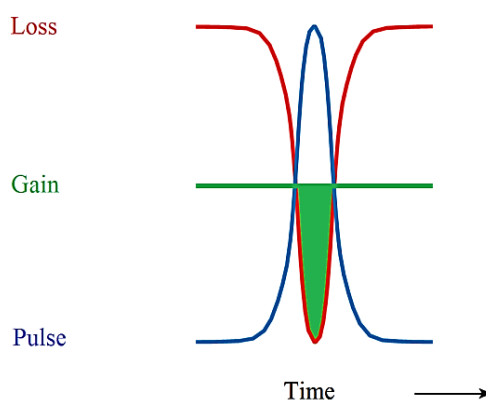


Figure 5-7 Fast Saturable absorber modelocking

In the case of an ideal fast saturable absorber, the loss recovers instantaneously.

Therefore it shows the same time dependence as the pulse envelope [159].

For UF solid-state lasers, there is no significant dynamic gain saturation taking place due to small gain cross-section and long upper state lifetime of gain material. A fast saturable absorber is necessary for solid-state lasers and the KLM is an almost ideal example of fast saturable absorber mode locking. Recent research also showed that a relatively slow saturable absorber can support significantly shorter pulses even though a net gain window remains open after the short pulse [148]. Loss modulation difference between active mode-locking and passive mode-locking is illustrated in Fig 5.8.

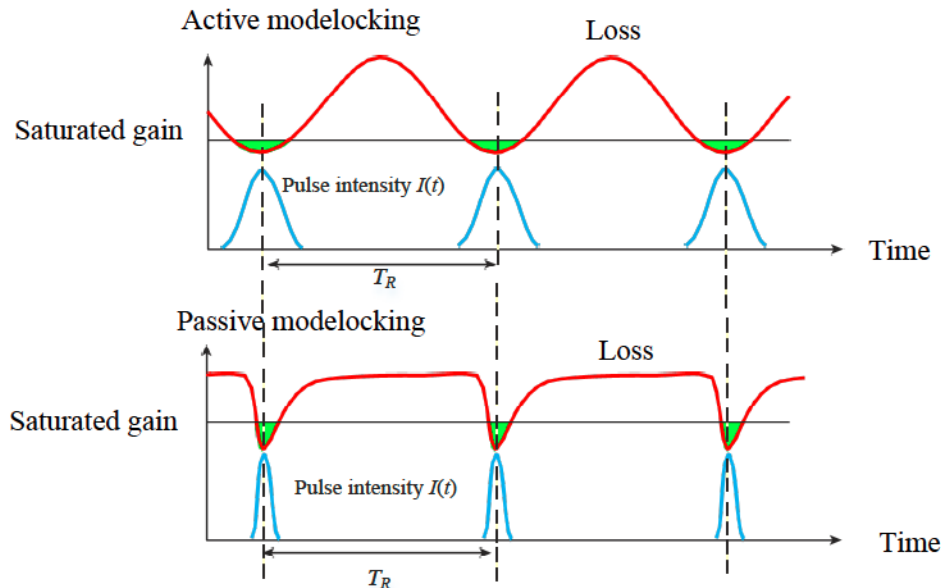


Figure 5-8 Loss modulation of active modelocking and passive modelocking [148]

5.6 SESAM mode-locking

A SESAM (semiconductor saturable absorber mirror) is typically made up by four components: top reflector, saturable absorber, bottom reflector and substrate [181] which are shown in Fig.5-9. The top reflector can be made from a multilayer

dielectric Bragg mirror made of materials such as SiO_2 and TiO_2 (In some SESAMs, it is replaced by a layer of AR coating film). This top reflector determines the intensity of light entering the semiconductor saturable absorber and can be used to control the saturation fluence of the saturable absorber [169]. In 980 nm to 1.5 μm wavelength region, the saturable absorber is usually made from single or multiple InGaAs/GaAs quantum wells. The bottom reflector is usually made from a highly-reflecting GaAs/AlAs dielectric Bragg mirror and the substrate is often made from GaAs [179]. Using epitaxial material deposition the material layer thickness can be controlled to sub-nanometer accuracy and thus we can precisely control the key parameters of SESAM: modulation depth (ΔR or saturable loss), nonsaturable loss, saturation fluence and recovery time τ_A [169] [179].

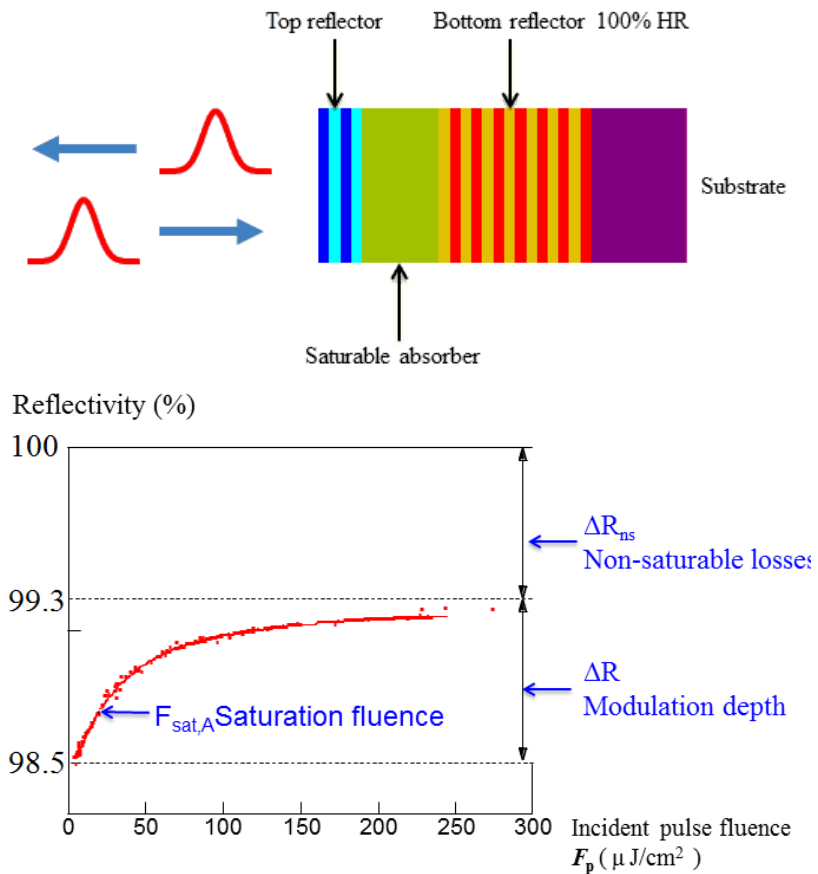


Figure 5-9 Typical layout of a SESAM (top) and a plot of typical reflectivity vs incident fluence (bottom) [161]

SESAM modelocking is a well-established process. In SESAM modelocking, a saturable absorber mirror acts as a saturable absorber and the loss modulation is achieved by intensity dependent changes in its reflection coefficient as shown in Fig. 5-9. In general conditions, the modulation depth ΔR ranges from a fraction of a percent to a few percent and the recovery time τ_A ranges from 500 fs to 10 ps [160]. Fig. 5-10 provides an example of a SESAM with 0.78 ps recovery time [181].

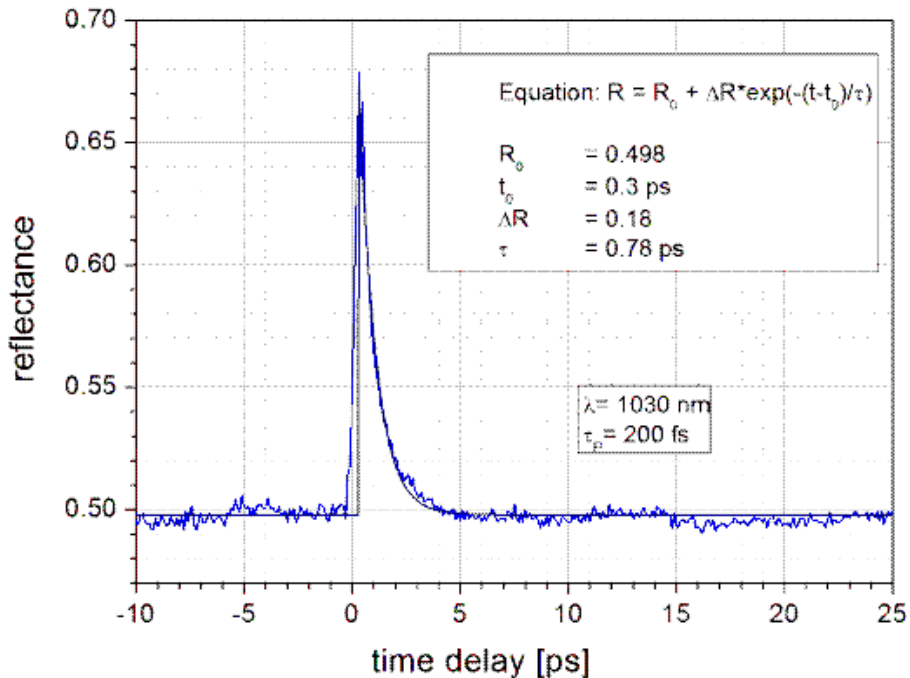


Figure 5-10 Time-dependent reflectivity for a SESAM with 0.78 ps recovery time

If $\tau_A \leq 10\tau_p$ where τ_p is the pulse duration and excludes SPM effects, dispersion and spatial hole burning effects a sech^2 -pulse pulse is expected. The pulse duration is estimated by [162]:

$$\tau_{p,\min} \approx \frac{1.5}{\Delta v_g} \sqrt{\frac{g}{\Delta R}} \quad 5.9$$

Where $\Delta\nu_g$ is the FWHM gain bandwidth. The mirror becomes saturated at high intensities allowing most of incident pulse energy reflected back. At low intensities SAM is unsaturated and absorbs a bit more incident pulse energy. A small absorption coefficient change is required to suppress QML operation. And the critical laser pulse energy E_p and intracavity power P_{intra} required to suppress the Q-switching instabilities are written as:

$$E_p \geq \sqrt{F_{\text{sat},l} \cdot A_{\text{eff},A} \cdot F_{\text{sat},A} \cdot A_{\text{eff},A} \cdot \Delta R} \quad 5.11a$$

$$P_{\text{intra}}^2 \geq F_{\text{sat},l} \cdot F_{\text{sat},A} \cdot \Delta R \cdot A_{\text{eff},L} \cdot A_{\text{eff},A} \frac{1}{T_R^2} \quad 5.11b$$

Where E_p is the intracavity pulse energy, P_{intra} is the intracavity power, $F_{\text{sat},l}$ is the gain medium saturation fluence, $F_{\text{sat},A}$ is the SESAM saturation fluence, $A_{\text{eff},L}$ and $A_{\text{eff},A}$ are effective laser mode areas inside gain medium and on the SESAM respectively, ΔR is the reflectivity modulation depth and T_R is the cavity round trip time. To avoid Q-switching instabilities, the $\Delta R < 1\%$ and $F_{\text{sat},A}$ is a few tens of $\mu\text{J}/\text{cm}^2$ should be employed.[163]

In the case of Q-switched modelocking, pulse energy is unstable and maximum peak pulse energy becomes very large which could create significant damage on the SESAM [164]. Such damage has been observed in the present experiments, Yb: CaF₂ SESAM modelocking laser, as shown in Fig 5-11. Due to the high saturation fluence of Yb:CaF₂ crystal, the laser system operated in Q-switched modelocking mode and then energetic pulses with very high peak intensity were generated. Although the SESAM damage threshold is as high as is 0.8 GW/cm², these pulses peak power were still strong enough to burn and crack the SESAM easily. Many burn spots with a few to tens of

micrometers diameters were observed by microscope. Furthermore the available SESAM saturable absorption modulation depth ΔR is also limited by increasing non-saturable loss. Greater modulation depth and shorter pulse operation is possible if in addition the Kerr-lens effect is used in the cavity.

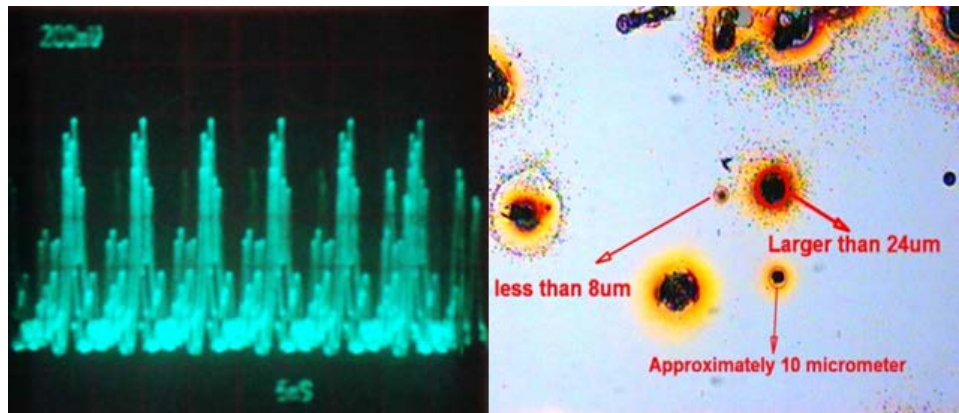


Figure 5-11 Q-Switching modelocking and burned SESAM

5.7 Kerr Modelocking

Kerr lens modelocking is an ideal fast saturable absorber technique for passive mode-locking without dynamic pulse-to-pulse gain saturation. It was first demonstrated as an intracavity fast self-amplitude modulator in a Ti:sapphire laser [139]. For an ideal fast saturable absorber, the master equation without GVD and SPM consideration is

$$\sum_i \Delta A_i = [g(1 + \frac{1}{\Omega_g^2} \frac{\partial^2}{\partial t^2}) - l + \gamma_A |A|^2] A(T, t) = 0 \quad 5.12$$

The amplitude solution is an unchirped sech-fuction [165]

$$A(t) = A_0 \operatorname{sech}(\frac{t}{\tau}) \quad 5.13$$

So the power solution is an unchirped sech^2 -pulse shape

$$P(t) = P_0 \operatorname{sech}^2(\frac{t}{\tau}) \quad 5.14$$

With a FWHM pulse width

$$\tau_p = 1.7627\tau = 1.7627 \frac{4D_g}{\gamma_A E_p} \quad 5.15$$

Where P_0 is the peak power of the pulse, D_g is the gain dispersion of the laser medium, γ_A is the absorber coefficient and E_p is the intracavity pulse energy. In a Kerr lens mode-locked laser the loss modulation is achieved by two ways, one is called “hard aperture KLM” and the other one is called “soft aperture KLM”.

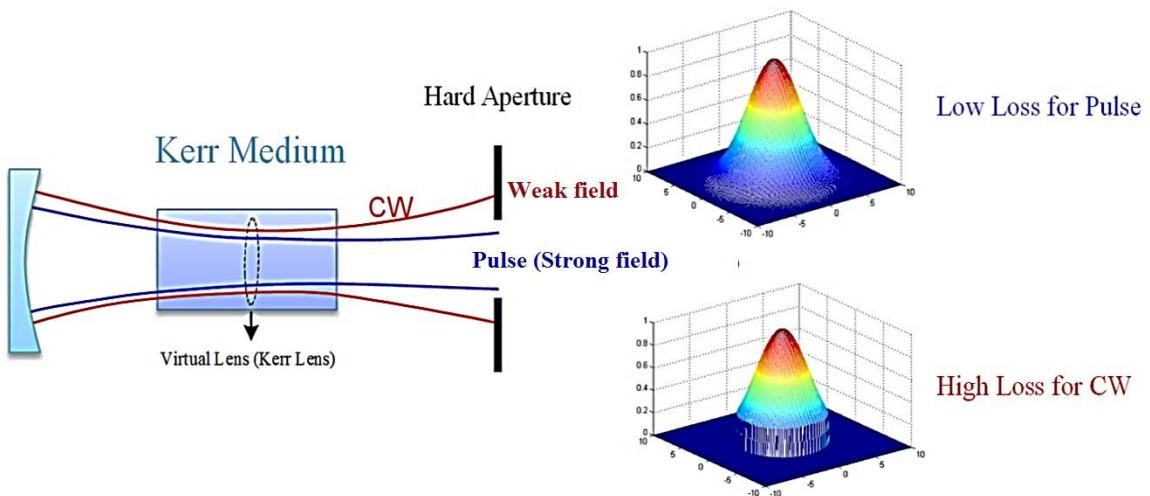


Figure 5-12 Hard Aperture Kerr lens modelocking [2]

In the case of the hard aperture KLM, an aperture element such as a pinhole or slit is inserted into the cavity. The self-focusing mechanism decrease pulse laser loss when it passes through the aperture. In the transverse plane perpendicular to optical axis, the radiant intensity distribution of a Gaussian beam TEM₀₀ mode with total power P and waist w is

$$I(r) = \frac{2P}{\pi w^2} e^{-2r^2/w^2} \quad 5.16$$

If the beam passes through a pinhole with radius R , the fraction power transmitted

$$T = \frac{2}{\pi w^2} \int_0^R 2\pi r e^{-2r^2/w^2} dr = 1 - e^{-2R^2/w^2} \quad 5.17$$

So the Loss is

$$L = 1 - T = e^{-2R^2/w^2} \quad 5.18$$

KLM is possible if the laser power transmittance increase with intensity rising $dT/dI > 0$. And the loss through the aperture decrease as intensity increase $dL/dI < 0$.

Aperture Transmission

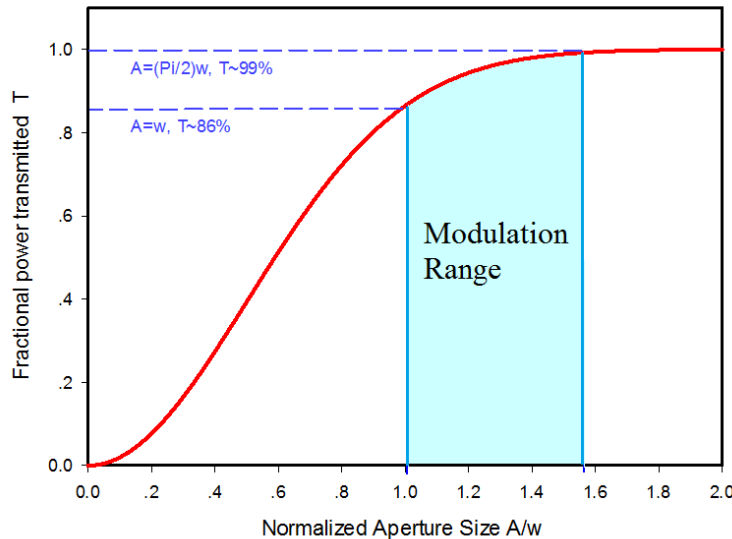


Figure 5-13 TEM₀₀ mode aperture transmission ratio

Without proper cavity configuration, the KLM operation would never be obtained. The cavity is typically operated near one end of its stability range, where the Kerr-lens-induced change of the beam diameter is large enough to sustain mode locking. Although KLM allows greater modulation depth than SESAM modelocking, to suppress QML the aperture loss modulation has to be designed to be small. The typical modulation range for hard aperture is shown by Figure 5-13. The magnitude of hard aperture Kerr-lens effect strongly depends on the cavity configuration and precise alignment is also needed. In KLM lasers mirrors and the laser crystal have to be

positioned to an accuracy of several hundred micrometers. Once the cavity is correctly aligned, KLM can be very stable and under certain conditions even self-starting.

In case of soft aperture KLM, there is no additional intracavity aperture. The pumping beam is usually focused to a narrower spatial profile than the lasing mode, so a radially dependent gain is created inside the gain medium. The pulsed laser mode experiences additional focusing and extra gain as mode matching between the pumping mode and the pulsed laser mode becomes more efficient than that of CW laser mode. The better mode matching also decreases the diffraction loss.

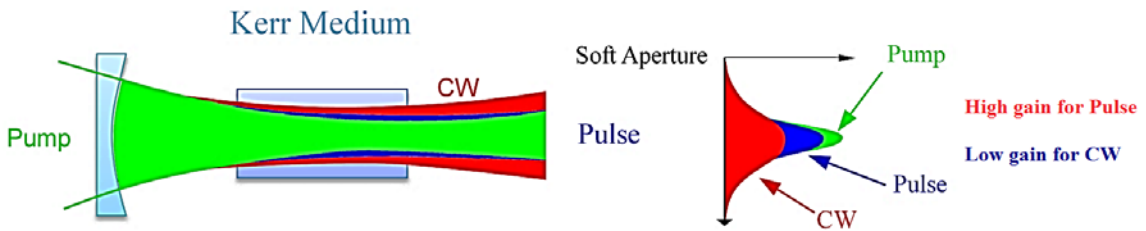


Figure 5-14 Soft aperture Kerr Modelocking [140]

An important parameter for analyzing the KLM cavity is the strength of the Kerr effect, which is also called small signal relative spot size variation, defined as [148]:

$$\delta = \left(\frac{1}{\omega} \frac{d\omega}{dp} \right)_{p=0} \quad 5.19$$

Where ω is the spot size at the aperture plane, p is the power normalized to the critical power for self-focusing. KLM is possible if δ is negative and sufficiently large, as the cavity is more suitable for pulsed laser operation.

KLM is able to generate very short pulses if a broadband pulse spectrum is given. However, so far there is no self-starting sub-50 fs KLM laser available. For a 10 fs Ti:sapphire laser with 100 MHz repetition rate, the peak power will be 10^6 times larger than CW mode [166]. So in order to initiate the ML process, additional elements have to be used. Furthermore a KLM laser needs critical cavity adjustments and operates

close to the stability limit where the Kerr-lens induced beam diameter variation is large enough to maintain mode-locking. Even after a large amount of research on the KLM technique there are still some details which need to be clarified (e.g. exact effective saturation fluence) [167]. Last but not least in the cases of sub-10-fs ML lasers, strong SPM effects make the evolution of the pulse shape far more complex and the linearized model does not fit well.

5.8 Soliton mode-locking

In soliton mode-locking, the pulse-shaping mechanism is dominated by soliton formation, i.e. nonlinear phase shift is balanced by negative GVD ($D < 0$) and positive SPM ($n_2 > 0$) [148]. In order to start the ML process and stabilize soliton pulse-forming process, a slow saturable absorber (compared with KLM) is used. In soliton mode locking, only the time-dependent Kerr effect $n(t) = n_0 + n_2 I_0(t)$ leading to SPM needs to be considered. Soliton mode locking does not critically depend on cavity design and there is no necessity for critical alignment, so in general it works over the full laser cavity stability range [168].

Including GVD, SPM and a slow saturable absorber $q(T, t)$ with a recovery time longer than the pulse duration, the Haus's master equation is [169]:

$$\sum_i \Delta A_i = \left\{ g + D_g \frac{d^2}{dt^2} - l_0 - q(T, t) \right\} A(T, t) + \left\{ iD \frac{d^2}{dt^2} - i\delta_L |A|^2 \right\} A(T, t) = 0 \quad 5.20$$

And we can expect a stable sech^2 shaped soliton pulse with pulse duration

$$\tau_p = 1.7627 \frac{2|D|}{\delta_L \cdot E_p} \quad 5.21$$

Where D is the dispersion parameter, δ_L is the SPM coefficient and E_p is the pulse energy. Another limiting effect becomes significant: the dispersive medium temporally

broadens the soliton pulse and shifts part of the pulse into the net loss time region, this part is usually called continuum [170]. The continuum pulse has a longer duration and a narrower spectrum than the soliton pulse. The minimal pulse duration is reached when the continuum loss, the soliton pulse loss and the saturated gain are all equal, which is given by [170]:

$$\tau_{p,\min} \approx 0.45 \left(\frac{1}{\Delta\nu_g} \right)^{3/4} \left(\frac{\tau_A}{\Delta R} \right)^{1/4} \frac{g^{3/8}}{\phi_s^{1/8}} \quad 5.22$$

Where $\phi_s = 0.5 \delta_L P_0$ is the phase shift of the soliton per cavity round trip, δ_L is the SPM coefficient, P_0 the peak power inside the laser cavity, and $\Delta R = 2q_0$ where q_0 is the unsaturated loss coefficient. Soliton shaping effects are able to generate significantly shorter pulses compared those without SPM. The shortest pulses are obtained by 1st order and higher order negative dispersion being fully compensated by SPM [171]. A soliton laser often tends to operate in continuum modes or break-up into two or three pulses. As compared with single pulse operation the other modes have narrower spectra so that they experience the gain profile peak which is higher than the gain for the soliton pulse. An additional saturable absorber is needed to stabilize the soliton and suppress the growth of continuum. The stability of the soliton against the continuum growth determines the allowed operating parameters, and then the shortest possible pulse duration.

KLM lasers often employ structures analogous to a soliton laser to counteract pulse dispersion for femtosecond regime pulse generation. Laser gain material and high nonlinearity crystal introduce positive group delay dispersion GDD which is usually compensated by negative GDD induced by negative dispersion prism pair. The GDD is expressed as [172]:

$$\frac{d^2\phi}{d\omega^2} = \frac{\lambda^3}{2\pi^2 c^2} \frac{d^2L}{d\lambda^2} \quad 5.23$$

Where L is the optical path length of the dispersive medium for wavelength λ_0 . For example for $\lambda_0=1050$ nm, the one way cavity travel GDD introduced by 5mm CaF₂ plate and 10mm SF57 plate (placed at Brewster angle) are ~ 108 fs² and ~ 1629 fs² respectively, thus the total GDD is 1737 fs². We can use SF10 negative dispersion prism pair to compensate positive GDD.

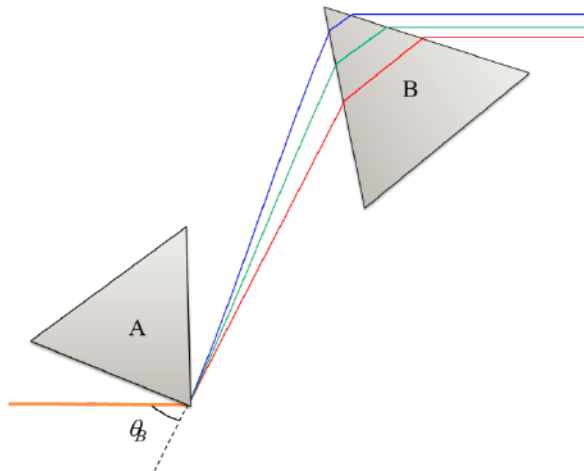


Figure 5-15 Negative dispersion prism pairs

The GDD of prism pair can be expressed by [173]:

$$\frac{d^2\phi}{d\omega^2} \approx \frac{\lambda_0^3}{2\pi c^2} \left[-4L_{sep} \left(\frac{dn}{d\lambda} \Big|_{\lambda_0} \right)^2 + L_{prism} \frac{d^2n}{d\lambda^2} \Big|_{\lambda_0} \right] \quad 5.24$$

Where L_{sep} is the prism tip-to-tip separation distance, L_{prism} is the pathlength of the beams propagating through the prism pair and θ_B is the Brewster angle for minimum reflection loss. The GDD of SF10 prism pair used in thesis is estimated to be

$$\text{GDD} \approx -5.5L_{sep} (\text{mm}) + 100.86 L_{prism} (\text{mm}) \quad [\text{fs}^2] \quad 5.25$$

In the femtosecond regime, QML instabilities are easier to overcome compared to pure saturable absorber mode-locked picosecond lasers. The femtosecond pulses have a

broader spectrum, and the strong SPM effects also broaden pulse spectrum. A broader pulse spectrum increase the loss due to finite gain bandwidth. The finite gain effects provide negative feedback to pulse energy increase caused by relaxation oscillations and reduce the necessary critical pulse energy for CW mode locking operation. The stability criterion for stable CW ML operation is [174].

$$E_{sat,L} \cdot g \cdot K^2 \cdot E_p^3 + E_p^2 > E_{sat,L} \cdot E_{sat,A} \cdot \Delta R \quad 5.26$$

Where K is given by

$$K \equiv \frac{0.315}{1.76} \cdot \frac{4\pi n_2 L_k}{D_2 A_{eff,L} \lambda_0 \Delta \nu_g} \quad 5.27$$

λ_0 is the center wavelength of mode-locked pulse, n_2 is the nonlinear refractive index, L_k is the propagation length in the Kerr medium per round trip, D_2 is the negative GDD per round trip which compensates for the chirp introduced by SPM, $A_{eff,L}$ is the effective laser mode area in gain media and $\Delta \nu_g$ is the FWHM of gain bandwidth.

5.9 Other Modelocking technology

Due to various reasons, the following modelocking techniques are not used very frequently anymore, so only a brief summary is given for them.

FM mode-locking

FM mode-locking is somewhat analogues to active mode locking. An electro-optic modulator (e.g. Pockels cell) generates a phase shift in the oscillating beam per round trip [175], which can link the modes together. Usually it leads to chirped pulses, and creates a mode hopping instability. Sometimes dispersive and nonlinear elements are used to remove or minimize the negative effects.

Synchronous pumping

The gain medium pumping is not continuous but pulsed, and the pumping repetition is synchronized with laser pulses envelop round-trip frequency. So a precise match between pump and lasing beam in the time domain is required. It is useful for converting longer amplitude-modulated (AM) pulses into shorter AM pulses. Yamashita et al. reported that a 0.79 ps dye (rhodamine 6G) laser pulse was obtained by 150 ps argon-ion pulse pumping [176].

Additive-pulse mode-locking (APM) or coupled-cavity mode-locking

Additive-pulse modelocking sometimes is also called coupled cavity mode locking. In APM two laser cavities with the same round trip time are coupled together. One is a regular laser cavity and the other is a resonator with single mode fiber inside. The cavities are coupled together with a semi-transparent dielectric mirror. Saturable absorber behavior is obtained by exploiting the nonlinear phase shifts in the fiber. Two pulse packets circulate in the two cavities and build constructive interference near the peak of the pulses and deconstructive inference in the wings of the pulses [177]. This technique can work at different wavelengths and generates extremely short pulses without any other special tools employed. However a critical resonator length adjustment is necessary and interferometric cavity-length stabilization is also required, so its suitability for industrial applications is limited [178].

6 Experiment Design and Result

In the present chapter various configurations of CW and modelocked Yb:CaF₂ laser cavities that were studied will be outlined. These include:

- Pump design and CW operation performance
- Passive mode-locking with SESAM
- KLM experiment with ZnS and SF57

CW performance is considerably affected by cavity stability and pump focusing spot size. For the SESAM ML, laser performance is mainly limited by saturable absorber characteristic. For the KLM laser with a highly nonlinear medium, the laser characteristics are principally determined by the gain medium gain saturation energy, Kerr medium properties and cavity geometric design.

6.1 Oscillator pump design and CW performance

For oscillator CW mode operation, a high power transfer efficiency, low pump threshold and circular TEM₀₀ beam mode is desirable. One of the main consideration is the volume overlap between the pump and laser mode as well as the Yb:CaF₂ active gain volume. Tight pump focusing can be easily achieved with diffraction-limited pump lasers such as Argon-ion lasers (514 nm) and frequency-doubled Nd:YAG lasers (532 nm) laser used to pump Ti:sapphire lasers. However the cost of a separate single mode pump source is quite high. Multiple-mode diode lasers offer a less expensive

alternative which could effectively reduce system cost. Two pump laser diodes (LD) were used in our experiments and their characteristic are listed in Table 6-1:

Table 6-1 Pump laser diode specification [182] [183]

	LIMO 32-F200-DL980-LM	Lumics LU0975T090
Output power CW (Maximum)	32 W	9 W
Center wavelength	980 ± 10 nm	975 ± 10 nm
Spectral width (FWHM)	4 nm	6 nm
Fiber core radius	100 μ m	52.5 μ m
Numerical aperture	0.22	0.22

The LIMO LD is a complete system while the Lumics LD is an OEM diode so a homemade power supply and a heat control system were built for pump operation.

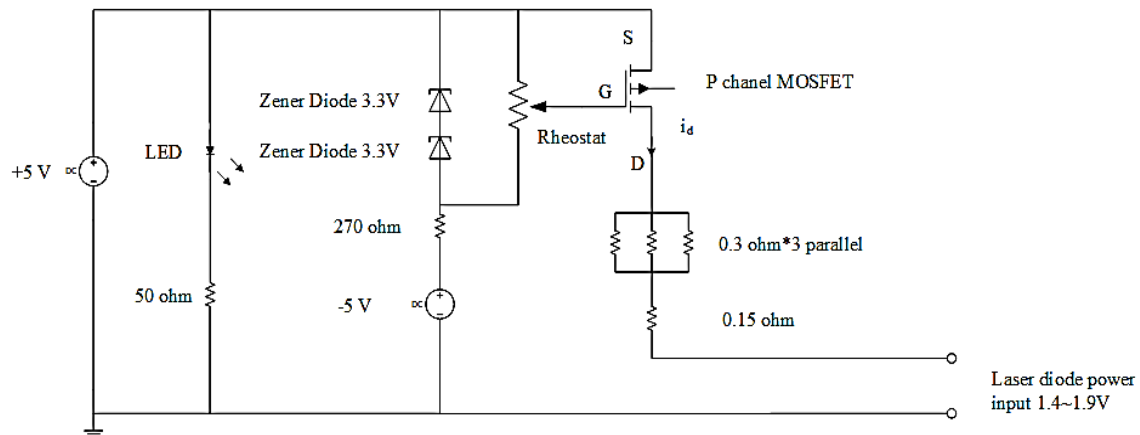


Figure 6-1 LU0975 diode drive diagram

As shown in Figure 6-1, the diode laser output power was controlled by a P-channel power MOSFET delivering drain current i_d to the laser diode. To prevent laser diode burn-out, the MOSFET V_{GS} is controlled by two 3.3 V Zener diodes and a rheostat. The MOSFET V_{DS} is controlled by attaching to a resistive divider (three parallel 0.3 ohm resistors serially connected with one 0.15 ohm resistor) and the DC power input to the diode. The MOSFET output characteristics and operating region in our experiment are shown in Fig. 6-2.

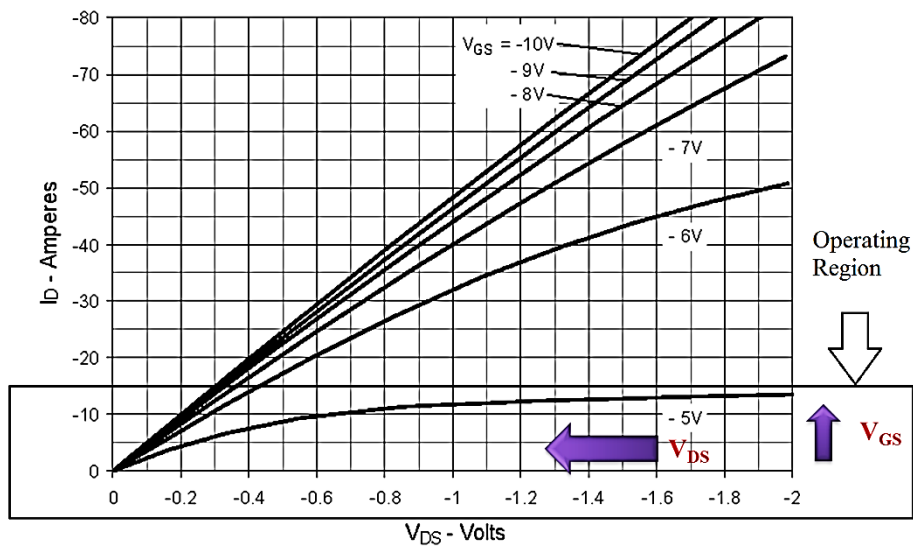


Figure 6-2 MOSFET output characteristics and diode current protect diagram

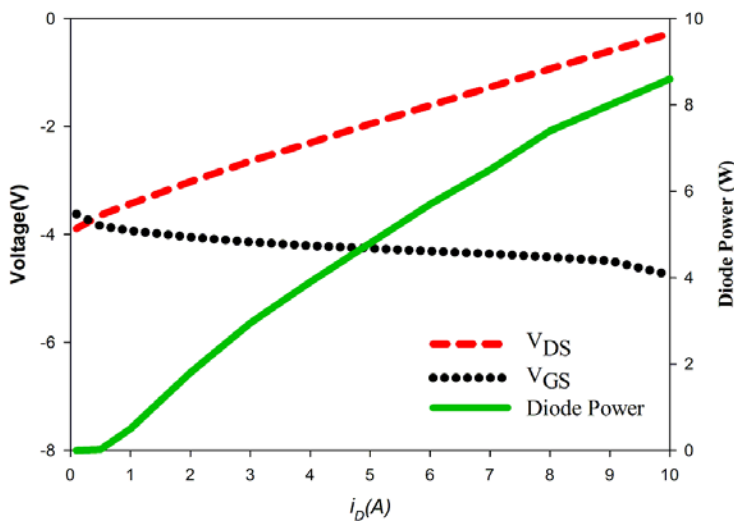


Figure 6-3 Luminous diode output power versus operating current

In our experiment, we varied the V_{GS} from -3.62 V to -4.75 V by changing rheostat resistance, then the V_{DS} is changed from -3.89 V to -0.28 V. As a result, the diode drive voltage and current range is 1.4 V to 1.9 V and 0 to 10 A respectively to prevent the diode from burn-out. The Lumic diode laser output power is adjustable from 0 W to 8.6 W as shown in Fig.6-3.

The LIMO diode output power versus operating current, the pump power transmission and absorption through a 2 at.% Yb doping, 5mm thickness crystal at Brewster angle where the pathlength is 6.07 mm are shown in Fig 6-4. The measurements were made for a Yb:CaF₂ crystal without lasing. The absorption fraction dropped from ~70% at 0.48 W incident power to ~55% at 18 W pump power.

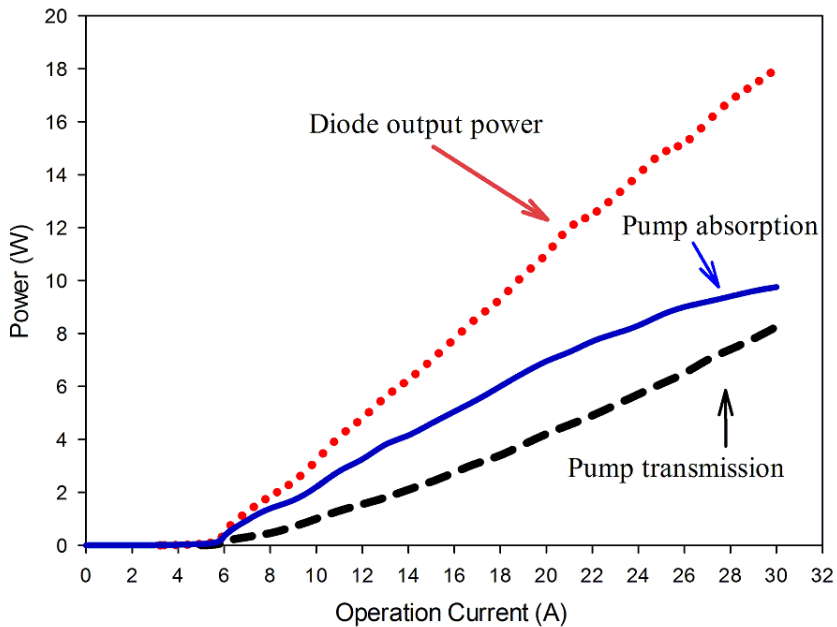


Figure 6-4 LIMO Diode performance and Yb:CaF₂ absorption without lasing

Both diodes output profiles are flat-top and two Thorlabs NIR achromatic doublet pairs (MAP105050-B, MAP104040-B) were used to pump the Yb:CaF₂ crystal. Due to quasi-three level system properties, a relatively high pumping intensity threshold is

required to achieve lasing. Mode matching is more challenging when using the LIMO diode system since the fiber radius is 100 μm and thus the pump optical intensity is lower compared to the Lumic diode for the same driving current. We utilized a z-shape cavity to test laser CW performance as shown in Fig. 6-5.

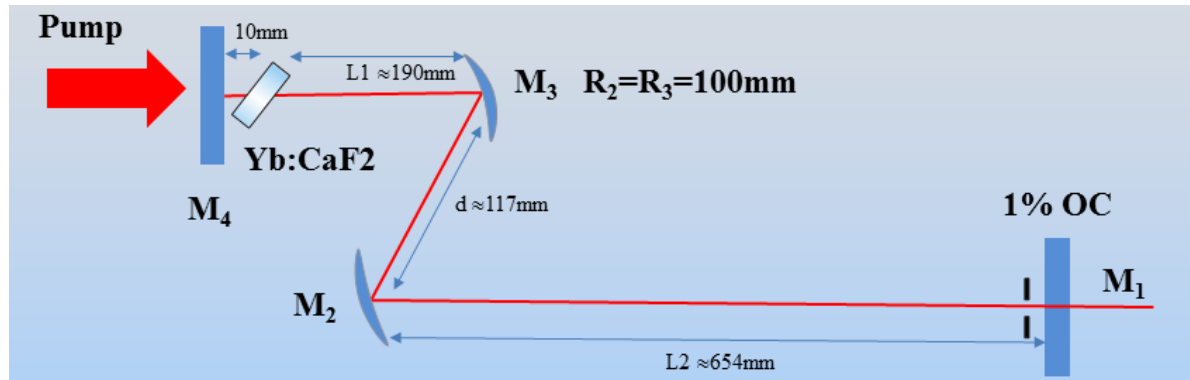


Figure 6-5 Yb:CaF₂ CW cavity configuration

With 1:1 pump imaging and using the Lumics diode (52.5 μm radius) as the pump diode, the output power is 900 mW at 8.4 W pump power. The optical-to-optical conversion efficiency is 10.7%. The CW experiment with LIMO diode (100 μm radius) was more tricky than expected. After several attempts of careful cavity alignment, the first CW lasing result with 1:1 pump imaging was only 400 mW output power at 18 W pump power with 2.2% optical efficiency. In addition, TEM₁₀, TEM₂₀ and higher order modes were generated during the experiment. In order to improve CW performance and improve TEM₀₀ operation performance, one approach is to use a pinhole aperture to introduce extra loss for higher modes. The other approach is to create a tighter pump focusing inside the gain medium thus favoring the fundamental mode with smaller spatial distribution will experience higher gain than higher modes.

The latter method would also improve the pump intensity which is the main reason for insufficient transfer efficiency. The pump imaging lens combination was adjusted to change the image ratio from 1:1 to 1: 0.8. As a result a tighter focal spot inside the Yb:CaF₂ was created and the pump intensity was increased. After this improvement, the CW output power was improved to 1.1 W at 9.1 W pump with ~12% optical-to-optical coupling efficiency. If we consider ~60% pump power absorptivity, about 20% of the optical pump power is transferred to laser power. This ratio is still low compared with theory. This can be explained by the following two reasons.

The first reason is that no active cooling was applied to the gain medium during pumping progress. The pump power causes a large thermal population in the higher Stark levels of the ground state manifold, which serves as the lower laser levels. Although an improved laser performance is expected if active cooling is applied, the chiller motor vibrations propagating through the cooling tubes led to some unwanted instabilities in the laser operation. As an interim measure, we placed the Yb:CaF₂ crystal on a 50 mm×50 mm×13 mm copper plate and used surrounding ambient air to dissipate the heat. Therefore the pump intensity required to reach laser threshold was significantly increased and the efficiency was degraded as well.

The second reason is the extra loss introduced by part of the Yb:CaF₂ crystal which was weakly pumped. At room temperature the lower lasing level of quasi-three-level system is thermally populated and absorbs the optical energy at the lasing wavelength.

In a longitudinally pumped configuration, the pump laser diode beam which is a combination of higher order modes diverges faster than laser beam (shown in Figure 6-6) and the pump power is usually absorbed in a short distance (shown in Figure 6-7) the portions of the laser medium that are not pumped strongly enough to provide gain would introduce loss for the oscillating beam.

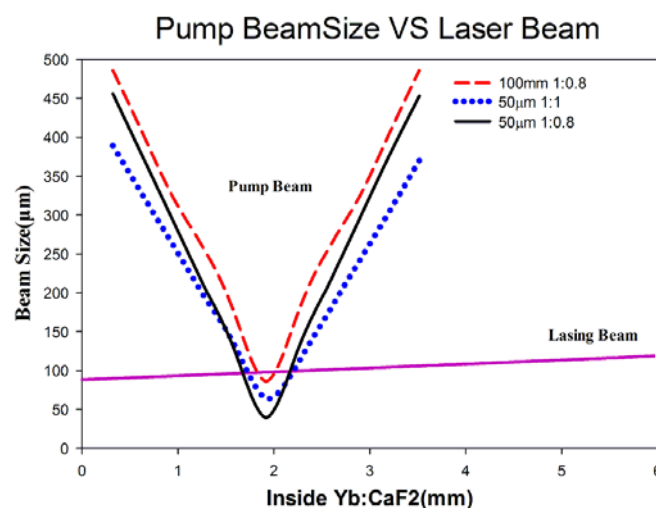


Figure 6-6 Pump and lasing beam divergence

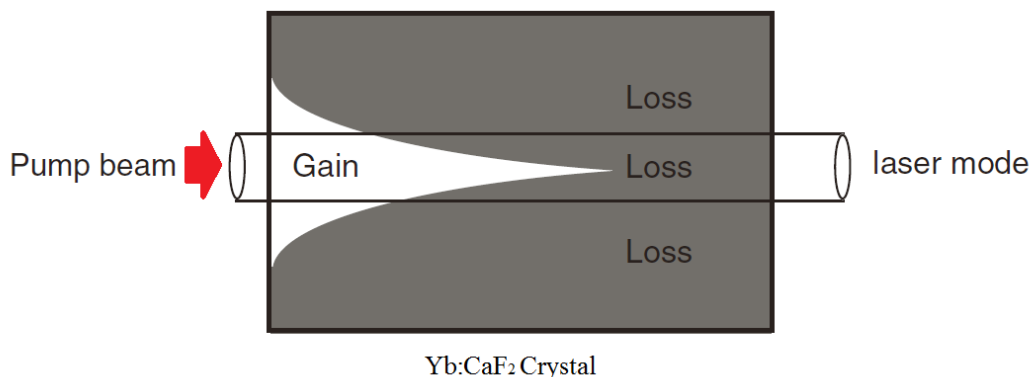


Figure 6-7 Pump absorption in Yb:CaF₂ crystal

An optimum power transfer efficiency is obtained if the residual pump intensity at the end of Yb:CaF₂ is exactly equal to the transparency intensity $I_{\text{transp}}(\lambda_l, \lambda_p)$ [184].

$$I_{\text{transp}}(\lambda_l, \lambda_p) = \frac{hc}{\lambda_p \left[\sigma_{\text{abs}}(\lambda_p) \times \frac{\sigma_{\text{em}}(\lambda_l)}{\sigma_{\text{abs}}(\lambda_l)} - \sigma_{\text{em}}(\lambda_p) \right] \tau} \quad 6.1$$

For Yb: CaF₂ crystal as used in this thesis, at room temperature the transition cross sections are given by [184]:

At $\lambda_l=1053$ nm, $\sigma_{\text{em}}(\lambda_l)=1.6\times10^{-21}$ cm² and $\sigma_{\text{abs}}(\lambda_l)=0.029\times10^{-21}$ cm²

At $\lambda_p=979.6$ nm, $\sigma_{\text{abs}}(\lambda_p)=5.4\times10^{-21}$ cm² and $\sigma_{\text{em}}(\lambda_p)=4.8\times10^{-21}$ cm²

The photon energy hc/λ_p at 979.6 nm is 2.03×10^{-19} joules and upper level life time τ is 2.4 ms, so $I_{\text{transp}}(\lambda_l, \lambda_p) \approx 288 \text{ W/cm}^2 = 2.88 \text{ W/mm}^2$

The coupled delivery fiber numerical aperture is 0.22 and focal spot is ~ 1 mm inside the first surface of the 5 mm Yb:CaF₂ crystal (6.07 mm pathlength in Brewster angle).

So at the exit the pump spot size is ~ 1.1 mm and the area is $A=\sim 3.8 \text{ mm}^2$. Assuming $\eta=\sim 45\%$ total pump power remains at the pump beam exit, so the optimal pump power P_{opt} can be expressed by

$$P_{\text{opt}} = \frac{I_{\text{transp}}(\lambda_l, \lambda_p) \cdot A}{\eta} \quad 6.2$$

So the optimal pump power is around 24 W

As no active cooling system was used, to avoid extensive heat accumulation inside the crystal and keep the thermal lens effect in a reasonable range, the pump was usually limited to 10 W. As a result the laser efficiency was further reduced. However on the other hand, this tapered gain regions could work like an aperture for the intra-cavity laser mode, so that the beam quality could be improved. In addition, due to this soft

aperture effect ML pulses may experience higher gain/less loss than CW which is preferred for ML operation. This aperture effect strength could be controlled by changing Yb concentration and reducing Yb:CaF₂ crystal length. Pumping efficiency can be significantly improved by using a single mode pumping source which would provide a much longer confocal parameter and tighter focusing than a flat-top diode. However such a high power single mode pump source is much more expensive and the system cost would be greatly increased.

Another important factor in the cavity design is to choose an optimum output coupler transmission. If the other laser resonator parasitic losses overwhelm the losses introduced by the output coupler, a low output coupler transmission would lead to a poor laser efficiency. However it will reduce the threshold pump power. In general the output coupler transmission value is often chosen to maximize the output power. In our experiment high output power was not our first priority. In order to maximize the intracavity optical intensities and suppress ML Q-switching instabilities, we used a 1% output coupler throughout all the experiments.

6.2 Passive mode-locking with SESAM

As introduced in Chapter 5, KLM lasers usually operate very close the cavity stability limit. In general the cavity is not optimized for best optical-optical efficiency and highest output power. This introduces some difficulties in cavity setup and alignment. The problem then becomes more severe at high power operation due to the changing

thermal lensing conditions. Alternatively, SESAM modelocked lasers have the same cavity stability range as CW lasers; they do not need critical cavity alignment and are a very attractive approach, as shown in Fig. 6-8.

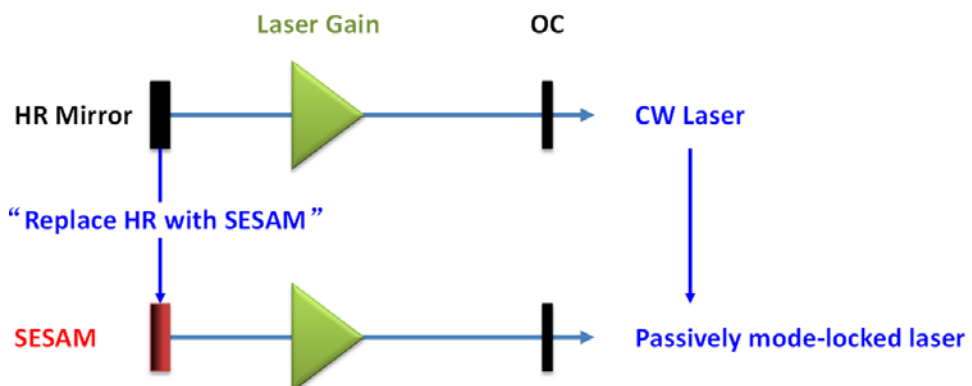


Figure 6-8 SESAM modelocking theoretical design

The SESAM utilized in the experiment is SAM-1040-1.5-25.4S-1ps from BATOP optoelectronics and its specifications are given in Table 6-2:

Table 6-2 SESAM specifications [185]

High reflection band ($R > 98\%$)	$\lambda = 990 \text{ nm to } 1050 \text{ nm}$
Small signal saturable absorption A_0	1.5%
Non-saturable loss A_{ns}	0.7%
Modulation depth ΔR	0.8%
Saturation fluence Φ_{sat}	$\sim 70 \mu\text{J/cm}^2$
Relaxation time constant	$\sim 1 \text{ ps.}$

Damage threshold 0.8 GW/cm^2

Chip area $4 \text{ mm} \times 4 \text{ mm}$

Chirp thickness $400 \mu\text{m}$

The experimental layout is shown by Fig.6-9, a Lumic diode was used as the pump diode and 1:1 pump image ratio was employed.

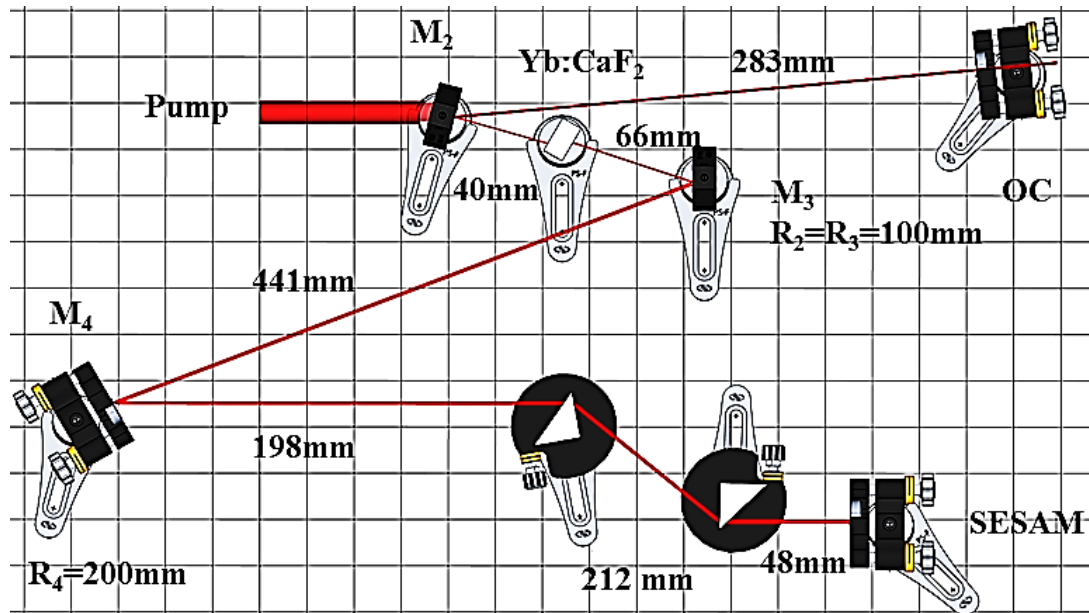


Figure 6-9 SESAM modelocking cavity design

An SF10 prism pair is used for GVD compensation, the cavity length is $\sim 1244 \text{ mm}$ corresponding to $\sim 8 \text{ ns}$ cavity round trip time. At 8 W pump, the laser output power was 1.1 W in CW mode (without the prism pair and SESAM) and 480 mW in ML mode (with the prism pair and SESAM). The resonator worked in Q-switched modelocking (QML) mode as shown in Fig. 6-10. The Q-switching pulse duration is about 2 μs and repetition frequency is around 2.3 kHz.

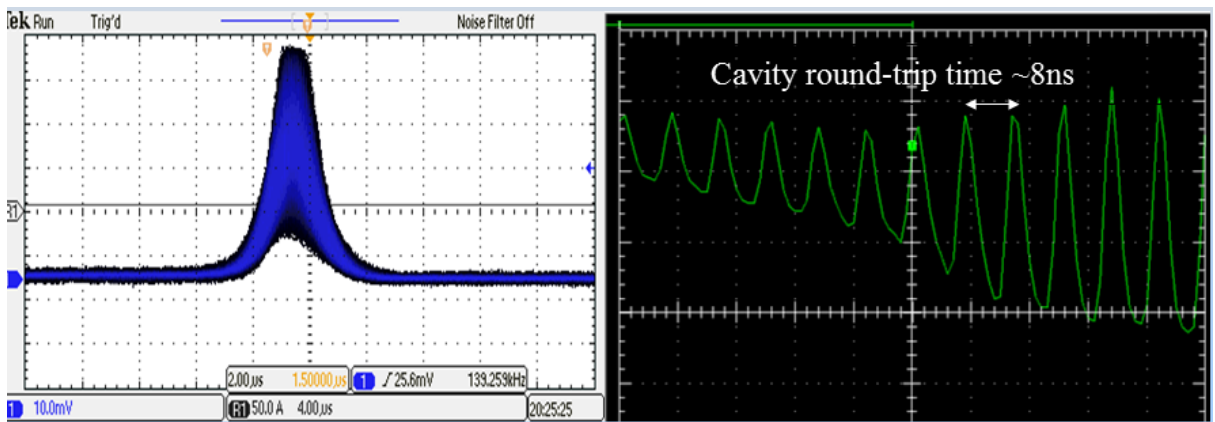


Figure 6-10 SESAM QML operations

This QML operation was unstable and power began dropping after 1-2 minutes. Burn spots were seen on the SESAM surface due to high intracavity power. The damaged SESAM then prevented QML and CW operation. Under the microscope, we found that the SESAM was badly burned and cracked as shown in Fig 6-11. The burn spot diameters were around 10-20 μm , and SESAM plate was cracked by the mechanical stress induced by the thermal loads.

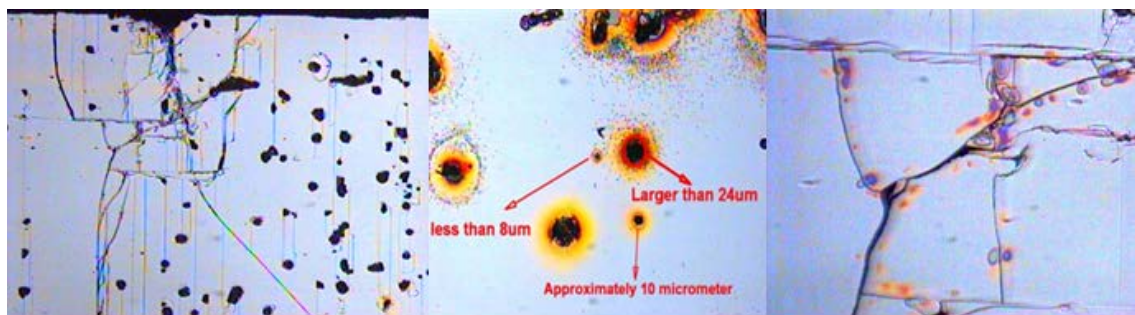


Figure 6-11 SESAM burn spot and surface crack

The very long metastable $^2F_{5/2}$ lifetime (2.4ms) make stabilized CW modelocking operation difficult to obtain for Yb:CaF₂ and its relatively small emission cross

sections lead to a huge gain saturation fluence. Thus energetic pulses beyond the damage threshold of the SESAM were generated during QML [186].

We evaluated our experiment result: as the output power is 480 mW with 1% OC, the intracavity power is 48 W. The cavity round trip time is 8 ns and the single pulse energy is 384 nJ. The mode radius on the SESAM is $\sim 200 \mu\text{m}$, then the area on the SESAM is $1.256 \times 10^{-3} \text{ cm}^2$ and the fluence is $\sim 0.3 \text{ mJ/cm}^2$. With 1 ps pulse duration assumption, the power intensity on SESAM is 0.3 GW/cm^2 which is close to the damage threshold 0.8 GW/cm^2 . All the calculations above are based on CW ML condition. If the system operates in QML then the intensity could be increased by a factor of 100, which is far beyond the damage threshold.

The necessary intracavity power to suppress Q-switching instabilities in picosecond regime is given by [186]:

$$P_{Intra} = \sqrt{F_{sat,L} \cdot A_{eff,L} \cdot F_{sat,A} \cdot A_{eff,A} \cdot \frac{1}{T_R^2} \cdot \Delta R} \quad 6.3$$

Where the gain saturation fluence $F_{sat,L} \approx 116 \text{ J/cm}^2$, the SESAM saturation fluence $F_{sat,A} \approx 70 \mu\text{J/cm}^2$, the effective laser mode area inside the gain medium $A_{eff,L} \approx 3.14 \times 10^{-4} \text{ cm}^2$ (100 μm radius), the effective laser mode area on the SESAM $A_{eff,A} \approx 1.256 \times 10^{-3} \text{ cm}^2$ (200 μm radius), the cavity round trip time $T_R \approx 8 \text{ ns}$ and the modulation depth $\Delta R \approx 0.8\%$. Then the P_{intra} is calculated to be $\sim 633 \text{ W}$ which is

much higher than CW intracavity power 120 W. As a result the resonator operated in QML mode and generated energetic pulses which burned the SESAM.

6.3 KLM experiment with ZnS

Since the Kerr lensing effect in Yb:CaF₂ is weak, it is difficult to obtain KLM behavior in a normal laser cavity. In this case an additional nonlinear element can be added to the cavity to enhance the KLM effect.

6.3.1 High nonlinearity crystal ZnS

KLM laser performance is not limited by the properties of a given SESAM has proven to be a powerful tool for ultrashort laser pulse generation. Unlike Ti:sapphire laser, where the gain medium also acts as the Kerr medium for modelocking, the 3rd order nonlinearity of the Yb: CaF₂ crystal is quite low ($n_2=1.26\times10^{-20}$ m²/W), so a very high intensity is required to generate a strong enough pulse shaping effect for KLM. This is very difficult to achieve with flat-top diode high order mode lasers pumping. In addition, to maintain a tight focusing of the pump over a long distance inside the Yb:CaF₂ crystal is also very challenging.

In order to achieve strong nonlinear pulse shaping strength, a practical approach is to insert an additional highly nonlinear Kerr medium into the cavity to enhance pulse shaping. The Yb:CaF₂ crystal solely acts as the laser gain medium and the high nonlinearity crystal is responsible for gain/loss modulation [187]. The cavity is

designed to minimize thermal lensing and astigmatism effects and maximize the pulse shaping strength for KLM.

Zinc sulfide (ZnS) was our first high nonlinear crystal candidate for a few reasons. First of all, its nonlinearity ($n_2=1.73\times10^{-18} \text{ m}^2/\text{W}$) is among the highest commercially available crystals. Secondly, the ZnS band gap 3.54 eV (cubic, 300 K) is far from Yb: CaF₂ photon energy 1.180 eV (1050 nm) and thus the two-photon absorption probability is quite low during ML operation. Thirdly, the ZnS transmission window in the near infrared regime is quite large. In fact its transmission window covers a large region from UV to FIR as shown in Fig 6-12.

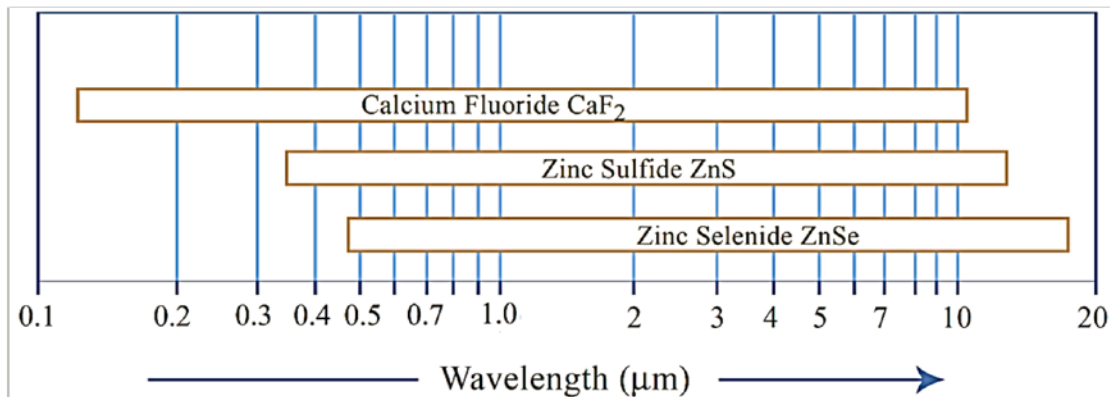


Figure 6-12 ZnS, CaF₂ and ZnSe transmitting windows [188]

The polycrystalline cubic multispectral grade ZnS crystal used in our experiment is from Crystran Ltd. They are manufactured by a hot isostatic pressing (HIP) process.

6.3.2 ZnS KLM Laser cavity design

A few factors are quite important for the KML laser cavity design.

1) Kerr lens strength

Comprehensive modeling of Kerr lens mode locking is difficult due to the complicated spatio-temporal dynamics and beam radius variations during the temporal pulse shaping process. We do not need to know all the laser pulse dynamic details to design our cavity. With the help of nonlinear ABCD matrix models, we can estimate the Kerr lens strength and identify a region of cavity designs favouring KLM operation. In order to obtain optimum mode matching, we chose the Z-shape cavity for our experiment.

The folding mirror incidence angle was adjusted to 8° to compensate astigmatism in the ZnS and Yb:CaF₂ Brewster plates. The cavity parameters were adjusted to generate the maximum pulse shaping strength for hard/soft aperture KLM.

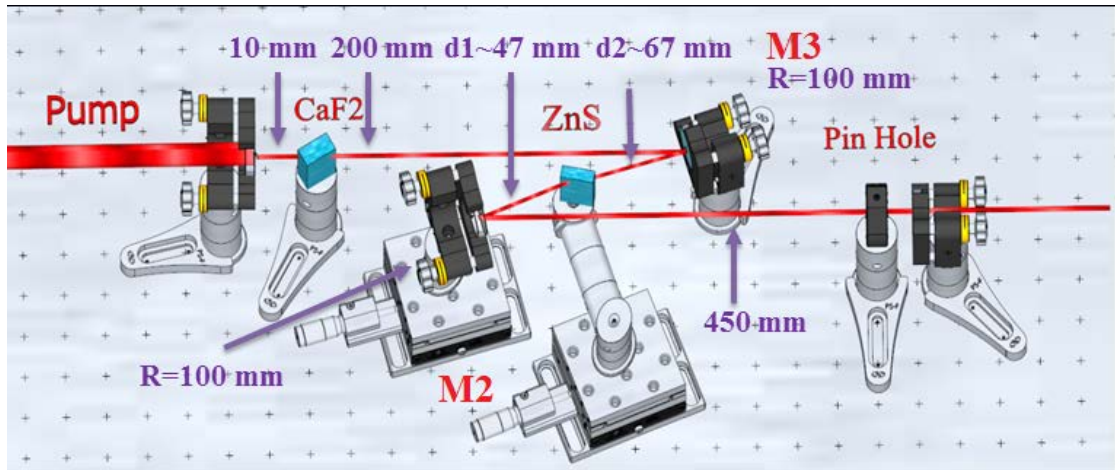


Figure 6-13 ZnS KML cavity

The laser beam size at each position was calculated by the ABCD matrix method, taking into account the Kerr-lens effect and astigmatisms of the folding mirrors and the Brewster plates (5 mm Yb:CaF₂ and 6 mm ZnS). The Kerr lens strength δ variation as defined in equation 5.18 with different cavity distances is shown in Fig. 6-14.

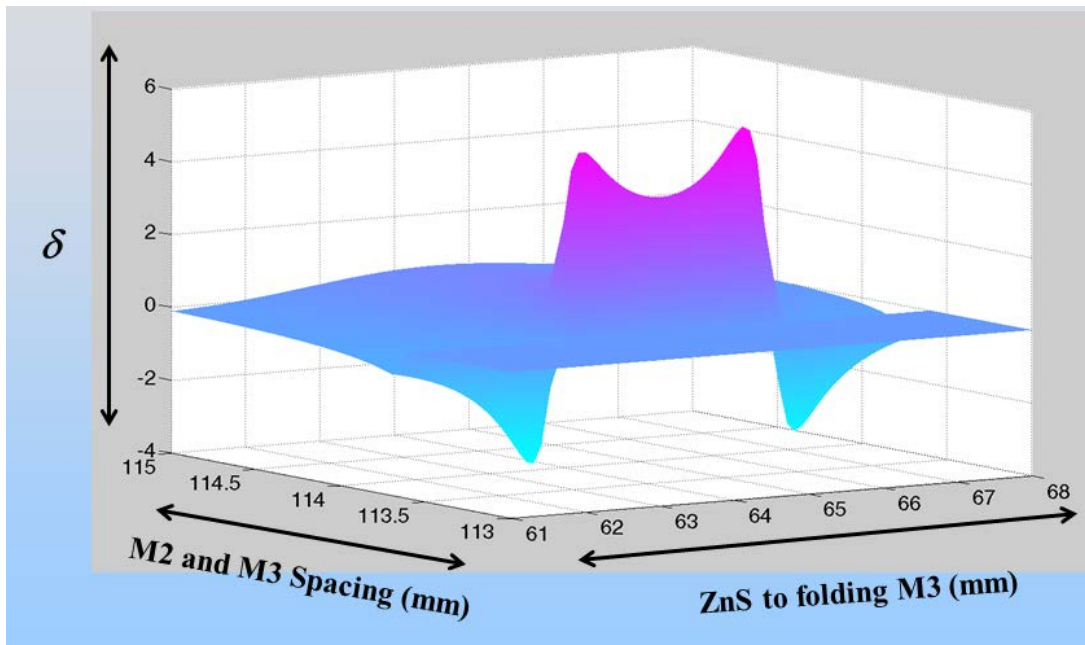


Figure 6-14 Kerr strength variation with cavity design

In order to achieve KML, δ has to be negative and its amplitude should be as large as possible. So the resonator alignment must be very close (~a few hundred micrometers) to the stability limit (~113.5 mm) and satisfying the optimum focusing condition is also necessary. The δ value is strongly dependent on the folding mirror separation (M2 to M3 spacing) and the Kerr element position.

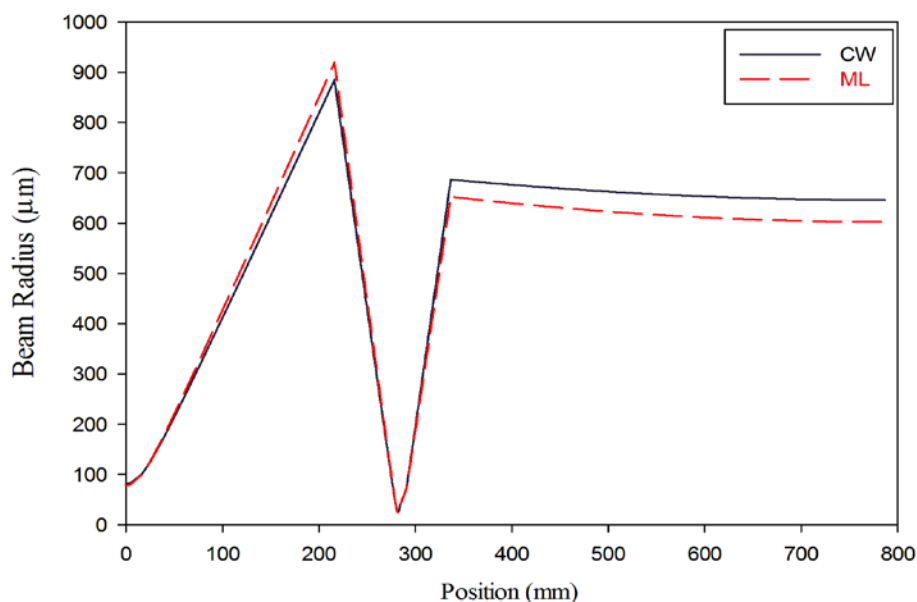


Figure 6-15 Beam radius as a function of position in the cavity

In theory the most suitable approach is to adjust the laser cavity to the stability limit. In reality we must operate some safe distance inside of the stability limit in case of small misalignments, so the parameters were set approximately to $d_1 \approx 47$ mm and $d_2 \approx 67$ mm. The intracavity beam radius for CW and ML mode at $0.6 P_c$ (P_c is ZnS critical self-focusing power) is shown in Fig.6-15.

A ~ 1.5 mm pinhole was placed close to output coupler to enhance KLM, which means the cavity loss must be reduced as the intracavity power was increased. In other words, the beam waist at the OC should be smaller for a higher intracavity power. So we also calculated the laser beam radius variation at the output coupler for different intracavity power to verify this assumption as shown in Fig.6-16.

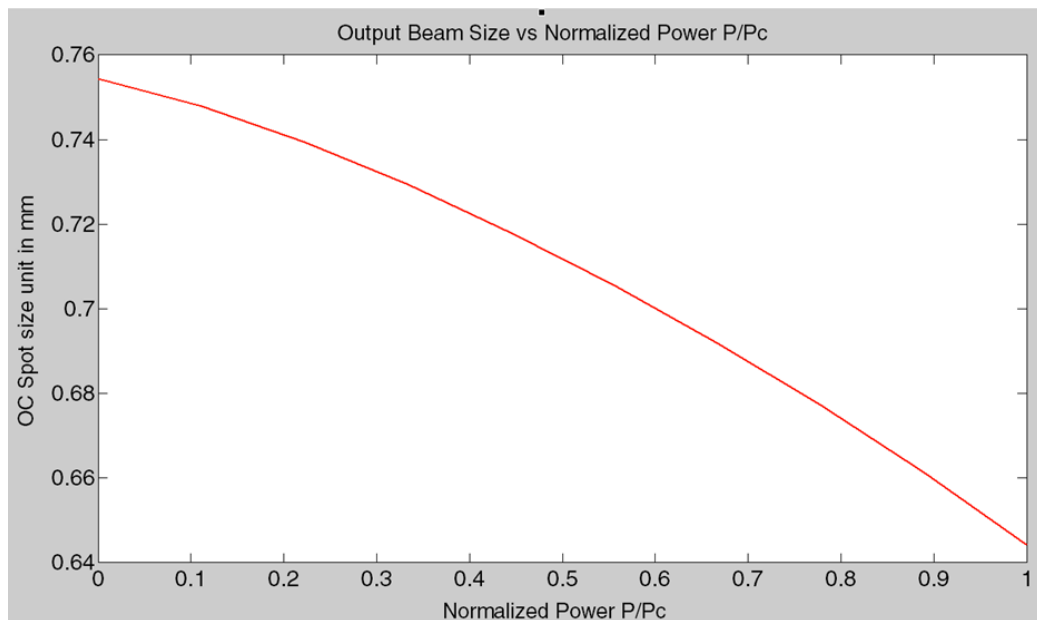


Figure 6-16 OC laser beam radius variation vs intracavity power

2) Thermal lens

As shown in Fig 6-14, Kerr lens strength is very sensitive to cavity alignment. So to optimize laser operation, it is necessary to minimize the effect of unknown cavity parameters. One of the major uncertainties is the exact value of Yb:CaF₂ thermal lens focal length induced by the diode laser pump. This thermal lens is affected by three thermo-optic effects: thermal expansion ($\chi_{\text{dilatation}} -10.4 \times 10^{-6} \text{ K}^{-1}$), refractive index variation ($dn/dT -10.6 \times 10^{-6} \text{ K}^{-1}$) and mechanical stress ($\chi_{\text{stress}} -11.1 \times 10^{-6} \text{ K}^{-1}$). At room temperature, these three effects combination results in a negative thermo-optic coefficient of $-11.3 \times 10^{-6} \text{ K}^{-1}$, whereas for YAG it is positive $\sim 8.9 \times 10^{-6} \text{ K}^{-1}$ [189].

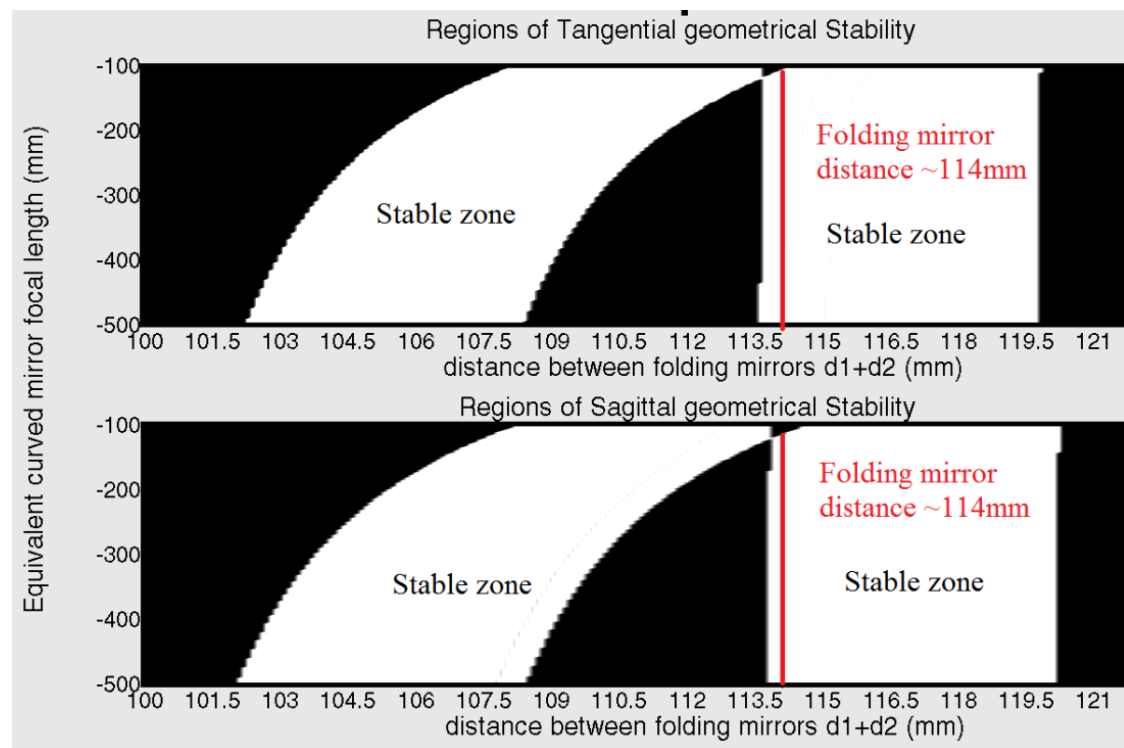


Figure 6-17 Regions of geometrical stability (in white) for cavity as a function of folding mirrors distance and the equivalent curved mirror focal length

As both tangential and sagittal stabilities are affected by the thermal lens and the exact value is tricky to determine. A practical way to evaluate these effects is to add an

equivalent negative lens at Yb: CaF₂ media location and exam cavity stability over a reasonable focal length range. In Fig 6-17, we calculated the cavity stability as a function of the folding mirrors spacing and the equivalent curved mirror focal length, the stable zones are noted.

The Y axis stands for the equivalent curved mirror (thermal lens) focal length from -100 mm to -500 mm. The X axis stands for the distance between two folding mirrors M2 and M3. One can see that for the folding mirror distance of 114 mm, the cavity remains stable for thermal lensing focal length of down to -150 mm. In chapter 7 we show that this thermal focal length is estimated to be around -418 mm [190]. In low power cases, the laser beam radius and curvature are weakly dependent on thermal effects. Further calculations also show that δ is also weakly depended on thermal effects if the laser operates in KLM mode. The thermal lens effect can thus be considered smaller than induced Kerr-lens effect in our experiment.

3) Thermal stress consideration

Another important thermal property is the thermal shock parameter. Yb:CaF₂ is fairly fragile and sensitive to thermal shocks (7 times lower threshold than YAG), so to avoid cracking the crystal by thermal stress the pump power should be changed slowly especially during high power operation [191][192].

6.3.3 ZnS KLM experiment results

At the beginning, the cavity was aligned for maximum output power and then after slight adjustment of the spherical mirrors and the ZnS position, we observed a mode beating effect as shown in Fig. 6-18. The pulses are separated by \sim 1.8 ns, which corresponds to round trip time from ZnS to the nearest end mirror.

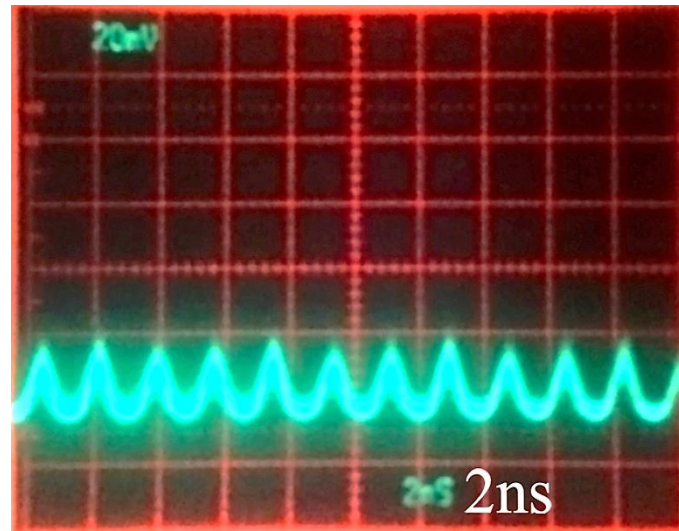


Figure 6-18 ZnS KLM mode beating

After adjusting the cavity parameters to maximize the mode beating effect, a mode locking operation starts spontaneously as shown in Fig.6-19.

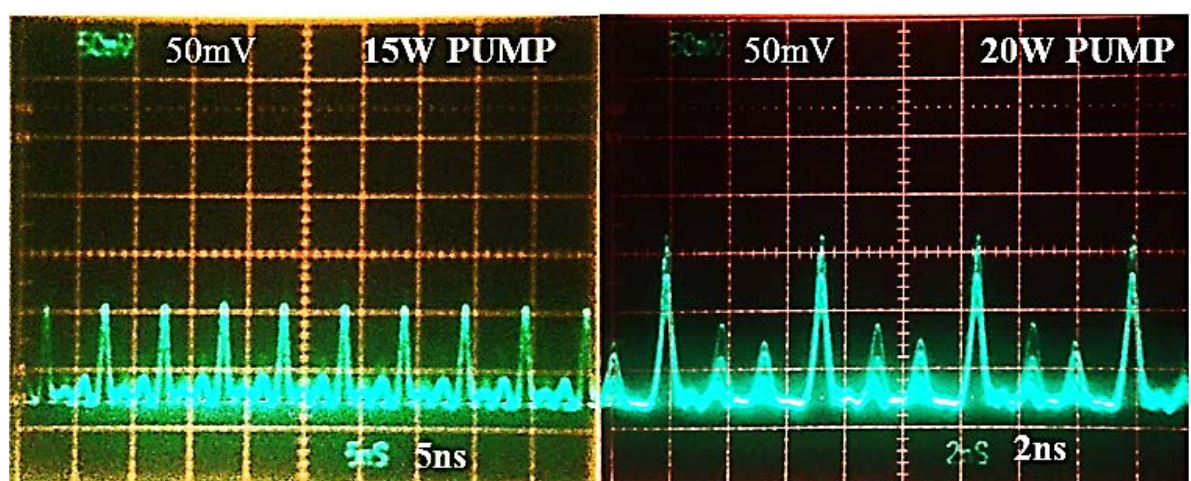


Figure 6-19 ZnS multiple-pulse KLM operation

The main peaks are separated by 5.3 ns which agrees with cavity round trip time (~790 mm, 5.26 ns). Increase the pump from 15 W to 20 W, two satellite pulses become noticeable and the oscillator operated in a multiple-pulse modelocking mode. It also indicates that ZnS acts as a self-amplitude modulator (SAM) providing strong enough pulse shaping ability to support multi-pulse mode-locking operation. However, the 6mm thick ZnS introduce a very large loss and the output is around only 160 mW at 20 W pump.

The ML pules are modulated by a ~13.3 kHz QS envelope. The QS frequency kept shifting over a small range which indicates that laser cavity gain/loss was varying with time. The cavity unstable properties limited the stable CW modelocking operation

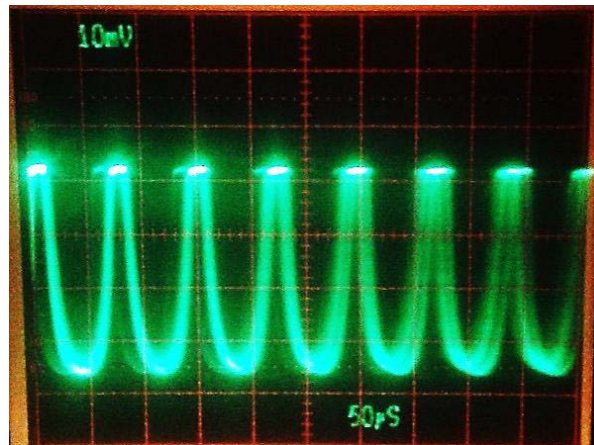


Figure 6-20 ZnS KLM Q-switching envelope

The output wavelength was centered at 1054.5 nm with ~3.3 nm spectral width as shown in Fig. 6-21. And green radiation (528.5 nm) also was observed emanating from the ZnS crystal in all configurations, which is the result of ZnS surface sum frequency generation (SFG). Spectrum measurement result also supports this

assumption. Similar to the results of Bohn et al. [193] for a Ti:Sapphire laser, the SFG radiation is brightest in QS operation, bright in pure ML operation and lowest in CW operation.

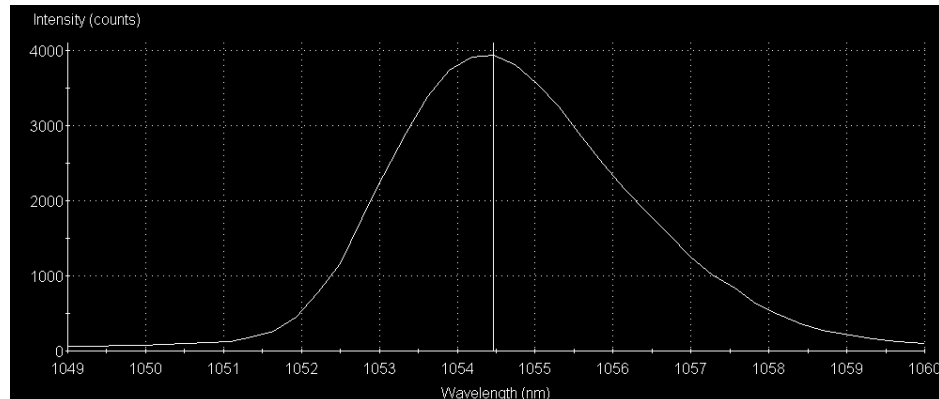


Figure 6-21 ZnS KLM spectrum

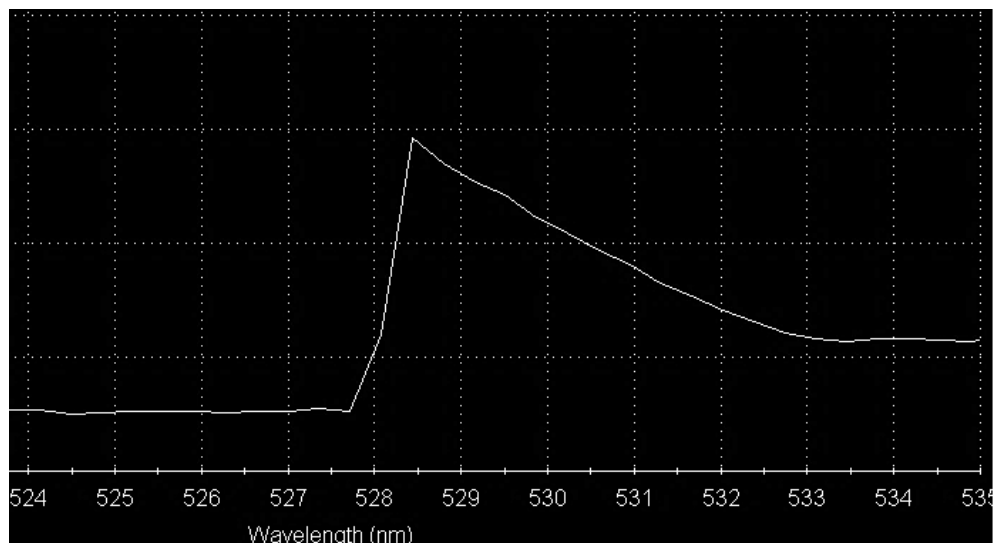


Figure 6-22 ZnS surface frequency generation

6.4 KLM experiment with 10mm SF57 nonlinear glass

6.4.1 High nonlinearity glass SF57

SF57 is a typical metal-doped silicate glasses made up of component (wt.%) 74.2% PbO and 23-26% SiO₂. In general SF57 glasses are centro-symmetric, therefore the second order nonlinear susceptibility ($\chi^{(2)}$) is zero. The third order nonlinear susceptibility ($\chi^{(3)}$) is homogeneous and wavelength independent. SF57 nonlinear refractive index is 0.96×10^{-12} esu or $4.44 \times 10^{-19} \text{ m}^2/\text{W}$ in SI units, which is the highest among commercially available lead silicate glasses [194]. They possess promising mechanical and thermal stability, and exhibit the low attenuation values between 1000 nm and 1300 nm ($\sim 0.3 \text{ dB/m}$) [195].

6.4.2 SF57 Z-cavity KLM design and result

Similar to the ZnS KLM experiment, we also used the Z-cavity for the SF57 KLM experiment as shown in Fig 6-23.

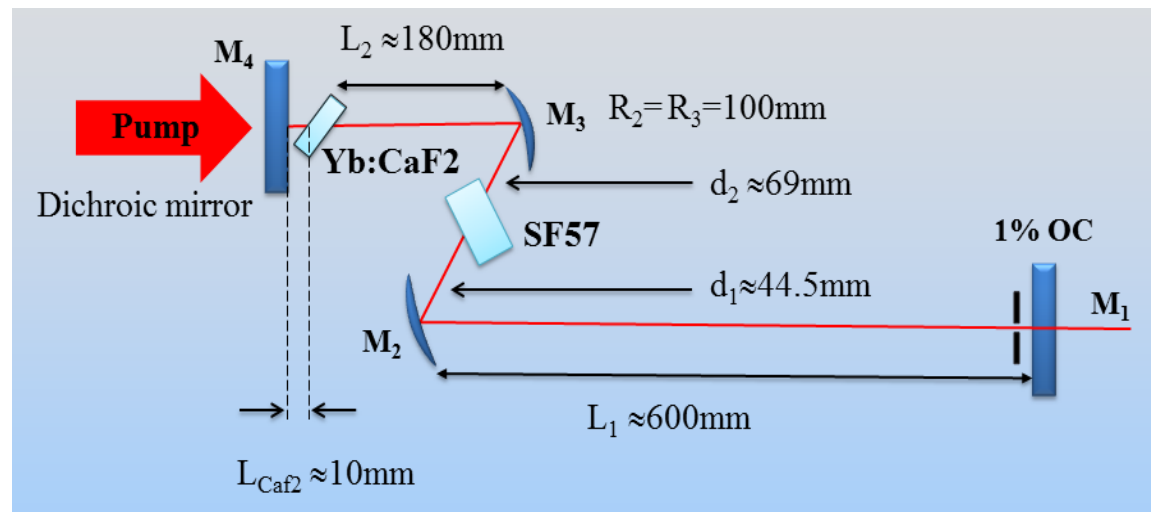


Figure 6-23 SF57 KLM cavity design

The folding mirror incidence angle is adjusted to 10.4 degree to compensate the astigmatism induced by the 10 mm SF57 plate and 5 mm CaF₂. All the other devices

are exactly the same as for the ZnS KLM experiment. In order to achieve maximum Kerr lens strength, the distance d_1+d_2 was adjusted to ~ 113.5 mm and d_2 is ~ 69 mm as shown in Fig.6-23. An interesting point is, as long as we keep d_1+d_2 constant, two strong Kerr lens zones can be reached by varying the SF57 position. The ML operation can be obtained in both these areas, these two ML areas are separated by a zone where modelocking should not occur. Our field experience showed that laser performance was slightly improved if d_2 was chosen close to 69 mm.

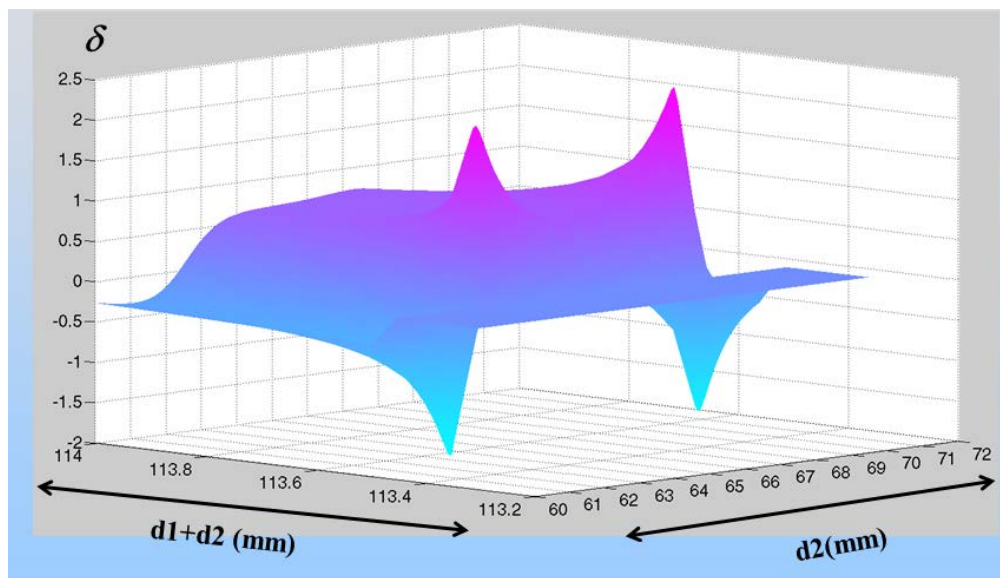


Figure 6-24 SF57 Kerr lens strength vs cavity design

Again, we also verified that cavity stability availability was acceptable with different thermal lens as shown in Fig 6-25. If we set $d_1+d_2=113.5$ mm, the resonator remained stable until the induced thermal lens focal length was shorter than 220 mm. So during the actual experiment we reserved a small safe distance (~ 0.5 mm) to keep the cavity

within the stable region. After cavity optimization, a stable 3 pulse per round trip Kerr lens modelocking operation was obtained as shown in Fig.6-26.

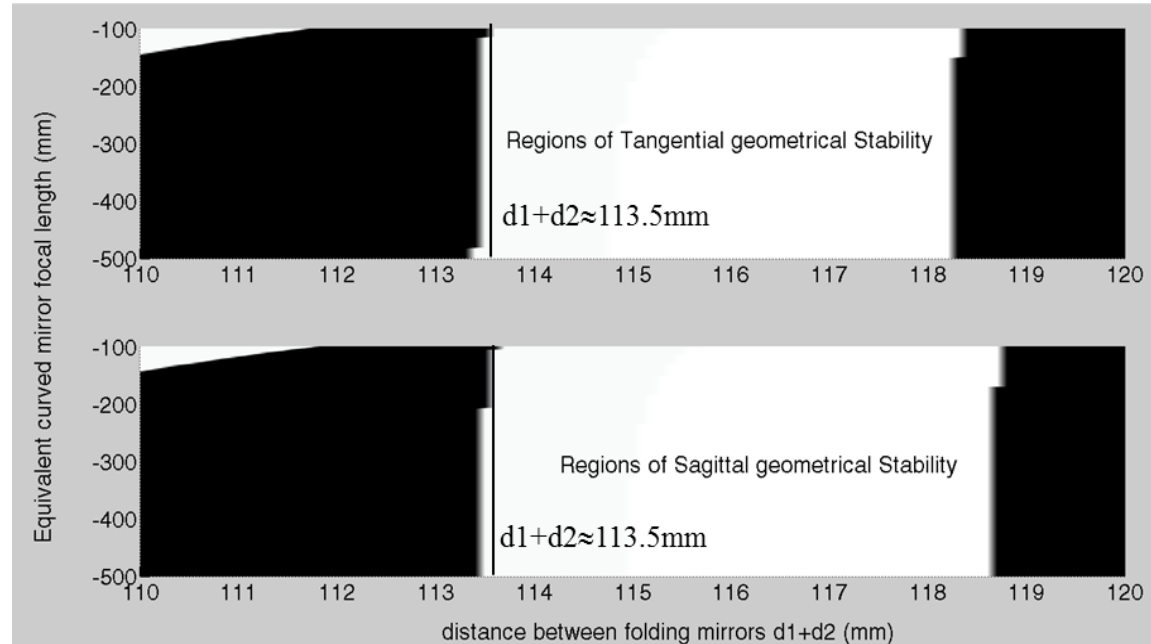


Figure 6-25 SF57 KLM laser cavity thermal stability

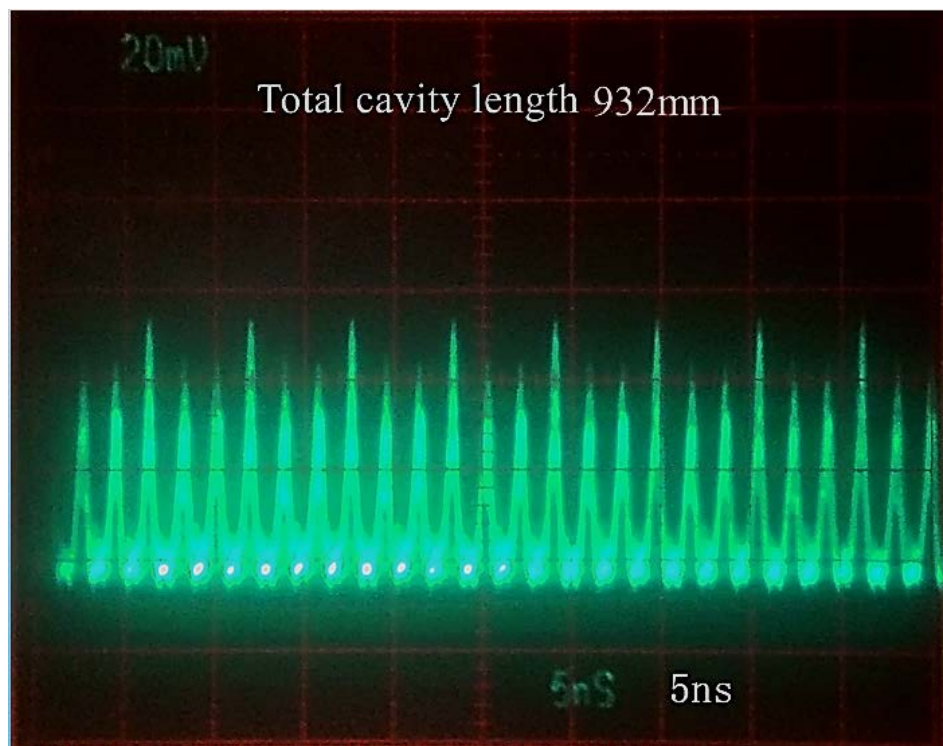


Figure 6-26 SF57 3-pulse per round trip KLM

The output is ~800 mW at ~10 W pump. The power transfer efficiency is much higher than ZnS. Due to SF57 symmetric structure, the second order nonlinear effect does not exist during ML operation and there was no other wavelength radiation generated from nonlinear SFG. The major peaks are separated by ~6 ns corresponds to the total cavity length ~932 mm. The ML pulse spectrum was centered at ~1053 nm with ~1.7 nm width. If we assume the beam is a transform limited Sech²-shape then the pulse duration would be ~700 fs.

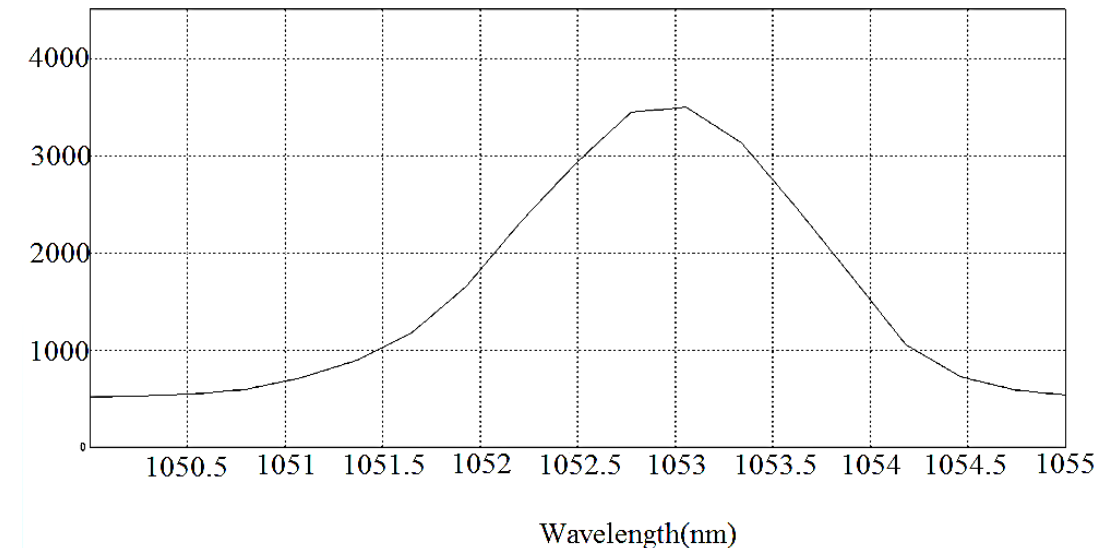


Figure 6-27 SF57 KLM 3-pulse per round trip spectrum

It is almost impossible to achieve sub-picosecond pulses without proper GVD compensation. So we speculate that it may be possible that there are a few ML pulse groups oscillating at different wavelengths around 1053 nm in the overall envelope shown in Fig 6-27. These pulse groups central wavelengths maybe close to each other but may not be coupled with each due to inhomogeneous gain broadening and other effects. So a wider spectrum than that of transform limited pulses could be obtained. It

appears that there are three pulses per round trip because total cavity length is almost 3 times the distance between SF57 and its nearest end mirror. The pulse shaping effect could be enhanced by the cooperation between colliding pulses for all the pulses in one round trip. We will further discuss this result in Chapter 7.

The laser always prefers to oscillate in a multiple ML pulse mode where there are more than one pulse per round trip. Unstable single pulse mode operation could only be reached by spoiling the laser cavity alignment by tuning the dichroic end mirror in vertical direction. As a result the output power was reduced and the beam becomes elliptical. The following experimental result showed that this type multiple-pulse ML laser operation was not quite as sensitive to pumping power as traditional KLM laser. It is probably because the latter part of beam region in the Yb:CaF₂ crystal in our experiment which is weakly pumped gives a pure loss for the oscillating beam . So even if the pump was reduced to the lasing threshold, where we can barely detect CW output by photodiode we can still observe the multiple pulse operation, which indicated that the pulse mode experience more gain than CW.

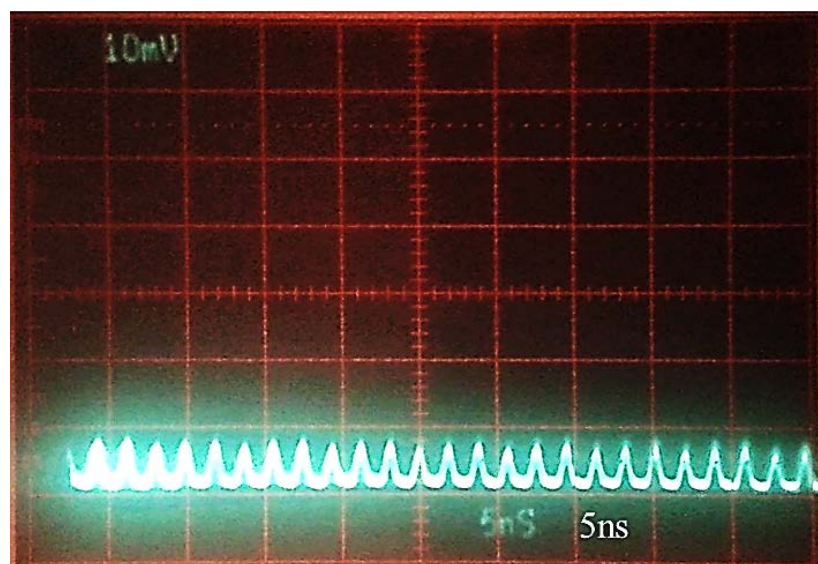


Figure 6-28 Laser performance at threshold

Although the laser cavity is designed for hard aperture KLM, the beam radius difference for CW and ML is maximized at the OC as shown in Fig. 6-31, where the intracavity power is assumed to be 0.6 times of SF57 critical self-focusing power. In fact soft aperture Kerr effect dominates the whole ML process.

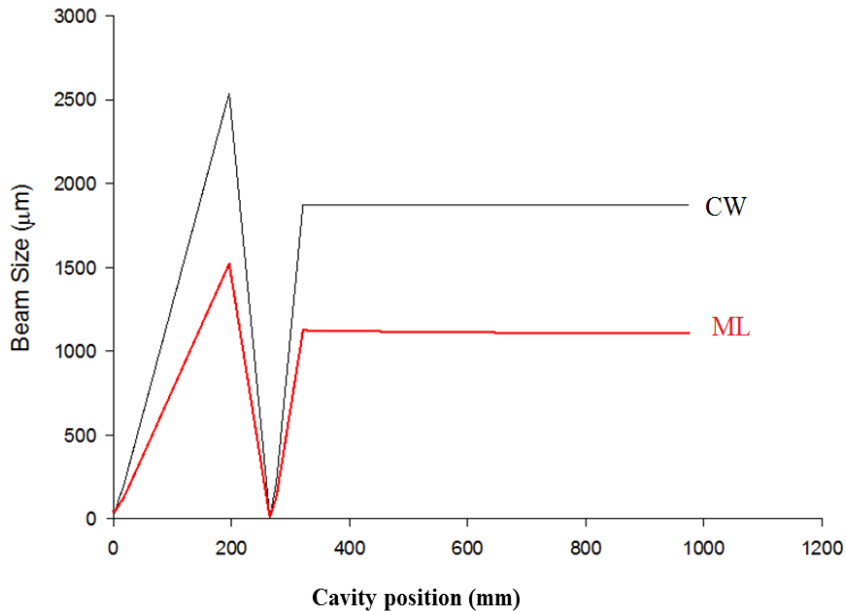


Figure 6-29 SF 57 ML and CW beam radius inside laser cavity

As multiple-pulse ML operation is directly affected by laser gain modulation, we performed a simulation to show how the Kerr lens effect affects the pump and laser mode overlapping as shown in Fig.6-30. The intracavity power is normalized to the SF57 critical self-focusing power. As the intracavity power increases, the beam waist on M4 keeps reducing. However due to the gap (~10 mm) between the Yb:CaF₂ crystal and M4, the beam radius on the Yb:CaF₂ surface closer to M4 reduces at a relatively slower rate and may rise up if the intracavity power is close to 1. As the strongest Kerr lens effect is only obtained near the beam waist, and the pump tight

focusing focal length distance is quite limited, we changed our cavity to a W-shaped semi-symmetric cavity to fully utilize Yb:CaF₂ gain region, and avoid an elliptical mode shape allowing for a stronger pulse shaping effect in the Yb:CaF₂ crystal from the Kerr lensing effect in the SF57 crystal.

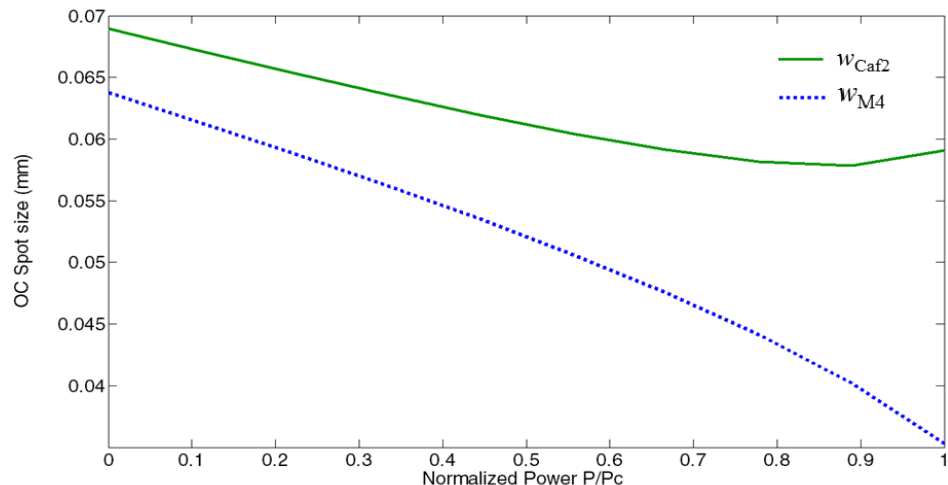


Figure 6-30 M4 and Yb:CaF₂ beam waist change vs intracavity power

6.4.3 SF57 W-cavity KML design and result

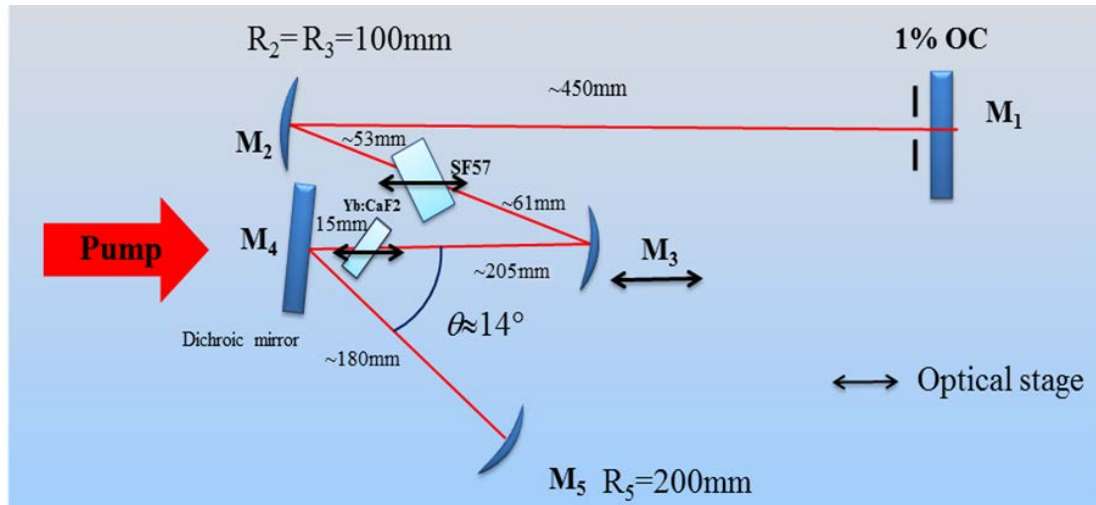


Figure 6-31 SF57 W-cavity KLM

The W-cavity design is shown in Fig. 6-31. The Yb:CaF₂ crystal was placed on an optical stage to find the best position for the soft aperture KLM effect and the dichroic mirror was tilted to fit the geometric requirements. Although the dichroic mirror is designed for normal incidence usage, it still worked well at 14° incidence angle. The ML output was increased to 970 mW at 10 W pump due to more optimized overlap of the laser mode and pump. The efficiency is a slightly lower than CW mode (1 W at 9.1 W pump). After fully optimizing the cavity, a 2-pulse per round trip KLM mode was obtained as shown in Fig. 6-32. To keep a strong Kerr lens effect, the SF57 axial position mis-alignment tolerance is only about 30 μm.

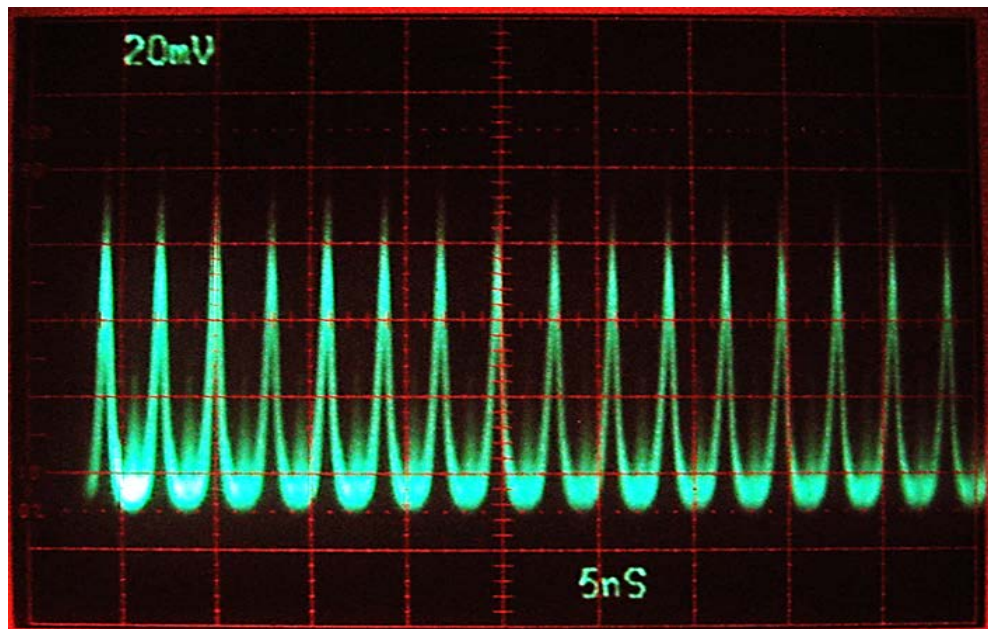


Figure 6-32 SF57 2-pulse per round trip KLM

The output spectrum FWHM is broadened to ~3 nm as shown in Fig 6-33, which would be able to support sub-400 fs transform limited Sech²-shape pulses in theory.

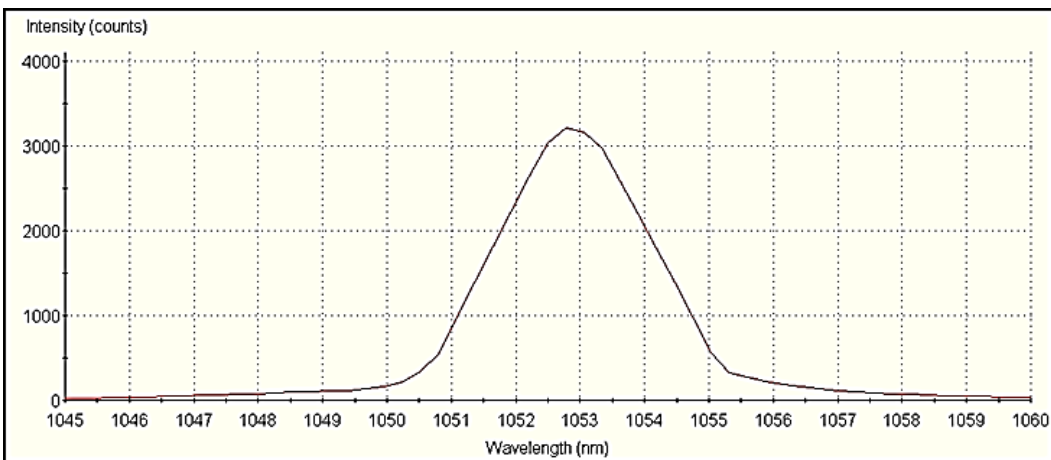


Figure 6-33 SF57 2-pulse KLM spectrum

A second type of multiple pulses operation has been observed during the cavity optimization as shown in Fig 6-36, a single pulse has been split into two twin pulses separated by $\sim 1\text{ns}$, which is very close to photo diode resolution ($\sim 500\text{ ps}$ including the cable and scope influence).

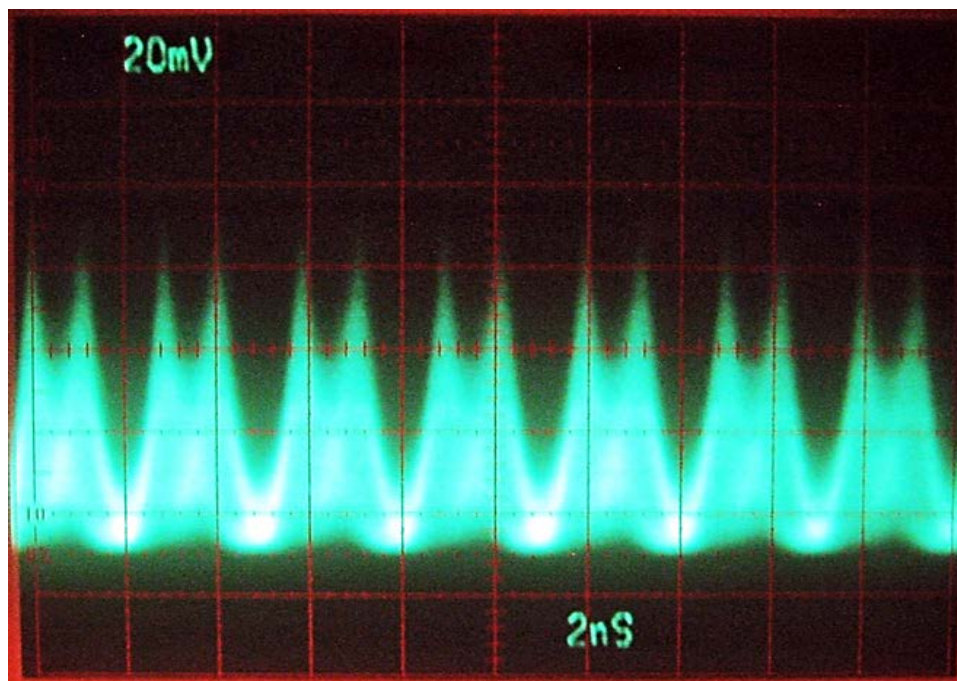


Figure 6-34 SF57 twin pulses KLM operation

Similar result has also been reported in Ti:sapphire laser by M. Lai et al. [196] and they suggested that when intracavity peak power approaches to the Kerr medium critical self-focusing power, the central part of pulse will be focused stronger and then SPM effect is enhanced substantially. Numerical analysis has showed that such enhanced SPM could split an ultrashort pulse in a normal dispersive medium [197] [198].

To further verify this result, shorter pulses with higher peak power to strengthen SPM effect are need. To compensate GVD, we added SF10 prism pair into the laser cavity as shown in Fig.6-35.

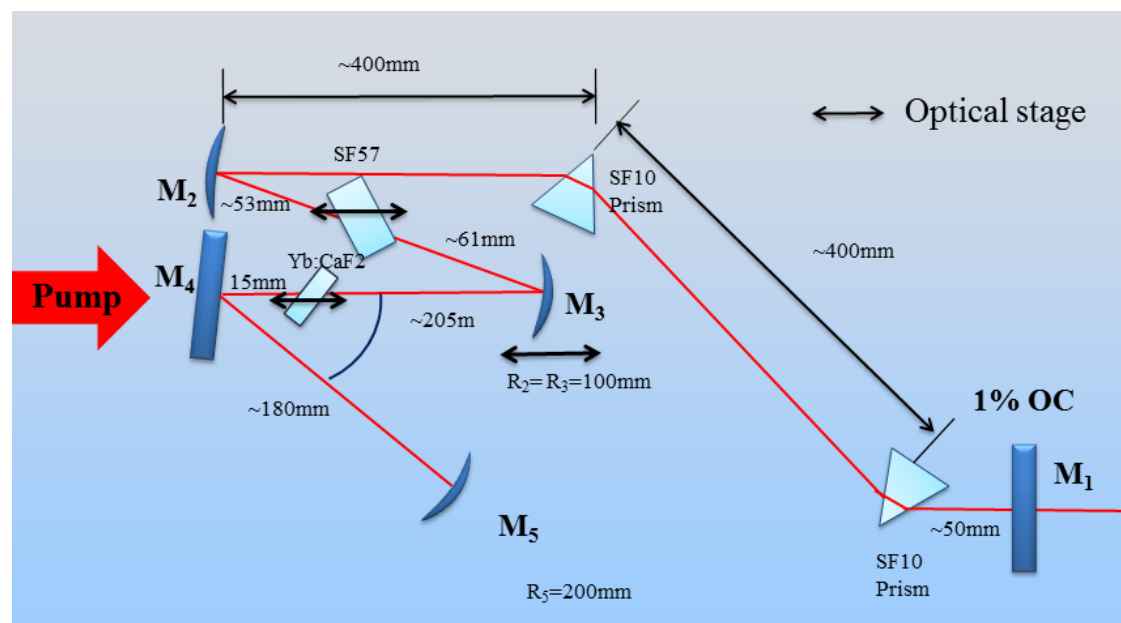


Figure 6-35 SF57 KLM W-cavity with GVD compensation

At the lasing wavelength (1050 nm), the system GDD per single pass is estimated as following:

For the Yb:CaF₂ crystal:

The GVD_{CaF₂}=17.78 fs²/mm, thickness $t=5$ mm and optical length path (at Brewster angle) is $L_{op}=6.1$ mm, so GDD_{CaF₂}≈108 fs².

For the SF57 plate:

GVD_{SF57}=142.57 fs²/mm, thickness $t=10$ mm and optical length path (at Brewster angle) is $L_{op}=11.42$ mm, then GDD_{SF7}≈1628 fs².

Thus for single pass Yb:CaF₂ crystal and SF57 plate the total GDD without SPM is GDD_{Total}=GDD_{CaF₂}+ GDD_{SF57}=1736 fs². Suppose the L_{prism} optical pass for each prism is around 2-3 mm and recall equation 5.25. The prism pair separation was set to be ~400 mm to provide the dispersion compensation.

At first we used 100 μm radius pump diode, and no obvious pulse splitting has been observed. We obtained 3-pulse per round trip KLM as shown in Fig 6-36.

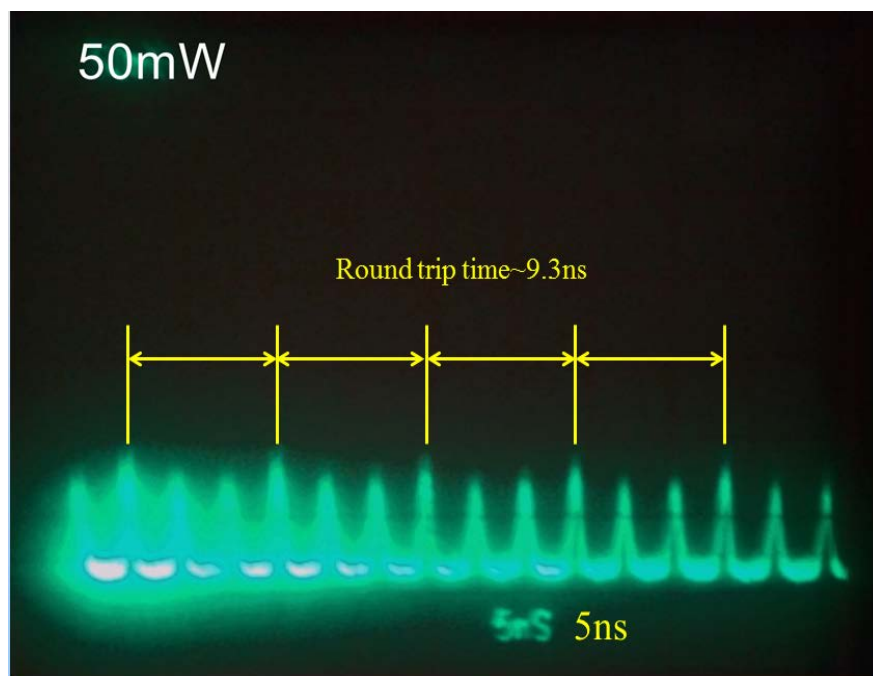


Figure 6-36 SF57 KLM with GVD compensation with 100μm radius diode pump

It was very similar to previous Z-cavity result but with a longer round trip time. The output was around 500 mW at 10 W pump.

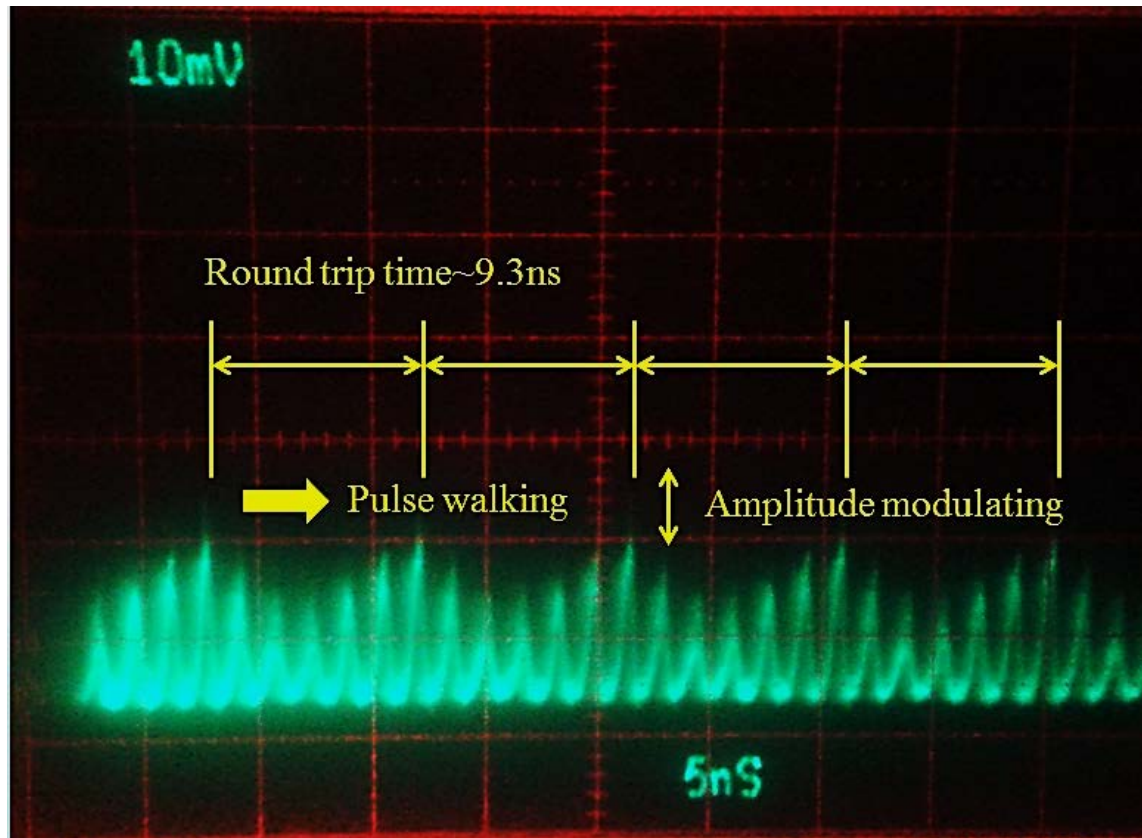


Figure 6-37 SF57 KLM with GVD compensation at $50\mu\text{m}$ radius diode pumping

To achieve a stronger pump fluence stronger beam interaction, we changed the pump to a $52.5 \mu\text{m}$ radius diode. After slightly adjusting cavity structure, pulse splitting and pulse walking phenomenon were observed as shown in Fig 6-37. 6 pulses per round trip KLM result was observed and pulse peaks amplitudes were modulated due to pulse walking. The output power dropped to 260 mW and center wavelength shifted to shorter wavelength 1049 nm due to higher cavity loss. The beam spectrum is narrowed down to ~ 2.2 nm perhaps because of the reduced round trip gain.

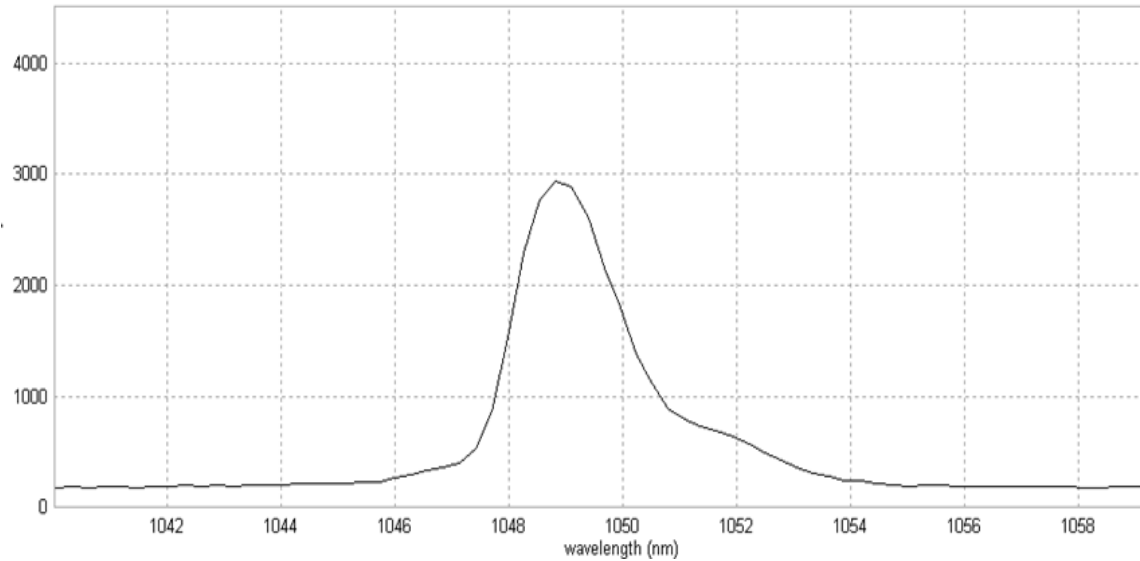


Figure 6-38 Spectrum of SF57 KLM 6 pulses per round trip

Last but not least, as the KLM cavity always works very close to the stability limit, so the power efficiency is lower than CW as a tradeoff. During the progress of cavity optimization, the laser sometimes operated in TEM_{01*} , TEM_{10} , TEM_{20} modes as shown in Fig.6-39. The presence of other higher order modes in ML operation indicates that the CW laser mode was not well overlapped with the pump gain volume when the cavity was optimized for self-starting mode-locking.

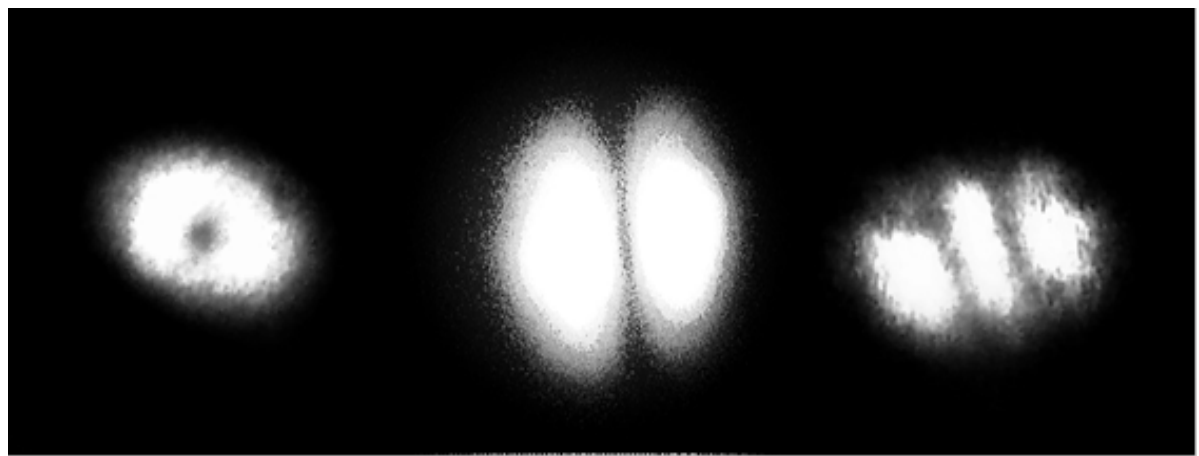


Figure 6-39 Other higher oscillating modes during KLM operation

6.5 Conclusion

A variety of modelocked regimes were explored in this chapter using a SESAM and additional nonlinear elements in the cavity. Complex behavior and either Q-switched modelocking or multipulse modelocking were observed. The behavior in the various regimes will be analyzed and discussed further in chapter 7.

7 Discussion of experimental results

In this chapter the results presented in the previous chapter will be discussed in detail.

7.1 CW operation stability

A laser cavity, especially a KLM cavity is very sensitive to all kinds of disturbances, so it is necessary to keep the laser system away from dust, mechanical vibrations and air flow. In a CW configuration, laser output stability is affected by these perturbations. The laser exhibits output spikes as shown in Fig.7-1 and instantaneous self-amplitude modulation (modulation depth over 50%) as shown in Fig.7-2.

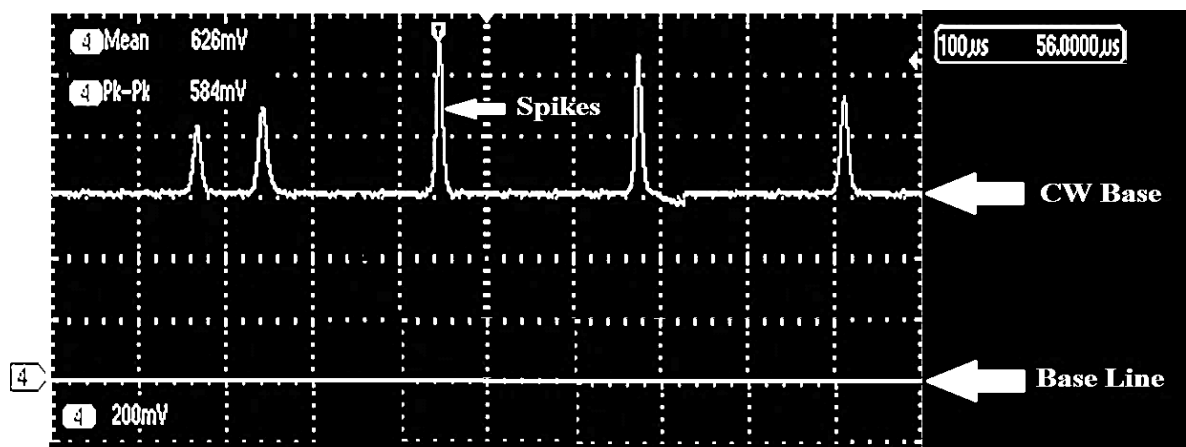


Figure 7-1 Yb:CaF₂ CW mode output spikes

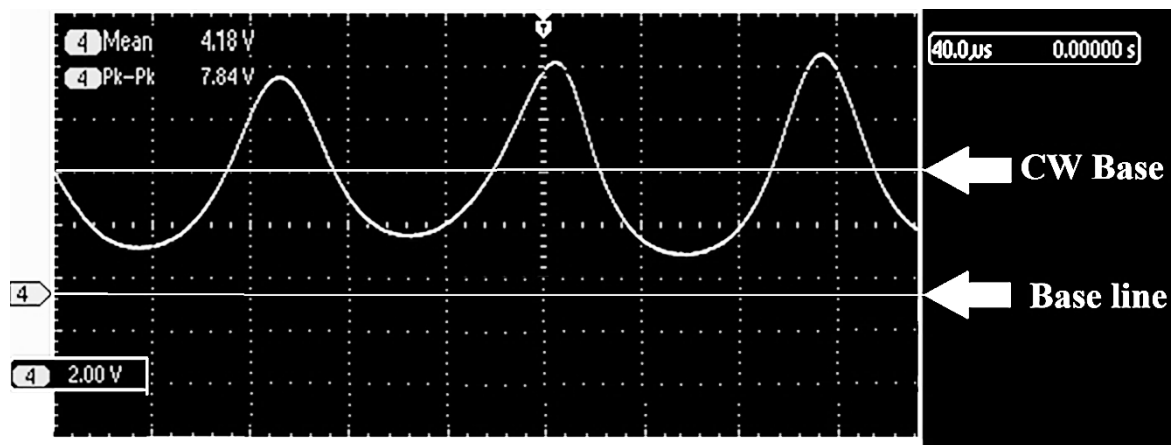


Figure 7-2 Yb:CaF₂ self-amplitude modulation

External instabilities especially mechanical vibration may severely affect laser output which makes laser operation more complex to analyze. In our experiment, the Yb:CaF₂ crystal was originally placed on a water cooling copper block. Later experiment showed that the mechanical vibration from the chiller motor can be transferred to the Yb:CaF₂ crystal through the cooling block and the water tubes. As one of the cavity end mirrors (dichroic mirror) was only 5-10 mm away from the Yb:CaF₂ and the vibration can also be transferred through optical table, so the mirror was unstable as well. This cavity instability drove the laser away from stable CW/ML operation and introduced random Q-switching (QS) and Q-switching modelocking (QML) operation.

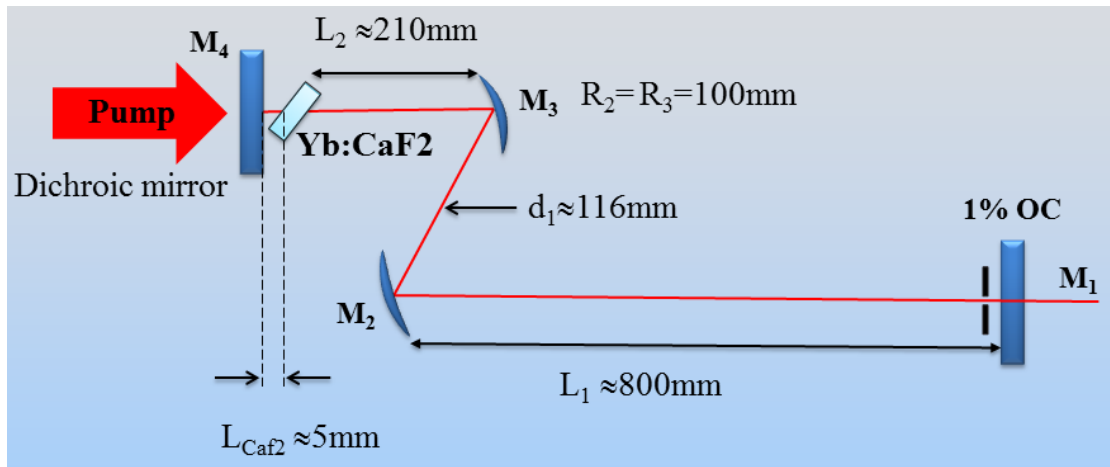


Figure 7-3 Yb:CaF₂ CW cavity configuration

A z-shape Yb:CaF₂ CW cavity configuration is shown in Fig.7-3, the total cavity length is close to 1140 mm. To minimize the other influences, the Yb:CaF₂ crystal was the only intracavity element. A random QS and QML operation was obtained when the water chiller was turned on as shown in Fig.7-4. Inside the Q-switching

envelope a noisy ML pulse training was observed, the pulse peaks separation is about 7.5 ns which corresponds to total cavity length.

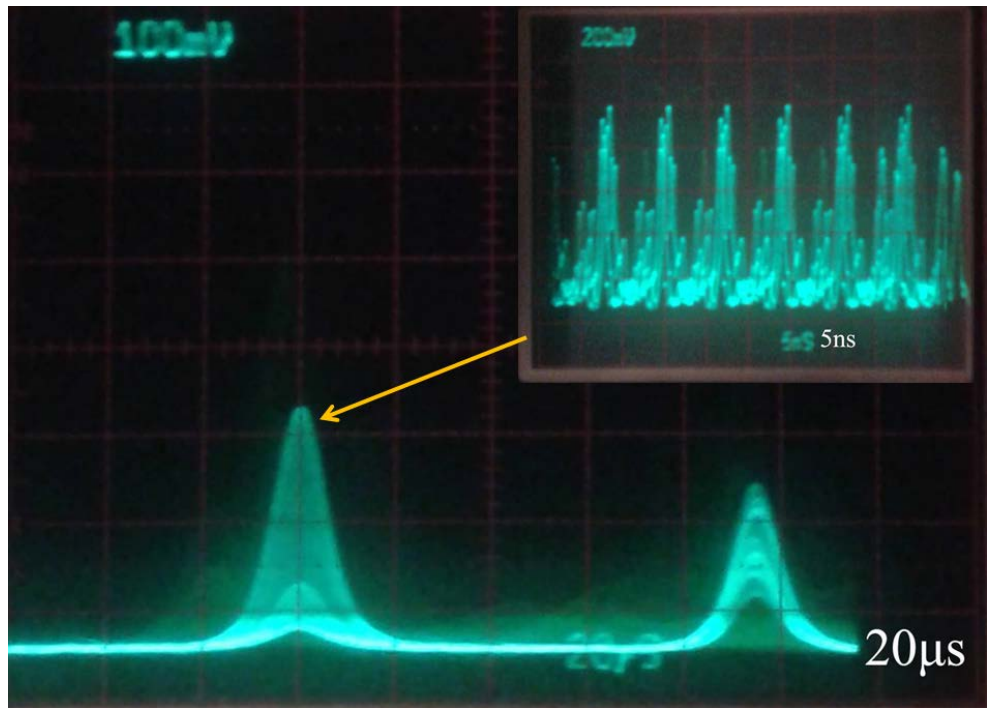


Figure 7-4 Yb:CaF₂ random QS and QML operation for the laser cavity configuration shown in Fig.7-3.

This random QML was initially thought to be random thermal Q-switching of the Yb:CaF₂ crystal. However after removed the extra Kerr medium and leaving the Yb:CaF₂ crystal as the only intracavity element this QML kept happening. Unlike typical KLM lasers which are very sensitive to cavity alignment and Kerr medium location, this type QML originating from cavity dumping was almost independent of the cavity structure. It was also independent of laser beam radius inside the Yb:CaF₂ crystal, as the beam size was changed from 100 μm to 300 μm and larger, similar results were observed with all the configurations tried until the chiller was turned off. This random

unpredicted QML may generate pulses with strong enough peak power to burn and crack the SESAM.

7.2 SESAM damage analysis

Due to a relatively small emission cross-section which leads to a high gain saturation fluence and a very long lifetime (2.4 ms) of the metastable $^2F_{5/2}$ state, Yb:CaF₂ crystal exhibits a strong tendency to store energy and to Q switch. Thus energetic pulses beyond the SEASAM's damage threshold can be generated during QML operation. It is a challenge for passively ML operation of Yb:CaF₂ with a SESAM and makes it difficult to stabilize CW mode-locked operation.

The Yb:CaF₂ emission cross sections at 1050 nm is $\sigma_{em} \approx 2.1 \times 10^{-25} m^2$ and the absorption cross sections at 1050 nm is $\sigma_{abs} \approx 0.2 \times 10^{-25} m^2$. The laser beam mode can be assumed to be symmetric with 120 μm average radius. The saturation energy is given by $E_{sat} = A_{effective} \times F_{sat}$ where $A_{effective}$ is the laser effective mode area within the Yb:CaF₂ crystal and F_{sat} is the laser gain saturation fluence, thus $E_{sat} \approx 37.2$ mJ. For a pulse duration of ~ 1 ps, the peak power would be $P_{peak} \approx 37.2$ GW [199]. Given a beam waist radius on the SESAM surface of ~ 300 μm , then the average intensity at the saturation would be ~ 13.2 TW/cm². It is not possible to generate such energetic pulses in our experiment. However in the QML process it is possible to generate 1/10000 of saturation intensity during SESAM transient regimes which is strong enough to damage the SESAM. The burn spot size was not consistent and much

smaller than the beam waist, which was because the intensity of beam center is higher. Once the central part was burned a little, the laser intracavity intensity was reduced immediately and left the surrounding part unburned, so the beam waist is larger than burn spot size.

We tried a few different cavity designs to avoid further damaging SESAM crystal. To reduce the laser mode size within the Yb:CaF₂ and enlarge the beam mode size at the SESAM surface. Two new cavities as shown in Fig.7-5 were tried.

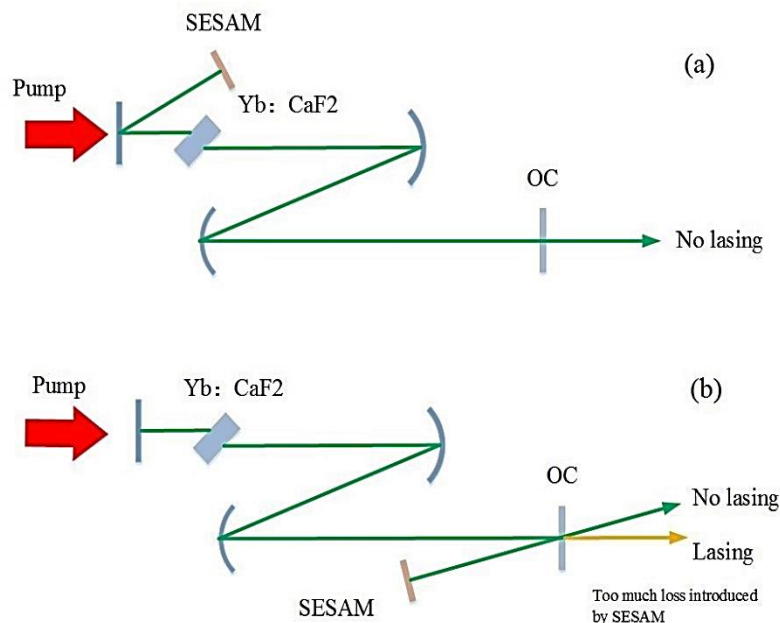


Figure 7-5 Modified SESAM ML Cavities

In the CW configuration (without SESAM), the lasing threshold was approximately 3W pump and the output was about 1 W at 9.1 W pumping. With the damaged SESAM, cavity loss become quite large and the lasing could only be obtained in the second configuration (b) of Fig.7-5 when the pump threshold was increased to 18 W. We

could only increase the pump to 20 W to avoid damaging the Yb:CaF₂ and the QML output power was limited to 130 mW. The cavity round trip time was ~7 ns and the Q-switching frequency was ~9 kHz. Although the output power is low, the peak power may still be quite high and further damage the SESAM. The best output obtained is shown in Fig 7-6. However the SESAM would still damage and such output was only stable for a few minutes.

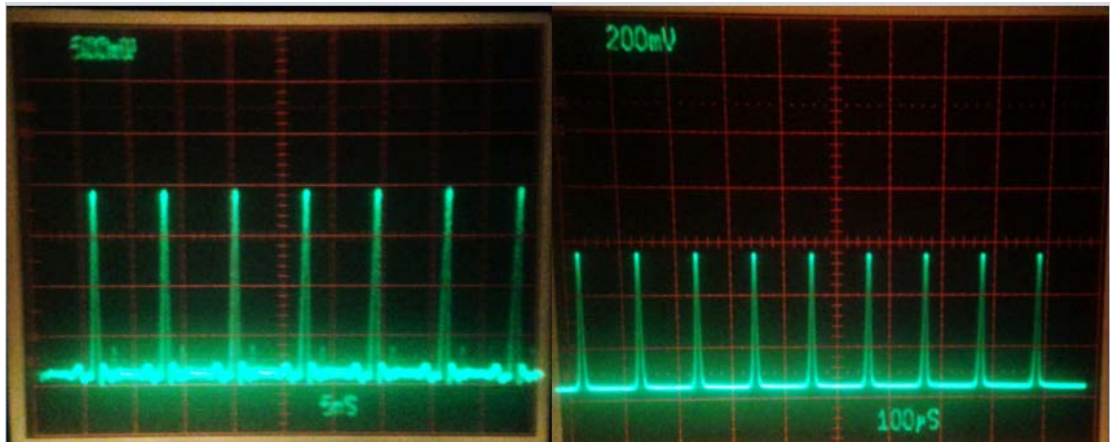


Figure 7-6 SESAM ML pulse trains and Q-switching envelop

Recall equation 5.11, the critical intracavity laser pulse energy E_p to suppress the Q-switching instabilities $E_p \geq \sqrt{F_{sat,L} \cdot A_{eff,L} \cdot F_{sat,A} \cdot A_{eff,A} \cdot \Delta R}$, with the laser saturation fluence $F_{sat,L} \approx 116 \text{ J/cm}^2$, the SESAM saturation fluence $F_{sat,A} \approx 70 \text{ } \mu\text{J/cm}^2$, the effective laser beam area inside the gain medium $A_{eff,L} \approx 3.14 \times 10^{-4} \text{ cm}^2$ (100 μm radius), the effective laser mode area on the SESAM $A_{eff,S} \approx 1.256 \times 10^{-3} \text{ cm}^2$ (200 μm radius), and the modulation depth $\Delta R \approx 0.8\%$, the threshold pulse energy to suppress QML is $E_p \approx 5 \text{ } \mu\text{J}$. This is very difficult to achieve in a seed oscillator. If we could reduce the mode size inside Yb:CaF₂ to 50 μm, the beam radius on SESAM surface to

50 μm and reflection coefficient to $\Delta R \approx 0.3\%$, then the $E_p \approx 388 \text{ nJ}$ which is possible to achieve in a compact oscillator. Although in femtosecond region, due to finite gain bandwidth there's a significant reduction on E_p , we have to safely transfer the laser operation from picosecond regime to femtosecond regime. So a small SESAM modulation depth and intracavity beam sizes inside the gain medium and on the SESAM surface are desirable for SESAM CW ML operation.

7.3 ZnS KLM experiment

When a 3 mm thickness ZnS crystal was used as a Kerr element for KLM, a similar self Q-switching behavior was observed as shown in Figure 7-7.

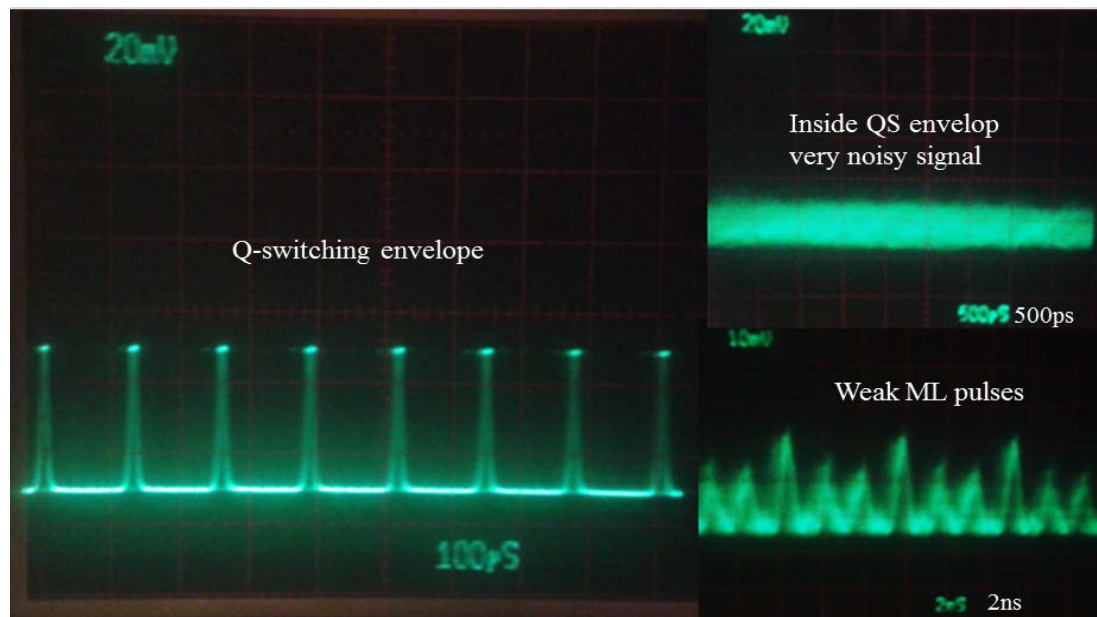


Figure 7-7 KLM experiment with 3mm ZnS

After the cavity was optimized for maximum CW output and moved close to the stability boundary where the nonlinear effect is stronger, a relatively stable

spontaneous QS operation was obtained. The Q-switching frequency is $\sim 1/120\mu\text{s}=8.3$ kHz and the output is about 300 mW at 10 W pump. In the Q-switching regime, strong green radiation was generated by surface sum frequency generation (SFG) as shown in Fig.6-8. At the position where SFG was maximized, very weak ML pulses were detected in the noisy signal.

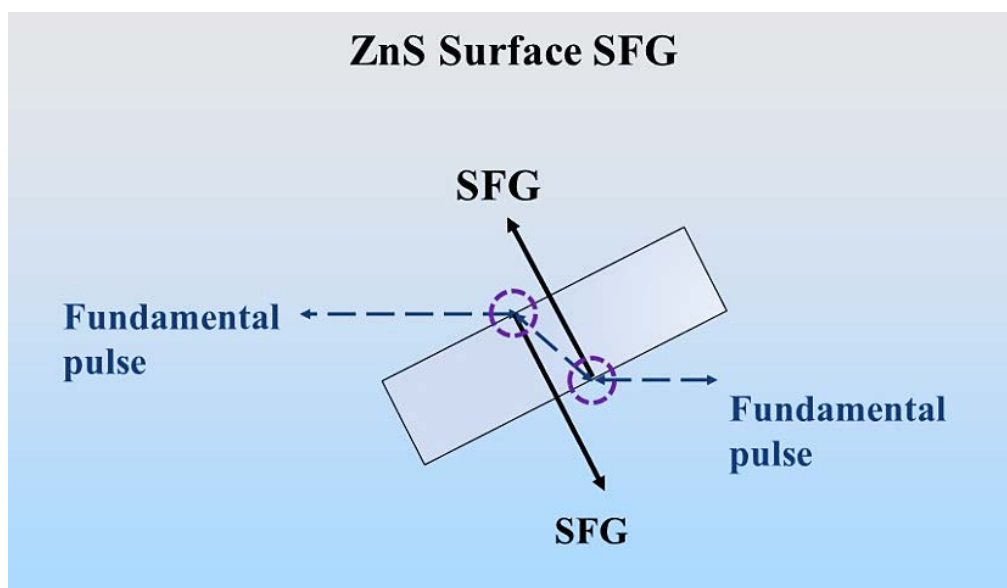


Figure 7-8 ZnS surface SFG

As ZnS is an almost cubic centrosymmetric crystal, birefringent phase matching is impossible. Furthermore ZnS was placed at Brewster's angle (66.4 degree) so collinear, non-phase matched second-harmonic green beam beyond the total reflection critical angle (24.6 degree) was generated and trapped inside the crystal. Last but not least, all the Brewster plates in the cavity were placed for horizontal polarized fundamental waves, they introduced large loss to SFG waves which were vertically polarized, so SFG intensity from OC was limited [200].

Compared with 13.3 kHz QML with 6mm ZnS, this 8.3 kHz Q-switching with 3mm ZnS modulation frequency is reduced because of weaker pumping and slower gain recovery. Recall equation 3.4, the cavity round-trip time T_R is ~ 5.3 ns and gain medium upper-state lifetime is 2.4 ms. For 6 mm ZnS, if we assume the round trip power gain is $g_0 \approx 0.25$ and the loss is $l \approx 0.2$, we get $f_{QML} \approx 14$ kHz. For the 3 mm ZnS, the round trip power gain and loss are assumed to be $g_0 \approx 0.15$ and $l \approx 0.13$ respectively yielding $f_{QS} \approx 8.9$ kHz. The QS frequency is strongly depend on intracavity loss [201] [202], and our estimation agrees with the experiment observations.

The QML result also indicates that a relatively larger modulation depth ΔR was generated during the modelocking process for the 6 mm ZnS which could be explained by 3 possible reasons are:

- 1) Enhanced SHG process due to pulse collisions, although a ZnS crystal is nearly symmetric, it still possesses a second-order nonlinear optical susceptibility of 12 pm/V (at 1047 nm) [203].
- 2) Transmission loss due to scattering [204] and polycrystalline structure [219].
- 3) Three photon absorption (TPA) process, the photon energy is 1.18 eV for 1050 nm radiation, the ZnS band gap is ~ 3.6 eV which means that TPA is a possible lossy process [205].

No SHG process has been observed during the SF57 glass KLM experiment, due to its symmetric structure.

7.4 SF57 multiple pulse ML operation

Two types of multiple pulses ML operation have been observed which depends on cavity design and can be categorized by the resultant pulse separations.

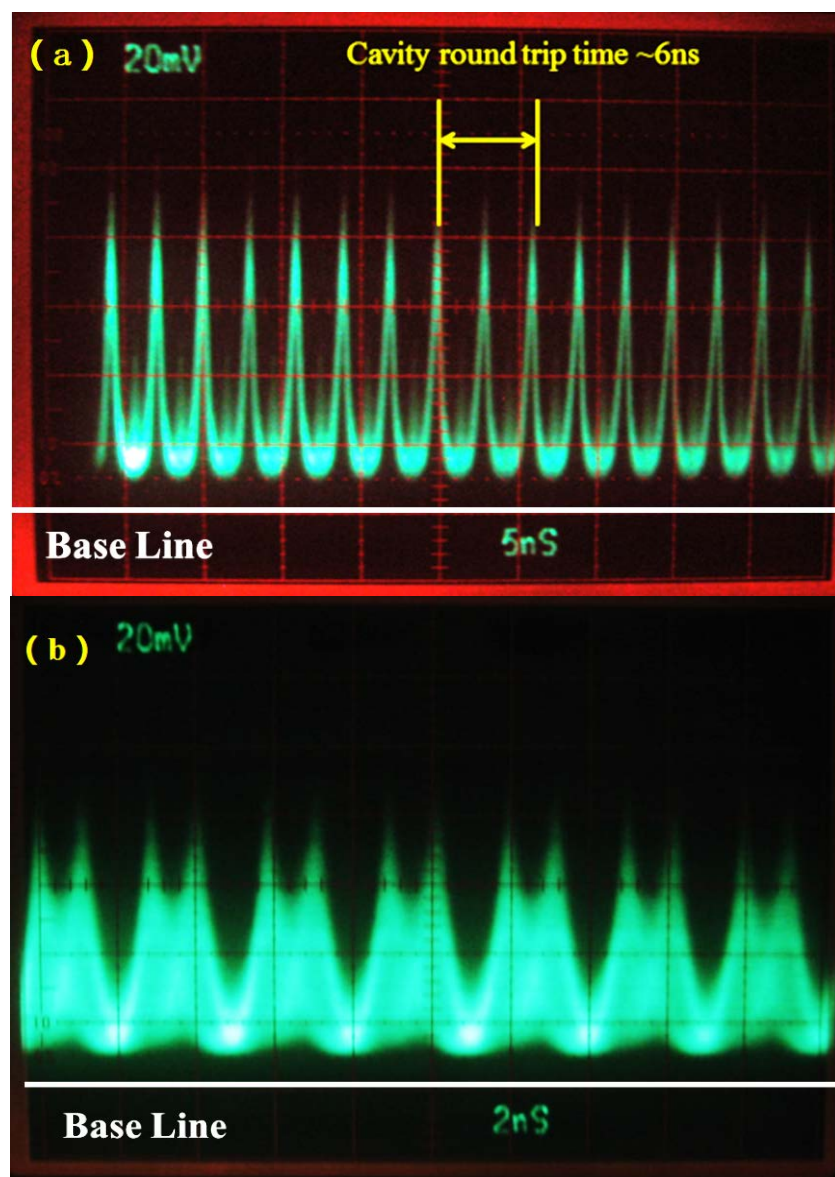


Figure 7-9 SF57 multiple pulse ML operation for the cases of (a) a few nanoseconds pulse separation and (b) $\sim 1\text{ns}$ pulse separation

- Pulse separation is in the fraction of cavity round time (a few nanoseconds)

- b) Two twin pulses and their separation is approximately 1 ns separation close to photo diode resolution limit.

7.4.1 Multiple-pulse ML operation with a few ns pulse separation

Collision of counter-propagating pulses inside the SF57 plate is the main reason for this multiple-pulse operation as shown in Fig.7-10 (b). The satellite pulses appear at fixed time interval, which is always equal to the round trip time from SF57 plate to the nearest end mirror. The pulse separation could be changed if the distance between SF57 and end mirror is varied. The total number of pulses per round trip N is determined by the quotient of division result $N=L_{\text{Cavity}}/L_{\text{Kerr}}$.

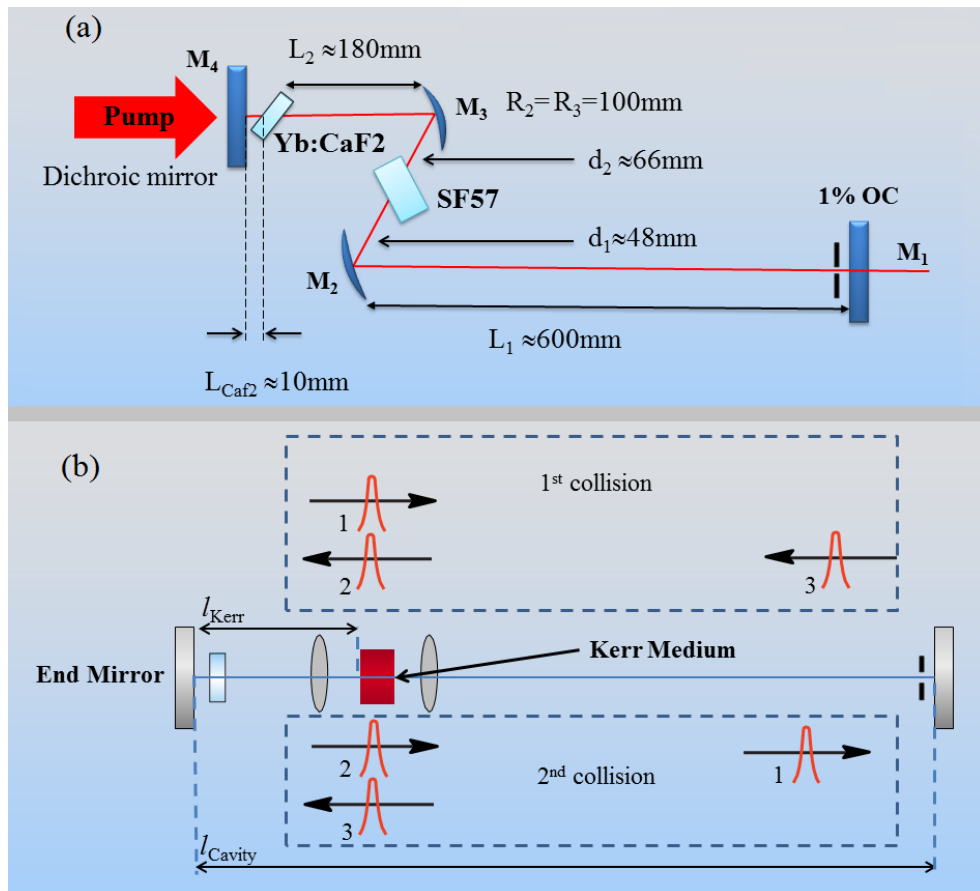


Figure 7-10 Pulses collide cavity configurations and scheme

The intensity-dependent lens is much stronger at the position where two pulses collide than at other locations or for single pulses. The maximum pulse shaping effect of colliding pulses is achieved near the beam waist where the nonlinearity is maximized. So a stable multiple-pulse soft aperture KLM operation can be achieved if the cavity design is optimized and the laser mode volume and pumped gain volume are well overlapped.

We have performed a numerical simulation to show the variations of the KLM strength parameter [214] $\delta = \lim_{p \rightarrow 0} \frac{1}{w} \left(\frac{dw}{dp} \right)$ as a function of the pulse collision position for single pulses, double pulses and triple pulses operation, where w is the spot size at the given plane (in our numerical simulation is the plane of dichroic mirror M4 in Fig7-10 (a)) and $p=P/P_{cr}$ is ratio of the laser peak power to the SF57 self-focusing critical power.

A negative δ indicates that ML is favored against CW for the chosen SF57 location. The Kerr medium (SF57 plate) was divided in to N (10-20) slices, the total effective thickness of the Kerr medium is t_{Kerr} , so the optical distance for each slice is $d=t_{Kerr}/N$ which has approximately the same length as the pulse envelop path length in its pulse duration. The cavity was evaluated by ABCD matrices formalism, including the nonlinear lensing, and each slice can be described by a matrix of

$$M_{Slice} = \begin{pmatrix} 1 & d \\ -1/f & 1 \end{pmatrix} \quad 7.1$$

$$\text{and } f = \frac{n_0 \pi w_0^4}{8n_2 P d} \quad [225] \quad 7.2$$

Where n_0 is the SF57 linear refractive index, w_0 is the beam waist at the entrance of the slice, n_2 is the SF57 nonlinear refractive index, P is the intracavity peak power and d is the thickness of the slice.

The simulation was based on the cavity configurations of Fig.7-10 (a). Starting with CW mode without nonlinear lens effect, the w_0 for each SF57 slice was calculated and then the M_{Slice} for each SF57 slice was firstly generated. Then based on the new cavity parameters, the ABCD matrix for the resonator was again calculated and generated new M_{Slice} for next iteration. This procedure was continued until a stationary state was reached, in our simulation the difference of the beam spot size on M4 (w_{M4}) for two successive iterations is less than 10^{-7} mm. It generally takes up to 7 iterations before a stable result was reached in small intracavity powers cases (p is on the order of 10^{-3}). The cavity may loss stability during the iterations if the p is close to 1, we did not obtain stable result when $p \approx 0.78$.

For the two pulses cases, we assumed the two counter-propagating pulses only interact in a single slice and the average output for the single and the double pulse mode was the same [206][211]. The peak power of single laser pulse in a slice was halved (p is also halved), and the collision point was identified by double the slice peak power. For the three pulses cases, the central pulse (No.2) of the train collides twice when propagating forward and backward as shown in Fig 7-10 (b). The peak

power for single slice was divided by three and collision point was calculated twice for two collisions per round trip [211]. Then the pulse collision point was scanned through the length of SF57 crystal.

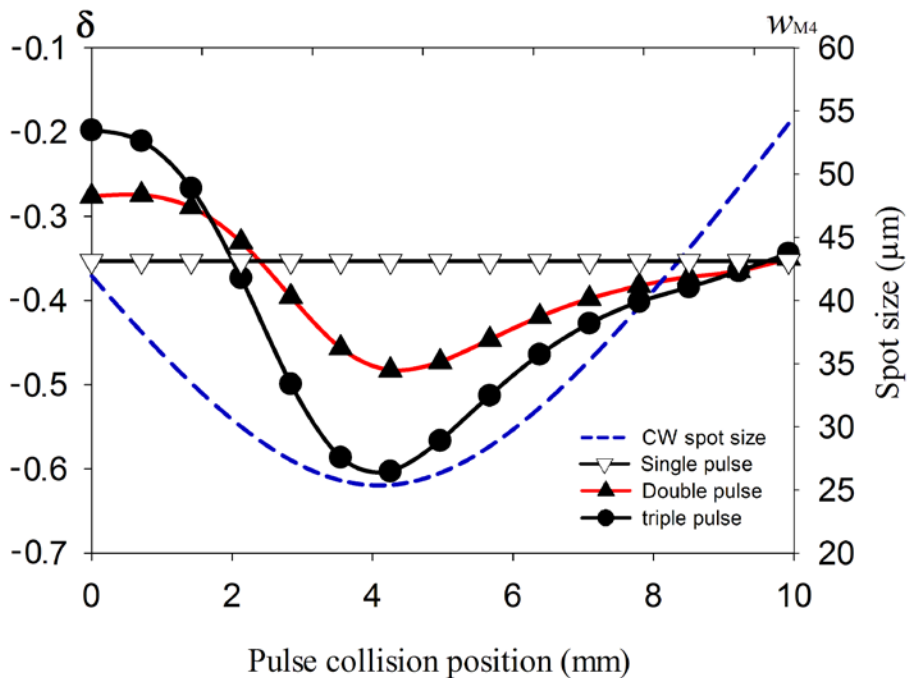


Figure 7-11 KLM strength variation with SF57 pulse collision position

As shown in Fig.7-11, δ is strongly dependent on the collision position in multiple pulse modes and we are expected to obtain strongest δ in triple pulse mode. Larotonda et al. [211] showed that in maximum we are able obtain more than four times stronger δ in double pulse mode than single pulse mode , and it could be more than eight times in triple pulse mode in spite of peak power was reduced. The optimal collision point is very close to CW mode beam waist with a tolerance below 0.4 mm, which agrees with the optimum focusing condition presented in Chapter 4 Section 4.3 as well as the results of Larotonda et al. [211] and M. Lai et al. [206]. It was also

noted that compared with CW mode, the beam waist between M2 and M3 shifted to M3 a distance of $\sim 200 \mu\text{m}$ in KLM mode due to self-focusing effect.

A stronger δ will favor ML rather than CW operation and maximize the intracavity power, which could explain the stabilization of the multiple-pulse mode operation. Self-amplitude modulation (SAM) is the main gain modulation mechanism in our KLM operation, the modelocked pulses experience more gain than CW for increasing intracavity power. SAM is affected by nonlinear self-focusing and gain aperture effects, which depend on nonlinear medium, pulse peak power and cavity geometrical design [211].

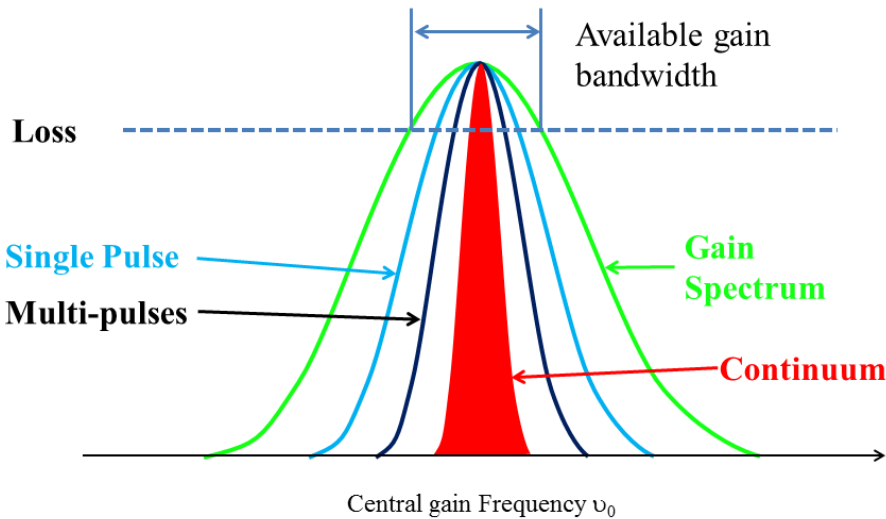


Figure 7-12 Spectrum width comparisons for gain, single and multiple pulses

A larger modulation depth could be introduced by a stronger SAM, therefore the ML pulses would have shorter duration and wider spectrum until limited by the available gain bandwidth. To maximum intracavity power, the system will then split the energy into multiple pulses [211]. These pulses with lower energy have weaker SAM, longer

pulse duration and narrower spectrum to fit the peak region of the available gain bandwidth as previously discussed in reference [212]. Finally, the weaker reduced SAM effect is compensated by an enhancement of SAM due to the pulses colliding effect [213].

Unlike the Nd:YAG experiments of M.A. Larotonda et al. where the laser system oscillates in single pulse mode at low pump power level [211], due to a relative high lasing threshold our oscillator tends to operate in multiple-pulse mode even at a very low pump power to maximize the intracavity power.

7.4.2 Multiple-pulse ML operation with 1 ns pulse separation

It has been shown that if the intracavity peak power approaches the Kerr medium critical self-focusing power, the pulse central part with highest peak intensity will first experience self-focusing. As a result, the self-phase modulation (SPM) will be further enhanced. A numerical analysis by Joshua [207] and experimentally varied by Jinedra et al. [208] showed that this SPM effect could split single pulse into two temporally separated pulses in a normal dispersive medium. In Ti:sapphire lasers, this separation can be tuned over the range from 200 fs to 1 ps [206] by adjusting the folding mirror spacing and changing pump power. We believe this theory should also be applied to our experiment. The 10 mm thickness SF57 glass plate could introduce normal dispersion to laser pulse during multiple pulse ML operation and split the pulse. The nonlinear refractive index for SF57 is $n_2=4.35\times10^{-19}$ m²/W and for Ti:sapphire is

$n_2 \approx 3 \times 10^{-20} \text{ m}^2/\text{W}$, so for SF57 ML operation the required peak intensity for pulse splitting is considerably lower. With a 1% output coupler the output power is around 0.8 W. With a $\sim 6\text{ns}$ cavity round trip time, 2 pulses per round trip and an assumed approximate pulse duration of ~ 1.5 ps, the intracavity peak power is estimated to be 160 KW. This estimate is close to the critical power for SF57 self-focusing of 203 KW given in section 4.2.2.

After the two pulses operation has been established, several effects can induce the relative walking of the two split pulses. Due to intensity dependent refractive index, the pulses with less energy will experience a relatively shorter optical path length than that with higher energy, therefore weak pulses move faster than strong pulses. An opposite affect is induced by gain saturation, the pulses with more energy saturate stronger than those with lower energy thus propagating a little faster. So the pulse walking stabilization could be achieved if these two effects are balanced [206].

The walking speed can be estimated from the difference in average pulse velocity. The index change due to the Kerr effect in the SF7 is $\delta n = n_2 I \approx 7.1 \times 10^{-5}$, where the optical intensity inside SF57 is estimated to be $I \approx 1.63 \times 10^{14} \text{ W/m}^2$, (160 KW peak power, a beam waist radius of $\sim 25 \mu\text{m}$ and intensity distribution is assumed to be in Gaussian shape). Then the walking speed is estimated by $v \approx c F n_2 \Delta I$. Where c is the speed of light, F is the ratio of the SF57 plate optical-path length to the total cavity optical-path length and ΔI is the intensity difference between the pulses. With $F \approx 1.2\%$

and $\Delta I \approx 0.05I$, we obtain $v \sim 13$ m/s. For the pulses to spread by 1 ns would require a walk off 30 cm requiring a period of 2.3×10^{-2} s. Stable operation of the cavity for this time period would be required for the walk off effect to take effect. It is expected that the observed pulse splitting would involve an interplay of several such nonlinear processes.

7.5 SF57 KLM cavity analysis

7.5.1 Cavity misalignment evaluation

In order to obtain large power dependent beam size variation, the resonator design must be very close to a stability limit (a few hundred micrometers) and satisfy the optimum focusing condition.

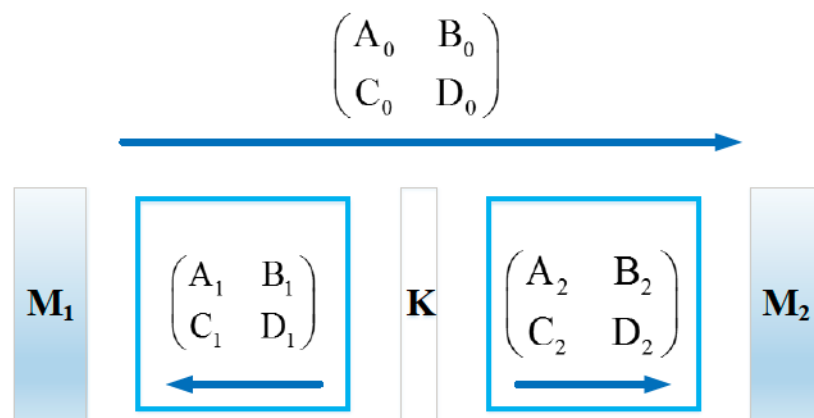


Figure 7-13 Matrix description of the resonator

Vittorio et al. showed that for a given resonator the maximum δ is reached at the plane of one of the flat end mirrors and the beam waists [214]. These positions are the most suitable for KLM as nonlinear gain/losses effects are maximized. Any resonator

can be generally described by Fig.7-13, where plane K is the Kerr medium central plane and the small signal relative spot size variation δ_1 at M1 can be expressed by:

$$\delta_1 = \lim_{p \rightarrow 0} \left(\frac{1}{w_1} \frac{dw_1}{dp} \right) = -\frac{1}{2} \frac{\alpha_1 + \alpha_2 S}{\alpha_1^2 + \alpha_2^2 + 2\alpha_1\alpha_2 S} \quad 7.3$$

$p=P/P_c$ is normalized power (P is the physical power and P_c is the Kerr material critical power for self-focusing)

$$\alpha_1 = 2B_1 D_1 / d_e - A_1 C_1 d_e / 2 \quad 7.4$$

$$\alpha_2 = 2B_2 D_2 / d_e - A_2 C_2 d_e / 2 \quad 7.5$$

$$S = A_0 D_0 + B_0 C_0 \quad 7.6$$

Where d_e is effective optical length, $A_{1/2}, B_{1/2}, C_{1/2}, D_{1/2}$ are the elements of one way matrices from plane K to the end mirror M1 and M2 in the direction as shown in Fig.7-13 respectively. A_0, B_0, C_0, D_0 are one way matrix elements for the propagation from end mirror M1 to M2. The resonator is stable if $-1 \leq S \leq 1$, and $\delta_{1\max, \min} = \pm 1/\left(2\sqrt{1-S^2}\right)$ when $\alpha_1 = \mp\sqrt{1-S^2}$, $\alpha_2 = 0$ [214].

To achieve large spot size variations and, hence, strong nonlinear gain/loss modulations, the resonator must be close to the stability limits $S \approx \pm 1$. From numerical simulation and experiment results we are able to show that Kerr effect pulse shaping effect is very sensitive to cavity structure and small variations would have a large effect on δ .

The OC beam waist variation vs intracavity power for the cavity design shown in Fig 7-14 is shown for two cases in Figure 7-15. In the first case we set $d_1=44.5$ mm and

$d_2=69$ mm, while in the second case we set $d_1=44.5$ mm and $d_2=68$ mm. All the other parameters are unchanged.

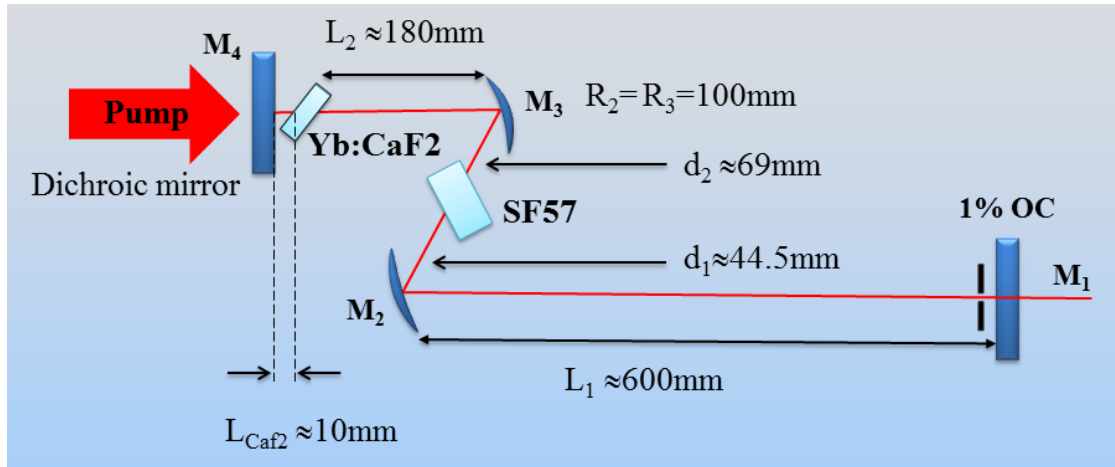


Figure 7-14 SF57 KLM cavity design

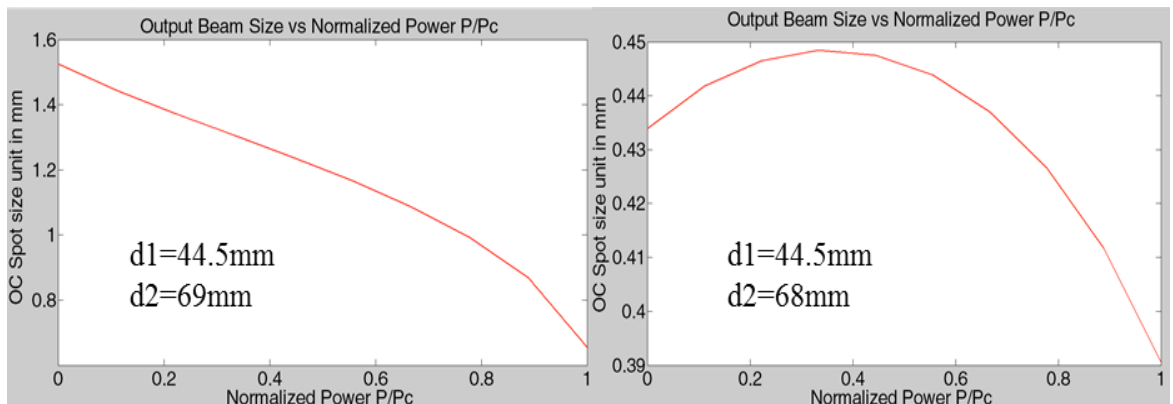


Figure 7-15 OC beam radius change vs intracavity power with different cavity design

In order to achieve KLM, the spot size at the aperture location must decrease to reduce diffraction losses as the intra-cavity power is increased. In the second case of Fig 7-15 KLM is hard to achieve as the nonlinear loss initially increases for increasing power and the size variation amplitude is too small. Only a continuous negative slope of the curve offers the possibility of KLM. Thus we expect to obtain KLM in the first case of

Fig 7-15. In the experiment we also found that in order to maintain KLM, d_2 axial misalignment tolerance was around 0.3 mm which agrees with numerical simulation.

Folding mirror incident angle alignment is also crucial in KLM cavity design. In our experiment the incidence angle is about 10.9 degree, intracavity beam radius calculations for angles of 10.5 degrees and 10.9 degrees are shown in Figure 7-16.

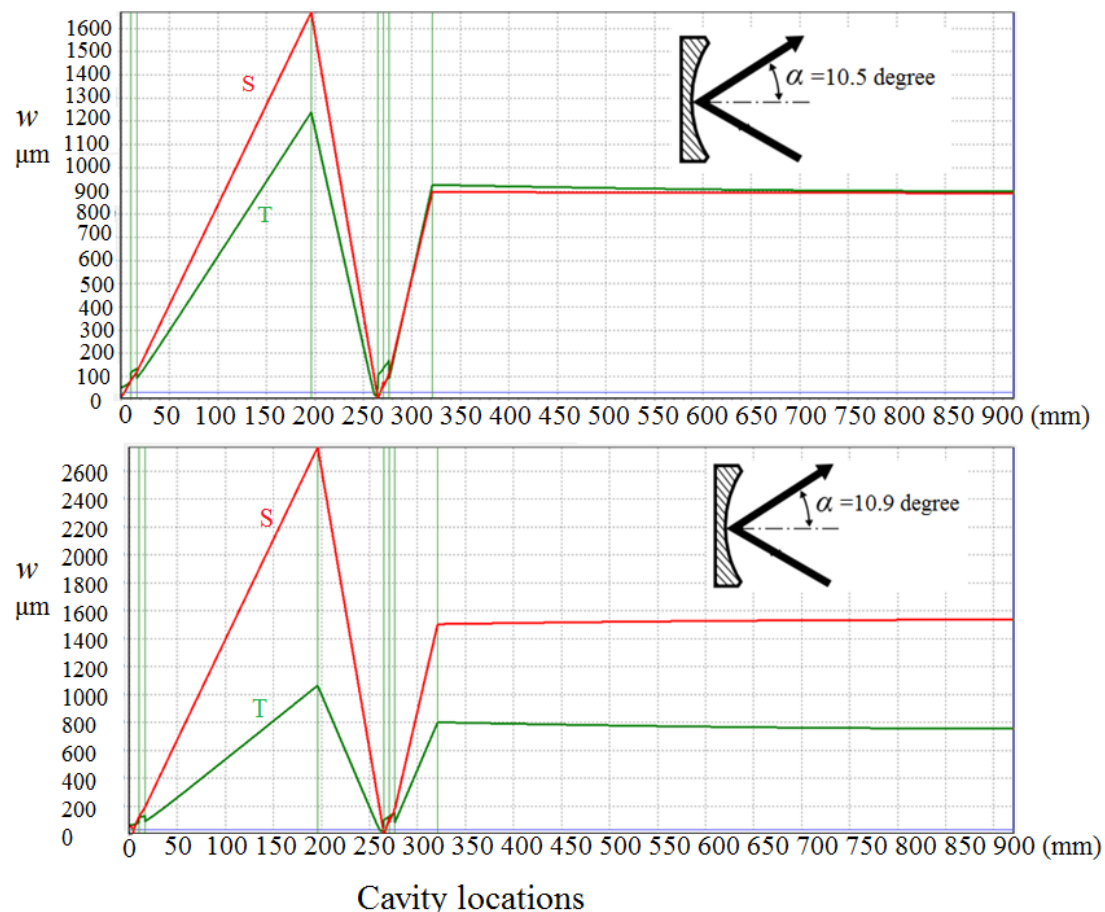


Figure 7-16 Beam radius affect by different folding mirror incidence angle

A large beam radius difference can be produced by the 0.4 degree misalignment on folding mirrors, so hard aperture KLM is quite challenging in our experiment. Luckily

the soft aperture Kerr lens effect generates a strong enough Kerr lens strength to start and maintain modelocking process

7.5.2 Lens effect

In order to optimize cavity design both the thermal lens effect D_{th} and the Kerr lens effect D_{Kerr} should be evaluated [206] [215].

$$D_{th} = \frac{1}{f_{th}} = \frac{\eta_h P_{abs} \chi}{2\pi\omega_p^2 \kappa_c} \quad 7.2$$

$$D_{Kerr} = \frac{1}{f_{Kerr}} = \frac{8n_2 L P_{intra}}{\pi\omega_l^4 f_R \Delta t} \quad 7.3$$

For Yb:CaF₂ crystal, assuming an efficiency of absorbed power transferred to heat of $\eta_h \approx 5\%$, $P_{abs} \approx 6.5$ W absorbed, thermo-optic coefficient $\chi \approx -11.3 \times 10^{-6}$ K⁻¹, equivalent pump effective waist is estimated to be $w_p = 250$ μm, thermal conductivity $\kappa_c = 6.1$ W m⁻¹ K⁻¹, yields $D_{th} \approx -1.53$ m⁻¹ and $f_{th} \approx -654$ mm

For Yb:CaF₂ crystal the nonlinear index $n_2 \approx 2 \times 10^{-20}$ m²/W, with an effective optical path length $L \approx 6.1$ mm, intracavity power $P_{intra} \approx 80$ W, repetition rate $f_R = 167$ MHz, pulse duration $\Delta t = 1.5$ ps, and laser beam waist inside the crystal $w_l = 80$ μm giving $D_{Kerr} = 2.42$ m⁻¹ and $f_{Kerr} = 413.2$ mm. This indicates that the negative pump thermal lens effect for the Yb:CaF₂ crystal could be fully compensated by the positive Kerr lens effect. As the Kerr lens strength is proportional to $1/w_l^4$ and $1/\Delta t$, further reduction in the laser beam waist and shorter pulse duration would lead to an increase in D_{Kerr} .

7.5.3 Minimizing degradation at the stability limit

During KLM cavity optimization, pushing the laser to the stability limit could induce degradation of laser performance. To overcome this challenge but still obtain a strong Kerr effect, we could use a symmetric or semi symmetric cavity. It has been shown that for any resonator the maximum achievable value of Kerr lens strength is limited by $|\delta|_{\max} = 1/4 [A_0 D_0 (1 - A_0 D_0)]^{1/2}$ [214], where A_0 and D_0 are the elements of the one-way matrix for the propagation from interested end mirror to the other end mirror. The simplest way to achieve $A_0=D_0=0$ in tangential plane is using a symmetric resonator ($L_1 = L_2$) with flat end mirrors and folding mirrors of radius R are placed at a distance of $z = z_m = \frac{4L_1 R_t - R_t^2}{4L_1 - 2R_t} + d(1 - \frac{1}{n^3})$, where L_1 is the distance between end mirrors to folding mirrors, $R_t = R \cdot \cos(\theta)$, and d is the length of the Brewster plate [217]. Our SF57 W-cavity KLM experiment is based on this result to form a semi-symmetric cavity.

7.6 KLM self-starting mechanism

One major drawbacks of a traditional KLM laser is that modelocking usually does not start automatically, so an external starting device is often needed. We overcome this challenge by cavity design and pump optimization to maximize gain saturation lens and Kerr lens effect. If the pump beams or laser intracavity beam path is blocked and then opened, the ML operation will restore automatically.

In principle every ultrafast nonlinear process can produce an ultrafast lens effect and we are able to build a gain/loss modulator based on it. Gain saturation lens effect can provides stronger gain modulation than Kerr lens effect at low peak power levels depending on the nonlinear strength of the Kerr medium and is a possible mechanism for self-starting. The theory for this lens effect is that the change in the refractive index caused by gain medium excitation is connected to the change in the gain [218]. Both positive and negative index change can be induced by gain saturation lens effect, depending on the relative position between gain center and laser wavelength. In our experiment a positive gain saturation lens is preferred as it consistent with the Kerr lens effect. For Ti:sapphire lasers, a typical value of loss modulation depth induced by gain saturation is estimated to be the order of 10^{-4} [210]. Self-mode locking only needs an extremely small saturable-absorber like gain/loss modulation ($<10^{-5}$) to start [220] [221]. So we expect to obtain this modulation from the joint effects of the SF57 Kerr lens effect and Yb:CaF₂ crystals gain saturation lens effect, which enhance each other.

A 1% output coupler was used since a lower cavity loss will reduce the threshold power for self-mode-locking. If the laser beam waist is $\sim 100 \mu\text{m}$, Yb:CaF₂ gain saturation energy at 1050 nm is 25.8 mJ, and out experiment pulse energy is estimated to be 240 nJ which is 9.5×10^{-5} of saturation energy, so the gain saturation effect is quite weak. The gain coefficient κ is linked to single-pass gain g by $g=4\pi\kappa L/\lambda$ [222], so for an unsaturated $g=0.2$ single-pass gain and the half-maximum value of gain

curvature is at 1055nm, $\kappa \approx 1.3 \times 10^{-6}$. Then 0.5% gain saturation modulation at 1055 nm induce to an index change of $\delta n \approx \delta \kappa \approx 0.5\% \kappa \approx 0.65 \times 10^{-8}$. To obtain the same index modulation by SF57 Kerr effect, laser pulse as short as ~2 ns (~100 ps for Yb:CaF₂) is required (240 nJ pulse energy and 40μm×55μm beam waist is assumed). Such pulse formation is possible from mechanical vibrations and initial mode beating. Thus in the case of a highly nonlinear material such as SF57 the effects of gain saturation and Kerr lensing both play a role in the ML pulse initiation. The Kerr lens effect is much less sensitive to wavelength variation than the gain saturation. Thus self-starting KLM is a complex process which occurs from a combination of these two mechanisms.

In KLM lasers, oscillating beam waist size together with gain variations along the gain medium length are both determining factors for gain saturation lens. So we are able to maximize gain saturation lens effect by adjusting the positions of the pump beam and laser beam waists, their confocal beam parameters and the folding mirrors spacing. The modelocking mechanism could be self-starting if the gain saturation lens is optimized and combined with the Kerr lens.

7.7 Symmetric cavity experiment and spectral analysis

In our experiment, the maximum spectral width was obtained from a Z-shaped symmetric cavity with SF57 without GVD compensation as shown in Fig 7-17. The total cavity length was ~765 mm corresponding to 5.1 ns cavity round trip time. The

maximum output was close to 1000 mW at 10 W pump. The spectral width was ~ 5 nm as shown in Fig 7-17 corresponds to 231.7 fs pulse duration for a transform limited Sech²-shape pulse. Two wavelength peaks were observed at 1052.2nm and 1054.2 nm, which may suggested that the measured spectrum is the combination of two ML pulses groups. Each group with different central wavelength, due to inhomogeneous gain mechanism, and the mode competition is weak. So both groups experienced enough gain and oscillated in the resonator.

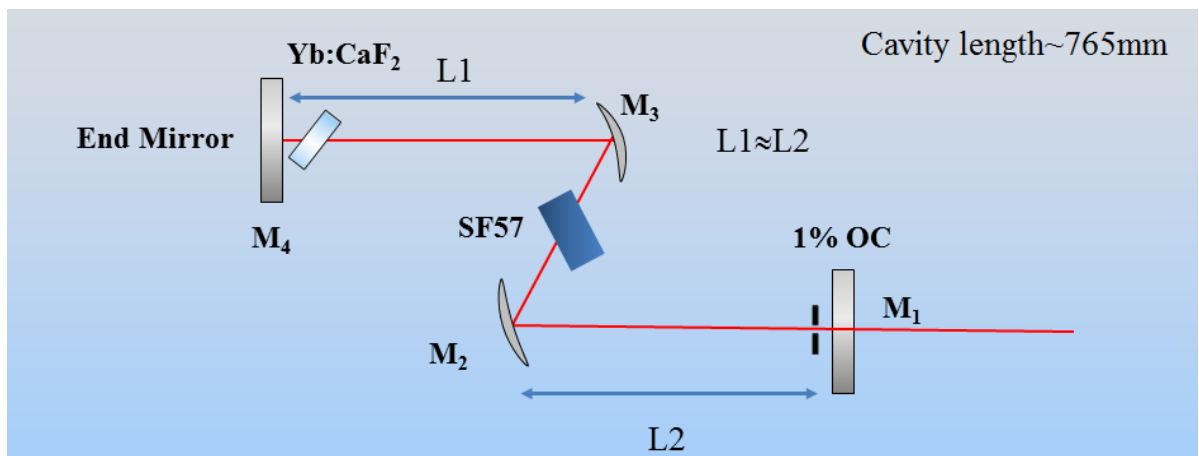


Figure 7-17 SF57 Z-shaped symmetric cavity

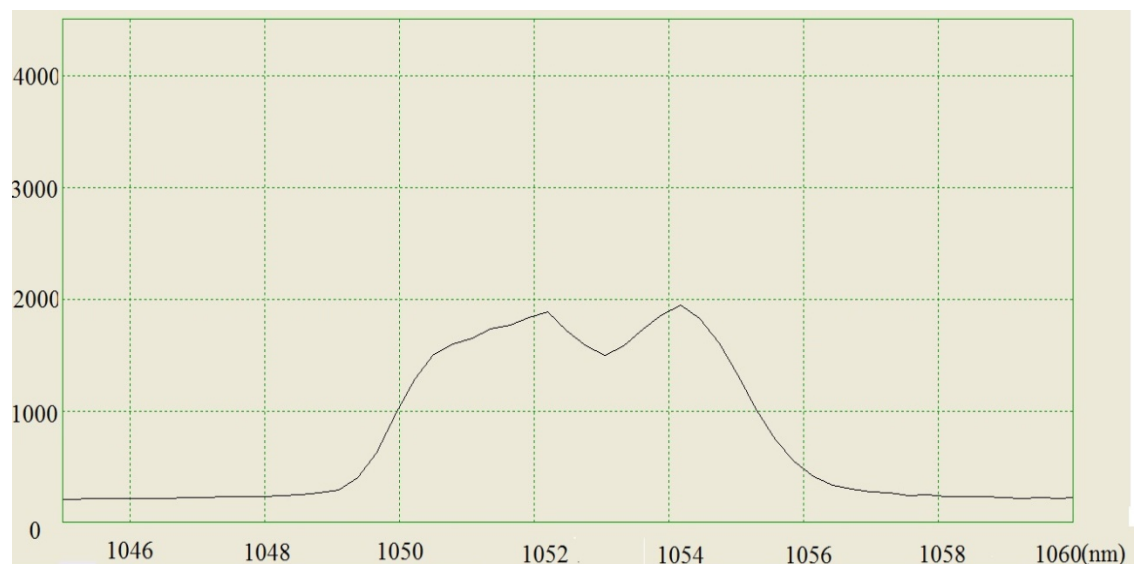


Figure 7-18 Spectrum of a symmetric cavity

Without GDD management, we expect the pulses will be linearly chirped, since the ML pulses experience a net positive dispersion from the linear material dispersion and nonlinear SPM effects. The pulse width broadening due to SPM and GVD can be estimated by [25]:

$$\tau^2 = \tau_0^2 \left[\left(1 + \frac{\sqrt{2}Ub\beta''z^2}{\tau_0^3} \right)^2 + \left(\frac{2\beta''z}{\tau_0^2} \right)^2 \right] \quad 7.4$$

Where τ_0 is the initial pulse duration, U is the intracavity pulse energy, b is the nonlinear SPM coefficient [224], β'' is the SF57 GVD coefficient and z is the light path length in the SF57. In our experiment we assume $\tau_0 \approx 1.5$ ps, $U=240$ nJ, $b \approx 3.9 \times 10^{-3}$ ps/nJ (for ~ 25 μm spot size), $\beta'' = 142.57$ fs $^2/\text{mm}$ and $z = 11.425$ mm. The pulse broadening factor is calculated to be 8.3×10^{-6} per pass. So the pulse broadening effect is very small for picosecond duration pulses and primarily important if one starts with pulses in the 100 fs regime. This is why lasers without dispersion compensation tend to produce pico-second duration pulses. However the spectrum result obtained in our experiment could also be a combination of multiple ML pulse groups oscillating near central wavelength. Unlike typical ML lasers with only one major oscillating pulse group, these groups are weakly coupled with each other due to inhomogeneous gain broadening and other effects. The extended spectrum may not give us the correct limiting pulse duration information, so direct measurements of pulse duration would be required to address this issue.

7.8 Conclusion

A number of features observed in the operation of the modelocked laser systems studied have been examined in the present chapter these include the regions of stability and completion between different mechanisms such as Kerr lensing, thermal lensing and gain saturation. Issues related to spectral broadening and multiple pulse behavior were discussed briefly and the mechanisms contributing to a stable self-starting KLM operation are explored. Overall, further work would be required to examine these issues in more detail.

8 Comparison to previous results

8.1 Comparison with previous Yb:CaF₂ modelocked systems

To date there are two groups that have published Yb:CaF₂ mode-locked resonator designs based on SESAM and KLM modelocking respectively.

The first Yb:CaF₂ femtosecond laser based on SESAM was reported in 2004 by Lucca et al. from Laboratoire Charles Fabry de l'Institut d'Optique (LCFIO) [226]. In their experiment, a 4-mm-long, 5 % at .% Yb doping Yb:CaF₂ crystal was placed on a water-cooled copper (12° C) mount with the use of indium foils for improved thermal contact. The SESAM used in their experiment possessed a 1% saturable absorption and a claimed saturation fluence of 30 mJ/cm². This would be much larger than the saturation fluence of the SESAM used in our experiment (70 μJ/cm²). With 4.5% OC, the one of the ML operations obtained was centered at 1049 nm with a 220 fs pulse duration and a 1.4 W average power at 15 W pump. A second mode of ML operation was obtained centered at 1043 nm with a 880 mW average power, a 150 fs pulse duration and a spectral width of 7.7 nm. The time-bandwidth products for both results are 0.33 close to that for a transform limited sech² temporal pulse.

In their experiment the cavity mode on SESAM was 100 μm×130 μm, thus the corresponding fluence on the SESAM was 893 μJ/cm² at 1.4 W output power with 4.5% OC. This is significantly higher than the SESAM experiments in CW operation, which is 546 μJ/cm² at 1.9 W output power with 10 % OC. However, in our case the

higher absorption of the SESAM used, 1.5%, led to Q-switched modelocking giving much larger peak fluence and damaging the SESAM. Lucca et al. also note in their paper [226] that when a SESAM with 2% absorption was employed that they obtained Q-switched modelocking and damaged the SESAM. Now the damage thresholds of all the available SESAMs in 1040nm region on Batop website are 3 mJ/cm^2 [227].

In 2009, F.Friebel also from LCFIO reported a 99 fs Yb:CaF₂ oscillator based on the joint effect of a SESAM and Yb:CaF₂ Kerr lensing effect [228]. This result is more comparable to our experiment. Their Yb:CaF₂ crystal was 6.1-mm-long, 2.6% at .%Yb and our Yb:CaF₂ crystal is 6.07mm (optical path length) with 2% at .%Yb. The pump was a 7 W, 50 μm diameter fiber coupled diode which is about 4 times brighter than our pump (105 μm diameter, 8 W). The SESAM used in their experiment was Batop GmbH SAM- 294-II.23 (1045 nm, 1% saturable absorption, 70 $\mu\text{J/cm}^2$ saturation fluence). The ML pulse duration was 99 fs with 13.2 nm spectrum width and the average was 380 mW. The time-bandwidth product was calculated to be around 0.36 which is also close to transform limited.

They also mentioned a metastable regime corresponding to the transition between cw ML and Q-switching with ~1Hz switching frequency by adjusting cavity round trip dispersion. In our KLM experiment with ZnS, we observed a modulation with similar frequency. In the regime with strongest SFG radiation, the green light intensity and Q-switching operation were also modulated by ~1-2 Hz. They suggested that based on

the characteristic time, it seems that pump absorption and negative thermal lensing were affecting each other in a bistable cycle and shifted the laser oscillation mode between cw ML and Q-switching.

Pure KLM operation of Yb:CaF₂ has been reported by Machinet et al. from Laboratoire CELIA in 2012 [229]. To achieve this they employed a very high mode quality pump laser to overcome Yb:CaF₂ low non-linear refractive index issue. They used a single-mode ytterbium-doped fiber laser as the pump source. With 8.5W pump power, they achieved an output power of 560 mW with 3% output coupler. The pulses duration was 117 fs with 10 nm spectral width which corresponds to a time-bandwidth product of 0.319. In 2013, they improved the output power to 2.3 W average output power and compressed the pulse duration to 68.2 fs with an additional extra-cavity compressor [230]. The spectral width was 19 nm and the time-bandwidth product was 0.35. A single mode pump source has obvious advantages in pump mode overlapping, in their experiment the pump beam was focused to a 32 μm radius (at 1/e²) beam with a 4.4 mm confocal parameter. While in our experiment the pump radius could be focused to ~40 μm with 52.5 μm radius Lumics diode and 1:0.8 doublet pair, however the confocal length is only ~0.15 mm (150.6 μm).

8.2 Comparison with other modelocked lasers using extra medium elements

In 1993, Czeslaw et al. reported that with the use of monocrystalline ZnS as

intracavity high nonlinear index crystal as the Kerr medium, the pump power threshold for Ti:sapphire laser self-modelocking can be reduced from 6.2 W to 3.7 W with a 10% output coupler [231]. They also tested the laser with polycrystalline ZnS, which reduced the pump threshold for modelocking in the similar way, but introduced much higher intracavity loss. The 3 mm and 6 mm ZnS crystals used in our experiment are both of polycrystalline cubic, which could explain that due to high cavity loss we were not able to achieve cw ML with ZnS.

In 2000, Larotonda et al. reported a KLM Nd:YAG resonator with SF57 as additional intracavity element. The average output power was 800 mW (at 1064 nm) at 3W pump (at 808 nm) and the pulse duration was 4.5 ps without GVD compensation [232]. In 2003, they reported the multipulse KLM result by changing pump power based on the same experiment setup [233]. Our experimental ML and multipulse KLM results with Yb:CaF₂ and SF57 are similar to their result. Due to the Nd:YAG large emission cross sections ($2.8 \times 10^{-19} \text{ cm}^2$ versus Yb:CaF₂ $2.1 \times 10^{-21} \text{ cm}^2$), the pump threshold to overcome cavity loss is considerably lower in their case. Thus they were able to achieve single pulse operation at lower pump power and then shift to multiple-pulse mode by increasing the pump power. In contrast our system prefers to operate in multipulse mode only. This may be related to the quasi 3-level dynamics and higher lasing threshold operation for Yb:CaF₂.

So far no groups have published results on Yb:CaF₂ KLM with diode laser pumping and extra intracavity nonlinear elements as the Kerr lens medium and the work here represents the first such investigation.

9 Summary and future work

9.1 Thesis summary

In this thesis an all solid-state, compact, cost-effective, self-starting passively mode locked high repetition diode-pumped Yb:CaF₂ oscillator has been investigated. The modelocking mechanism based on SESAM absorption modulation and Kerr nonlinear lensing have been studied

In the case of the SEASM ML laser, the long upper-level lifetime and large gain saturation energy led to a strong tendency to Q-switch. Energetic pulses which exceeded the SESAM damage threshold were generated during the QML process.

Q-switched modelocked trains with 3.3 nm spectra bandwidth were generated which in principle could support pulses as short as 351 fs if proper dispersion compensation were introduced. However, the system operation was not stable leading to SESAM burn damage after a brief period of operation.

Further studies pursued the Kerr nonlinear lens effect to create rapid gain/loss modulation and large enough modulation depth for short laser pulse generation. KLM laser performance strongly depends on the resonator cavity configurations and is very sensitive to external perturbations, so it is necessary to optimize cavity design and isolate the cavity from mechanical vibrations, dust and air current.

For the issue of Yb:CaF₂ the low n_2 value and weak Kerr lensing can be overcome by inserting an extra intracavity high nonlinear index crystal as the Kerr lens medium.

Two nonlinear crystals ZnS and SF57 were investigated. Although ZnS crystal possesses the higher nonlinearity, the KLM performance was limited by self Q-switching operation, generation of second harmonic radiation and significant scattering losses. SF57 does not have any 2nd order nonlinear processes because of its symmetric structure and isotropic characteristics. The scattering loss is very low.

Unlike many typical KML laser systems which exhibit strong suppression effect of multi-pulsed operation, the KML Yb:CaF₂ laser configuration studied here always preferred to oscillate in multiple-pulse mode even at very low pumping power. Two kinds of multiple pulse ML operations have been observed and categorized by the pulse separation time. The first multiple-pulse operation mode with a few nanoseconds pulse separation is due to strong self-amplitude modulation (SAM) SAM effects. The system will split the pulse energy into multiple pulses and weaken the SAM effect to maximize intracavity power. The SAM effect is then balanced by counter-propagating pulse collision in the Kerr medium to give a stronger KLM enhancement of the roundtrip gain. The second regime is pulse splitting into a pair of twin pulses with a separation of the order of a nanosecond. It is possible that self-phase modulation in the Kerr crystal leads to the splitting of the single pulse into two pulses which then walk off from each other to a stabilized separation of close to a nanosecond. In the dispersion compensated cavity configuration (with the SF10 prism pair), even more complex pulse splitting and pulse walking effects have been observed.

While there are a number of mechanisms which can contribute to the multipulse behavior observed, further work is needed to clarify this issue.

9.2 Future work

Cavity loss control is one of the major considerations for Yb:CaF₂ CW ML operation. BATOP has released a new SESAM (SAM-1040-0.5-1ps), compared with the SESAM used in our experiment, it exhibits lower absorption and higher damage threshold (0.5% absorbance, 0.3% modulation depth, 0.2% non-saturable loss, 120 μJ/cm² saturation fluence and 3 mJ/cm² damage threshold [234]) which is more suitable for Yb:CaF₂ CW ML. Such a SESAM should be tried in place of the one used in the correct experiments. For the use of an external KLM element a monocrystalline ZnS will introduce much less cavity loss than the polycrystalline ZnS used in the present KLM operation. So it would be worthwhile to try these two new elements in our resonator designs.

The prism pair adds extra intracavity loss and forces the laser to oscillate in the horizontal polarization mode only. A 35% output power decrease for each prism has been reported by Lucca et al [235]. Chirped mirrors are a promising alternative choice for GVD compensation without average power loss if high quality mirrors are used.

The time-bandwidth products of our system under different operating configurations were not accurately measured. A better understanding of system operation could be

obtained if the pulse width were measured for all the different regions of operation reported here.

Due to Yb:CaF₂ relatively low emission cross-section ($2.1 \times 10^{-21} \text{ cm}^2$) and high gain saturation fluence, the availability of suitable SESAMs has been limited. Yb:KGW with one of the highest emission cross-sections ($2.8 \times 10^{-20} \text{ cm}^2$) [236] among Yb-doped materials is another promising candidate for use in femtosecond oscillators. A 3 W output power, 67 fs pulse duration, 16.8 nm (FWHM) bandwidth centered at 1032 nm, SESAM-assisted Kerr-lens mode-locked Yb:KGW laser has been reported in 2013 [237]. Yb:KGW exhibits a broader emission bandwidth 20 nm but a lower thermal conductivity of $\sim 3.3 \text{ W m}^{-1} \text{ K}^{-1}$ [236]. So more attention should be focused on crystal cooling if using Yb:KGW as a working material. It would be useful to try Yb:KGW as a femtosecond oscillator gain medium for the planned TW laser system.

The use of a thin-disk laser enables highly efficient cooling and also eliminates the requirement of high beam quality pump source [238]. A bright broad-spectrum pump diode and stable effective cooling could also improve laser efficiency. Such a thin-disk laser could also be explored as a femtosecond oscillator system.

With such future work it should be feasible to develop a stable fs oscillator serve as the seed system for a TW class direct diode pump Yb:CaF₂ laser in the future.

Bibliography

- [1] G. Steinmeyer, D. H. Sutter, L. Gallmann, N. Matuschek, U. Keller *Science* 286, 1507, 1999.
- [2] Christensen, James J. *The Structure of an Atom*. London: Wiley, 1990: 60-65.
- [3] E. Hecht and A. Zajac. *Optics*. Addison-Wesley, Menlo Park, CA, 1987
- [4] "Press Release: The Nobel Prize in Chemistry 1999". Nobelprize.org
- [5] Hopkins, John-Mark, and Wilson Sibbett. "Ultrashort-Pulse Lasers: Big Payoffs in a Flash." *Scientific American* 283.3 (2000): 72-79
- [6] Huang, D. *et al.* Optical coherence tomography. *Science* 254, 1178–1181 (1991).
- [7] Boivin, L., Wegmueller, M., Nuss, M. C. & Knox, W. H. 110 Channels x 2.35 Gb/s from a single femtosecond laser. *IEEE Photonics Technology Lett.* 11, 466–468 (1999).
- [8] Gabrielse G. *et al.*, *Phys. Rev. Lett.*, 97 (2006) 030802.
- [9] "Press Release: The 2005 Nobel Prize in Physics". Nobelprize.org
- [10] T. Südmeyer *et al.*, *Nature Photonics* 2, 599, 2008
- [11] Siders, C. W. *et al.* Detection of nonthermal melting by ultrafast X-ray diffraction. *Science* 286, 1340–1342 (1999)
- [12] Hammer, D. X. *et al.* Experimental investigation of ultrashort pulse laser induced breakdown thresholds in aqueous media. *IEEE J. Quantum Electron.* 32, 670–678 (1996)
- [13] Dr. Stefan Nolte. B. N. Chickov, et. al., *Applied Physics A, Mat. Sci. Proc.*, 63, 109-115 (1996).
- [14] G. M. Petrov and J. Davis, "Laser acceleration of light ions from high-intensity laser-target interactions," *Applied Physics B*. 2009

- [15] T.Bartel et al Focussing of short-pulse high intensity laser accelerated proton beams. *Nature Physics* 8, 139 (2012)
- [16] Gergely, L. Á., and T. Harko. "Testing general relativity with laser accelerated electron beams." arXiv preprint arXiv:1207.3770 (2012).
- [17] Jaroszynski, D. A., R. Bingham, and R. A. Cairns. *Laser-plasma Interactions*. Chapter 1 Page 5 Boca Raton: CRC/Taylor & Francis, 2009. Print.
- [18] P. F. Moulton, Spectroscopic and laser characteristics of Ti:Al₂O₃, *J. Opt. Soc. Am. B* 3, 125–133 (1986).
- [19] R. Ell, U. Morgner, F. X. KÄÄrtner, J. G. Fujimoto, E. P. Ippen, V. Scheuer, G. Angelow, T. Tschudi, M. J. Lederer, A. Boiko, and B. Luther-Davies, “Generation of 5-fs pulses and octave-spanning spectra directly from a Ti:sapphire laser,” *Opt. Lett.* 26, 373-375 (2001).
- [20] E. Deichsel, D. Schröder, J. Meusel, R. Hülsewede, J. Sebastian, S. Ludwig, P. Hennig, *Proc. SPIE* 6876, 68760K (2008)
- [21] F. Friebel, F. Druon, J. Boudeile, D. N. Papadopoulos, M. Hanna, P. Georges, P.Camy, J. L. Doualan, A. Benayad, R. Moncorgé, C. Cassagne, and G. Boudebs, “Diode-pumped 99 fs Yb:CaF₂ oscillator,” *Opt. Lett.* 34, 1474-1476 (2009)
- [22] Siebold, M., et al. "Yb: CaF₂—a new old laser crystal." *Applied Physics B* 97.2 (2009): 327-338.
- [23] J. Boudeile, J. Didierjean, P. Camy, J. L. Doualan, A. Benayad, V. Me'nard, R. Moncorge', F. Druon, F. Balembois, and P. Georges, B Thermal behaviour of ytterbium-doped fluorite crystals under high power pumping,[*Opt. Exp.*, vol. 16, no. 14, pp. 10 098–10 109, Jul. 2008.
- [24] <http://www.korth.de/index.php/162/items/10.html>

- [25] G. Machinet, P. Sevillano, F. Guichard, R. Dubrasquet, P. Camy, J.-L. Doualan, R. Moncorgé, P. Georges, F. Druon, D. Descamps, and E. Cormier, "High-brightness fiber laser-pumped 68 fs–2.3 W Kerr-lens mode-locked Yb: CaF₂ oscillator," *Opt. Lett.* 38, 4008-4010 (2013)
- [26] Pearson, Gary W., Czeslaw Radzewicz, and Jerzy S. Krasinski. "Use of ZnS as a self-focusing element in a self-starting Kerr lens modelocked Ti: sapphire laser." OE/LASE'94. International Society for Optics and Photonics, 1994.
- [27] Mukhopadhyay, P. K. "Femtosecond pulse generation and amplification in Yb-doped fibre oscillator-amplifier system." *Pramana* 75.5 (2010): 787-805.
- [28] Okhotnikov, Oleg, Anatoly Grudinin, and Markus Pessa. "Ultra-fast fibre laser systems based on SESAM technology: new horizons and applications." *New journal of physics* 6.1 (2004): 177.
- [29] Chang, Guoqing, et al. "Femtosecond Yb-fiber chirped-pulse-amplification system based on chirped-volume Bragg gratings." *Optics letters* 34.19 (2009): 2952-2954.
- [30]] Keller, Ursula. "Ultrafast solid-state lasers." *Progress in Optics* 46 (2004): 1-116.
- [31] L. E. Hargrove, R. L. Fork, and M. A. Pollack, “Locking of He–Ne laser modes induced by synchronous intractivity modulation,” *Appl. Phys. Lett.*, vol. 5, pp. 4–6, 1964
- [32] H. W. Mocker and R. J. Collins, “Mode competition and self-locking effects in a Q-switched ruby laser,” *Appl. Phys. Lett.*, vol. 7, pp. 270–272, 1965
- [33] E. P. Ippen, C. V. Shank, and A. Dienes, “Passive mode locking of the cw dye laser,” *Appl. Phys. Lett.*, vol. 21, pp. 348–350, 1972.

- [34] C. V. Shank and E. P. Ippen, "Sub-picosecond kilowatt pulses from a mode-locked cw dye laser," *Appl. Phys. Lett.*, vol. 24, pp. 373–375, 1974.
- [35] Keller, U., et al. "Solid-state low-loss intracavity saturable absorber for Nd: YLF lasers: an antiresonant semiconductor Fabry–Perot saturable absorber." *Optics letters* 17.7 (1992): 505-507.
- [36] Keller, U. "Ultrafast solid-state laser oscillators: a success story for the last 20 years with no end in sight." *Applied Physics B* 100.1 (2010): 15-28.
- [37] Spence, David E., P. Np Kean, and Wilson Sibbett. "60-fsec pulse generation from a self-mode-locked Ti: sapphire laser." *Optics letters* 16.1 (1991): 42-44.
- [38] E.P. Ippen, "Principles of Passive Mode Locking," *Appl. Phys. B*, 58, pp. 159-170, 1994.
- [39] McClung, F.J., Hellwarth, R.W.: Giant optical pulsations from ruby; *J. Appl. Phys.* 33(1962) 828–829
- [40] Collins, R.J., Kisliuk, P.: Control of population inversion in pulsed optical masers by feedback modulation; *J. Appl. Phys.* 33 (1962) 2009–2011.
- [41] New, G.H.C.: Pulse evolution in mode-locked quasi-continuous lasers; *IEEE J. Quantum Electron.* 10 (1974) 115–124
- [42] Kuizenga, D.J., Siegman, A.E.: FM and AM mode locking of the homogeneous laser –Part II: Experimental results in a Nd:YAG laser with internal FM modulation; *IEEEJ. Quantum Electron.* 6 (1970) 709–715.

- [43] Haus, H.A.: Theory of modelocking with a fast Saturable absorber; *J. Appl. Phys* 46(1975) 3049–3058.
- [44] E.P. Ippen, C.V. Shank, A. Dienes: "Passive mode locking of the cw dye laser," *Appl. Phys. Lett.* 21, 348-350 (1972)
- [45] Ippen, E.P., Eichenberger, D.J., Dixon, R.W.: Picosecond pulse generation by passive modelocking of diode lasers; *Appl. Phys. Lett.* 37 (1980) 267–269.
- [46] Fork, R. L., B. I. Greene, and C. V. Shank. "Generation of optical pulses shorter than 0.1 psec by colliding pulse mode locking." *Applied Physics Letters* 38.9 (1981): 671-672.
- [47] J. A. Valdmanis et al., *Opt. Lett.* 10, 131, 1985
- [48] R. L. Fork et al., *Opt. Lett.* 12, 483, 1987
- [49] C. Hönninger, G. Zhang, U. Keller, and A. Giesen, "Femtosecond Yb:YAG laser using semiconductor saturable absorbers," *Opt. Lett.* 20, 2402-2404 (1995)
- [50] F. Salin, J. Squier, M. Piché: Mode locking of Ti:Al₂O₃ lasers and selffocusing: A Gaussian approximation, *Opt. Lett.* 16, 1674-1676 (1991).
- [51] U. Keller et al. *Opt. Lett.* 17, 505, 1992
- [52] Kerr-lens mode-locked Ti:sapphire laser producing pulses in the two-cycle regime; *Opt. Lett.* 24 (1999) 631–633
- [53] Morgner, U., Kärtner, F.X., Cho, S.H., Chen, Y., Haus, H.A., Fujimoto, J.G., Ippen, E.P., Scheuer, V., Angelow, G., Tschudi, T.: Sub-two-cycle pulses from a Kerr-lens mode-locked Ti:sapphire laser; *Opt. Lett.* 24 (1999) 411–413.

- [54] Ell, R., Morgner, U., Kärtner, F.X., Fujimoto, J.G., Ippen, E.P., Scheuer, V., Angelow,G., Tschudi, T., Lederer, M.J., Boiko, A., Luther-Davis, B.: Generation of 5-fs pulsesand octave-spanning spectra directly from a Ti:sapphire laser; Opt. Lett. 26 (2001)373–375,
- [55] Schenkel, B., Biegert, J., Keller, U., Vozzi, C., Nisoli, M., Sansone, G., Stagira, S., Silvestri, S.D., Svelto, O.: Generation of 3.8-fs pulses from adaptive compression of a cascaded hollow fiber supercontinuum; Opt. Lett. 28
- [56] Biegert, J., et al. "Generation of 3.8-fs Pulses Through Adaptive Cascaded Hollow Fiber Compression." Ultrafast Optics IV. Springer New York, 2004. 91-96.
- [57] M.Y Shverdin, D. R. Walker, D.D. Yavuz, G.Y. Yin and S.E. Harris, "Generation of a Single-Cycle Optical Pulse," Phys.Rev.Lett. 94, 033904 (2005)
- [58] H. Hentschel, R. Kienberger, Ch. Spielmann, G. A. Reider, N. Milosevic,T. Brabec, P. Corkum, U. Heinzmann, M. Drescher, F. Krausz: "Attosecond Metrology," Nature 414, 509-513 (2001).
- [59] E. Goulielmakis, M. Schultze, M. Hofstetter, V. S. Yakovlev, J. Gagnon, M. Uiberacker, A. L. Aquila, E. M. Gullikson, D. T. Attwood, R. Kienberger, F. Krausz, U. Kleineberg "Single-Cycle Nonlinear Optics" Science, June 20, 2008
- [60] Kun Zhao, Qi Zhang, Michael Chini, Yi Wu, Xiaowei Wang, and Zenghu Chang, "Tailoring a 67 attosecond pulse through advantageous phase-mismatch," Opt. Lett. 37, 3891-3893 (2012)

- [61] Brabec, T. & Krausz, F. Intense few-cycle laser fields: Frontiers of nonlinear optics. *Rev. Mod. Phys.* 72, 545–591 (2000)
- [62] Siebold, M., et al. "High-energy, diode-pumped, nanosecond Yb: YAG MOPA system." *Optics express* 16.6 (2008): 3674-3679.
- [63] <https://www.llnl.gov/news/newsreleases/2013/Aug/NR-13-08-04.html>
- [64] Steinmeyer, G., et al. "Frontiers in ultrashort pulse generation: pushing the limits in linear and nonlinear optics." *Science* 286.5444 (1999): 1507-1512.
- [65] T.Y. Fan and R.L. Byer, Diode pumped solid state lasers, *IEEE J. Quantum Electron.* 24, 895, 1988.
- [66] A. Giesen, H. Gudel, A. Voss, K. Witting, U. Brauch, H. Opower, Scalable concept for diode-pumped high power solid state laser, *Appl. Phys. B* 58, 365–372, 1994.
- [67] F. Druon, F. Balembois and P. Georges, ‘Laser crystals for the production of ultra-short laser pulses’, *Annales de Chimie Science des Matériaux*, Éditions scientifiques et médicales Elsevier SAS, Vol. 28, Issue 6 , Pages 47-72
- [68] Hönniger, C., et al. "Femtosecond Yb: YAG laser using semiconductor saturable absorbers." *Optics letters* 20.23 (1995): 2402-2404.
- [69] C. Hönniger, F. Morier-Genoud, M. Moser, U. Keller, L. R. Brovelli, and C. Harder, “Efficient and tunable diode-pumped femtosecond Yb:glass lasers,” *Opt. Lett.* 23, 126-128 (1998)

- [70] Liu, H., J. Nees, and G. Mourou. "Diode-pumped Kerr-lens mode-locked Yb: KY (WO₄)₂ laser." *Optics letters* 26.21 (2001): 1723-1725.
- [71] F. Druon, S. Chénais, P. Raybaut, F. Balembois, P. Georges, R. Gaumé, G. Aka, B. Viana, S. Mohr, and D. Kopf, "Diode-pumped Yb:Sr₃Y(BO₃)₃ femtosecond laser," Opt. Lett. 27, 197-199 (2002)
- [72] Frédéric Druon, François Balembois, and Patrick Georges, "Ultra-short-pulsed and highly-efficient diode-pumped Yb:SYS mode-locked oscillators," Opt. Express 12, 5005-5012 (2004)
- [73] A. A. Lagatsky, A. R. Sarmani, C. T. A. Brown, W. Sibbett, V. E. Kisel, A. G. Selivanov, I. A. Denisov, A. E. Troshin, K. V. Yumashev, N. V. Kuleshov, V. N. Matrosov, T. A. Matrosova, and M. I. Kupchenko, "Yb-doped YVO₄ crystal for efficient Kerr-lens mode locking in solid-state lasers," Opt. Lett. 30, 3234-3236 (2005)
- [74] S. Rivier, X. Mateos, J. Liu, V. Petrov, U. Griebner, M. Zorn, M. Weyers, H. Zhang, J. Wang, and M. Jiang, "Passively mode-locked Yb:LuVO₄ oscillator," Opt. Express 14, 11668-11671 (2006)
- [75] S. Rivier, X. Mateos, J. Liu, V. Petrov, U. Griebner, M. Zorn, M. Weyers, H. Zhang, J. Wang, and M. Jiang, "Passively mode-locked Yb:LuVO₄ oscillator," Opt. Express 14, 11668-11671 (2006)
- [76] J. Boudeile, F. Druon, M. Hanna, P. Georges, Y. Zaouter, E. Cormier, J. Petit, P. Goldner, and B. Viana, "Continuous-wave and femtosecond laser operation of

Yb:CaGdAlO₄ under high-power diode pumping," Opt. Lett. 32, 1962-1964 (2007).

- [77] Simon Rivier, Andreas Schmidt, Christian Kränkel, Rigo Peters, Klaus Petermann, Günter Huber, Martin Zorn, Markus Weyers, Andreas Klehr, Götz Erbert, Valentin Petrov, and Uwe Griebner, "Ultrashort pulse Yb:LaSc₃(BO₃)₄ mode-locked oscillator," Opt. Express 15, 15539-15544 (2007)
- [78] García-Cortés, J. M. Cano-Torres, M. D. Serrano, C. Cascales, C. Zaldo, S. Rivier, X. Mateos, U. Griebner and V. Petrov, "Spectroscopy and Lasing of Yb-Doped NaY(WO₄)₂:Tunable and Femtosecond Mode-Locked Laser Operation," IEEE J. Quantum Electron. 43, 758-764 (2007)
- [79] S. Uemura and K. Torizuka, "Kerr-Lens Mode-Locked Diode-Pumped Yb:YAG Laser with the Transverse Mode Passively Stabilized," Appl. Phys. Express 1, 012007 (2008)
- [80] F. M. Bain ; A. A. Lagatsky ; C. T. A. Brown ; W. Sibbett; High-power Kerr-lens mode-locked ytterbium lasers. Proc. SPIE 6871, Solid State Lasers XVII: Technology and Devices, 68712L (February 14, 2008); doi:10.1117/12.762933
- [81] F. Friebel, F. Druon, J. Boudeile, D. N. Papadopoulos, M. Hanna, P. Georges, P. Camy, J. L. Doualan, A. Benayad, R. Moncorgé, C. Cassagne, and G. Boudebs, "Diode-pumped 99 fs Yb:CaF₂ oscillator," Opt. Lett. 34, 1474-1476 (2009)
- [82] Masaki Tokurakawa, Akira Shirakawa, Ken-ichi Ueda, Hideki Yagi, Meichin Noriyuki, Takagimi Yanagitani, and Alexander A. Kaminskii, "Diode-pumped

- ultrashort-pulse generation based on Yb³⁺:Sc₂O₃ and Yb³⁺:Y₂O₃ ceramic multi-gain-media oscillator," Opt. Express 17, 3353-3361 (2009)
- [83] Uemura, Sadao. "Sub-40-fs pulses from a diode-pumped Kerr-lens mode-locked Yb-doped yttrium aluminum garnet laser." Japanese Journal of Applied Physics 50.1 (2011): 0201.
- [84] Machinet, Guillaume, P. Sevillano, F. Guichard, R. Dubrasquet, P. Camy, J-L. Doualan, R. Moncorgé et al. "High-brightness fiber laser-pumped 68 fs–2.3 W Kerr-lens mode-locked Yb: CaF₂ oscillator." *Optics letters* 38, no. 20 (2013): 4008-4010.
- [85] Haitao Zhao and Arkady Major, "Powerful 67 fs Kerr-lens mode-locked prismless Yb:KGW oscillator," Opt. Express 21, 31846-31851 (2013)
- [86] Frédéric Druon, Sandrine Ricaud, Dimitris N. Papadopoulos, Alain Pellegrina, Patrice Camy, Jean Louis Doualan, Richard Moncorgé, Antoine Courjaud, Eric Mottay, and Patrick Georges, "On Yb:CaF₂ and Yb:SrF₂: review of spectroscopic and thermal properties and their impact on femtosecond and high power laser performance [Invited]," Opt. Mater. Express 1, 489-502 (2011)
- [87] Ito, Masahiko, et al. "Crystal growth, Yb³⁺ spectroscopy, concentration quenching analysis and potentiality of laser emission in Ca_{1-x}Yb_xF_{2+x}." Journal of Physics: Condensed Matter 16.8 (2004): 1501.
- [88] Druon, Frédéric, Francois Balembois, and Patrick Georges. "New materials for short-pulse amplifiers." Photonics Journal, IEEE 3.2 (2011): 268-273.

- [89] J. Boudeile, J. Didierjean, P. Camy, J. L. Doualan, A. Benayad, V. Me'nard, R. Moncorge', F. Druon, F. Balembois, and P. Georges, B Thermal behaviour of ytterbium-doped fluorite crystals under high power pumping,[Opt. Exp., vol. 16, no. 14, pp. 10 098–10 109, Jul. 2008.
- [90] M. Siebold, M. Hornung, R. Boedefeld, S. Podleska, S. Klingebiel,C. Wandt, F. Krausz, S. Karsch, R. Uecker, A. Jochmann, J. Hein, and M. C. Kaluza, "Terawatt diode-pumped Yb:CaF₂ laser," Opt. Lett. 33, 2770–2772 (2008).
- [91] Siegman, Anthony E. "Lasers, 1986." p2.
- [92] W. Koechner, Solid-State Laser Engineering, Springer Series in Optical Sciences, Volume 1, Second Edition, Springer-Verlag 1985
- [93] D. E. McCumber, "Einstein relations connecting broadband emission and absorption spectra", Phys. Rev. 136 (4A), A954 (1964)
- [94] S. Chénais, F. Balembois, F. Druon, G. Lucas-Leclin, P. Georges, Thermal lensing in diode-pumped ytterbium laser — Part II Evaluation of quantum efficiencies and thermo-optic coefficients, IEEE J. Quantum Electron. 40(9), 1235, 2004.
- [95] Fermann, Martin E., Almantas Galvanauskas, and Gregg Sucha, eds. Ultrafast lasers: Technology and applications. Vol. 80. CRC Press, 2002. P52
- [96] W. P. Risk, "Modeling of longitudinally pumped solid-state lasers exhibiting reabsorption losses", J. Opt. Soc. Am. B 5 (7), 1412 (1988)
- [97] D. C. Brown, J. M. Singley, K. Kowalewski, J. Guelzow, and V. Vitali, "High sustained average power cw and ultrafast Yb:YAG near-diffraction-limited cryogenic solid-state laser," Opt. Express 18, 24770–24792 (2010)

- [98] Frédéric Druon, Sandrine Ricaud, Dimitris N. Papadopoulos, Alain Pellegrina, Patrice Camy, Jean Louis Doualan, Richard Moncorgé, Antoine Courjaud, Eric Mottay, and Patrick Georges, "On Yb:CaF₂ and Yb:SrF₂: review of spectroscopic and thermal properties and their impact on femtosecond and high power laser performance [Invited]," Opt. Mater. Express 1, 489-502 (2011)
- [99] V. Petit, J. L. Doualan, P. Camy, V. Menard, and R. Moncorgé, —CW and tunable laser operation of Yb³⁺ doped CaF₂, Appl. Phys. B 78(6), 681–684 (2004)
- [100] A. Lucca, M. Jacquemet, F. Druon, F. Balembois, P. Georges, P. Camy, J. L. Doualan, and R. Moncorgé, "High-power tunable diode-pumped Yb³⁺:CaF₂ laser," Opt. Lett. 29, 1879-1881 (2004)
- [101] Yb-doped YLF and CaF₂ crystal laser at room temperature Optical Materials (30 August 2010), doi:10.1016/j.optmat.2010.07.019 by Angela Pirri, Guido Toci, Daniele Alderighi, Matteo Vannini
- [102] Günter, Peter, and Jean-Pierre Huignard, eds. Photorefractive materials and their applications. Vol. 2. Berlin: Springer, 1989.
- [103] M. Robinson and C. K. Asawa, "Stimulated Emission from Nd³⁺ and Yb³⁺ in Noncubic Sites of Neodymium- and Ytterbium-Doped CaF₂," J. Appl. Phys. 38, 4495 (1967)
- [104] P. Sorokin, M. Stevenson, IBM J. Res. Dev. 5, 56 (1961)
- [105] J. Lawson, S. Payne, J. Opt. Soc. Am. B, Opt. Phys. 8, 1404 (1991)
- [106] Y. Kariss, P.P. Feofilov, Opt. Spectrosk. (USSR) 14, 169 (1963)
- [107] Kaminskii, L. Kornienko, L. Makarenko, A. Prokhorov, M. Fursikov, Sov. Phys. JETP 19, 262 (1964)
- [108] R. Keyes, T. Quist, Appl. Phys. Lett. 4, 50 (1964)

- [109] S. Hatch, W. Parsons, R. Weagley, Am. Ceram. Soc. Bull. 44, 410 (1965)
- [110] Stephen A. Payne, John A. Caird, L. L. Chase, L. K. Smith, N. D. Nielsen, and William F. Krupke, "Spectroscopy and gain measurements of Nd³⁺ in SrF₂ and other fluorite-structure hosts," J. Opt. Soc. Am. B 8, 726-740 (1991)
- [111] Petit, V., et al. "CW and tunable laser operation of Yb³⁺ doped CaF₂." Applied Physics B 78.6 (2004): 681-684.
- [112] Koerner, Joerg, et al. "Measurement of temperature-dependent absorption and emission spectra of Yb: YAG, Yb: LuAG, and Yb: CaF₂ between 20° C and 200° C and predictions on their influence on laser performance." JOSA B 29.9 (2012): 2493-2502.
- [113] Siebold, M., et al. "Yb: CaF₂—a new old laser crystal." Applied Physics B 97.2 (2009): 327-338.
- [114] Uemura, Sadao. "Sub-40-fs pulses from a diode-pumped Kerr-lens mode-locked Yb-doped yttrium aluminum garnet laser." Japanese Journal of Applied Physics 50.1 (2011): 0201
- [115] Machinet, Guillaume, P. Sevillano, F. Guichard, R. Dubrasquet, P. Camy, J-L. Doualan, R. Moncorgé et al. "High-brightness fiber laser-pumped 68 fs–2.3 W Kerr-lens mode-locked Yb: CaF₂ oscillator." *Optics letters* 38, no. 20 (2013): 4008-4010.
- [116] Robert Adair, L. L. Chase, and Stephen A. Payne, "Nonlinear refractive-index measurements of glasses using three-wave frequency mixing," J. Opt. Soc. Am. B 4, 875-881 (1987)

- [117] Welch, David F. "A brief history of high-power semiconductor lasers." Selected Topics in Quantum Electronics, IEEE Journal of 6.6 (2000): 1470-1477.
- [118] Goubau, George, and F. Schwering. "On the guided propagation of electromagnetic wave beams." Antennas and Propagation, IRE Transactions on 9.3 (1961): 248-256.
- [119] H. Kogelnik and T. Li,"Laser Beams and Resonators," Appl. Opt. 5,pp. 1550 — 1566 (1966)
- [120] Astigmatically compensated cavities for CW dye lasers H. Kogelnik, E. Ippen, A. Dienes, C. Shank
- [121] F. A. Jenkins and H. E. White, Fundamental of Optics. New York: McGraw-Hill, 1957, p95
- [122] D. C. Hanna, "Astigmatic Gaussian beams produced by axially asymmetric laser cavities", IEEE J. Quantum Electron. QE-5, 483-488 (1969)
- [123] Franken, P.; Hill, A.; Peters, C.; Weinreich, G. (1961). "Generation of Optical Harmonics". Physical Review Letters 7 (4): 118.
- [124] Nonlinear Optics, Third Edition, Robert W. Boyd Sec.1.1
- [125] J. Kerr, Phil. Mag. 3 (1877) p.321.
- [126] Janice E. Aber, Maurice C. Newstein, and Bruce A. Garetz, "Femtosecond optical Kerr effect measurements in silicate glasses," J. Opt. Soc. Am. B 17, 120-127 (2000)

- [127] Robert Adair, L. L. Chase, and Stephen A. Payne, "Nonlinear refractive-index measurements of glasses using three-wave frequency mixing," J. Opt. Soc. Am. B 4, 875-881 (1987)
- [128] R. Y. Chiao, E. Garmire, and C. H. Townes, "Self-trapping of optical beams", Phys. Rev. Lett. 13 (15), 479 (1964) Critical Power
- [129] Gaeta, Alexander L. "Catastrophic collapse of ultrashort pulses." Physical Review Letters 84.16 (2000): 3582.
- [130] Trofimov, V. A., and T. M. Lysak. "Catastrophic self-focusing of axially symmetric laser beams due to cascading SHG." Laser Optics 2010. International Society for Optics and Photonics, 2010
- [131] R. W. Boyd, Nonlinear Optics (Academic, Boston, Mass., 1992), Sec. 6.2.
- [132] E. Schulz *et al.*, App. Phys. B 95: 269 (2009)
- [133] D. E. Spence, P. N. Kean, and W. Sibbett, "60-fsec pulse generation from a self-mode-locked Ti:sapphire laser," Opt. Lett. 16, 42-44 (1991)
- [134] M. Pich~, Optics Comm. 86 (1991) 156.
- [135] S. Chen and J. Wang, Optics Lett. 16 (1991) 1689.
- [136] G.W. Pearson, C. Radzewicz and J.S. Krasinski, Optics Comm. 94 (1992) 221
- [137] Vittorio Magni, Giulio Cerullo, Sandro De Silvestri, ABCD matrix analysis of propagation of gaussian beams through Kerr media, Optics Communications, Volume 96, Issues 4–6, 15 February 1993, Pages 348-355

- [138] L. E Hargrove, R. L Fork, M. A Pollock, "Locking of He-Ne laser modes induced by synchronous intracavity modulation (diffraction by phonons in crystals E)," Appl. Phys. Lett. **5**, 4 (1964)
- [139] D. E. Spence, P. N. Kean, and W. Sibbett, "60-fsec pulse generation from a self-mode-locked Ti: sapphire laser," Opt. Lett. **16**, 42-44 (1991)
- [140] Keller, U., et al. "Femtosecond pulses from a continuously self-starting passively mode-locked Ti: sapphire laser." Optics letters **16**.13 (1991): 1022-1024.
- [141] Dzhibladze, M. I., et al. "Mode locking in a fiber laser." Quantum Electronics **13**.2 (1983): 245-247.
- [142] "Solid-state lasers," J. Appl. Phys. **34**, 2289 (1963).
- [143] WALL, KEVINF, and Antonio Sanchez. "Titanium sapphire lasers." The Lincoln Laboratory Journal **3**, no. 3 (1990): 447-462.
- [144] V. Petit, P. Camy, J-L. Doualan, X. Portier, and R. Moncorgé, "Spectroscopy of Yb³⁺:CaF₂ : From isolated centers to clusters," Phys. Rev. B **78** (8), 085131-1 – 085131-12 (2008).
- [145] C. L. Tang, H. Statz, and G. deMars, "Spectral output and spiking behavior of solid-state lasers," J. Appl. Phys. **34**, 2289 (1963).
- [146] H. A. Haus, "Short pulse generation," in *Compact Sources of Ultrashort Pulses*, I. I. N. Duling, Eds. (Cambridge University Press 1995, New York, 1995) pp. 1-56.

- [147] Honninger, C., Paschotta, R., Morier-Genoud, F., Moser, M., Keller, U.: Q-switchingstability limits of cw passive modelocking; J. Opt. Soc. Am. B **16** (1999) 46–56.
- [148] Keller, U. "2.1 Ultrafast solid-state lasers." Laser Physics and Applications. Springer Berlin Heidelberg, 2007. 33-167.
- [149] Haus, H.A.: A theory of forced mode locking; IEEE J. Quantum Electron. **11** (1975) 323–330.
- [150] U. Keller, J. A. Valdmanis, M. C. Nuss, and A. M. Johnson, "53ps pulses at 1.32 μm from a harmonic mode-locked Nd:YAG laser" IEEE J. Quantum Electron., vol. 24, pp. 427-430, 1988
- [151] Mode locking and Q switching of a diode laser pumped neodymium - doped yttrium lithium fluoride laser Download PDF G. T. Maker and A. I. Ferguson.
- [152] High-frequency acousto-optic mode locker for picosecond pulse generation. Keller U, Li KD, Khuri-Yakub BT, Bloom DM, Weingarten KJ, Gerstenberger DC.
- [153] Kopf, D., et al. "Pulse shortening in a Nd: glass laser by gain reshaping and soliton formation." Optics letters 19.24 (1994): 2146-2148.
- [154] Laser Physics and Applications". Chapter 2.1 Ultrafast solid-state lasers U. Keller
- [155] Q-switching stability limits of continuous-wave passive mode locking, Hönninger, Paschotta, Morier-Genoud, Moser and Keller [1999]

- [156] Solid-state low-loss intracavity saturable absorber for Nd:YLF lasers: an antiresonant semiconductor Fabry-Perot saturable absorber" Optics Letters, **17**, 505-507 (1992).
- [157] New, G.H.C.: Modelocking of quasi-continuous lasers; Opt. Commun. **6** (1972) 188–192.
- [158] Kartner, F. X., I. D. Jung, and U. Keller. "Soliton mode-locking with saturable absorbers." Selected Topics in Quantum Electronics, IEEE Journal of **2.3** (1996): 540-556.
- [159] Haus, H.A.: Theory of modelocking with a fast saturable absorber; J. Appl. Phys **46** (1975) 3049–3058.
- [160] Appl. Phys. B **79**, 285, 2004
- [161] D. J. H. Maas, et al., *Optics Express* **16**, 7571, 2008
- [162] Paschotta, R., Keller, U.: Passive mode locking with slow saturable absorbers; Appl. Phys. B **73** (2001) 653–662.
- [163] C. Hönniger, R. Paschotta, F. Morier-Genoud, M. Moser, U. Keller, JOSA B **16**, 46-56 (1999)
- [164] U. Keller et al. Opt. Lett. 17, 505, 1992 IEEE JSTQE 2, 435, 1996
- [165] H. A. Haus, J. G. Fujimoto, E. P. Ippen, “Structures for additive pulse modelocking,” J. Opt. Soc. Am. B **8**, 2068, 1991.
- [166] Sub-10-fs Ti:sapphire Kerr-lens Mode Locked Oscillator Eugen Slobodchikov, Shuji Sakabe, Tomoyuki Kuge, Sakae Kawato, Masaki Hashida, Yasukazu Izawa

- [167] Brabec, T., Spielmann, C., Krausz, F.: Mode locking in solitary lasers; Opt. Lett. **16**(1991) 1961–1963.
- [168] H. A. Haus, J. G. Fujimoto, E. P. Ippen, "Structures for additive pulse modelocking," J. Opt. Soc. Am. B **8**, 2068, 1991
- [169] Keller, U., Weingarten, K.J., Kartner, F.X., Kopf, D., Braun, B., Jung, I.D., Fluck,R., Hönninger, C., Matuschek, N., Aus der Au, J.: Semiconductor saturable absorbermirrors (SESAMs) for femtosecond to nanosecond pulse generation in solid-state lasers; IEEE J. Sel. Topics Quantum Electron. **2** (1996) 435–453
- [170] Kartner, F.X.; Jung, I.D.; Keller, U., "Soliton mode-locking with saturable absorbers," Selected Topics in Quantum Electronics, IEEE Journal of , vol.2, no.3, pp.540,556, Sep 1996
- [171] Paschotta, R., Keller, U.: Passive mode locking with slow saturable absorbers; Appl.Phys. B **73** (2001) 653–662.
- [172] J. P. Gordon and R. L. Fork, Opt. Lett. **9**,153 (1984).
- [173] Diels, Jean-Claude, and Wolfgang Rudolph. Ultrashort laser pulse phenomena. Academic press, 2006. P115
- [174] C. Hönninger, R. Paschotta, F. Morier-Genoud, M. Moser, and U. Keller, " Q -switching stability limits of continuous-wave passive mode locking," J. Opt. Soc. Am. B **16**, 46-56 (1999)

- [175] D. J. Kuizenga and A. E. Siegman, "FM and AM mode locking of the homogeneous laser - Part I: Theory", IEEE J. Quantum Electron. 6 (11), 694 (1970)
- [176] Picosecond gain spectroscopy of a laser dye during mode-locked laser action Yamashita, Mikio Sato, Takuzo
- [177] J. Mark *et al.*, "Femtosecond pulse generation in a laser with a nonlinear external resonator", Opt. Lett. 14 (1), 48 (1989)
- [178] E. P. Ippen *et al.*, "Additive pulse mode locking", J. Opt. Soc. Am. B 6 (9), 1736 (1989)
- [179] Keller, U. "Ultrafast solid-state laser oscillators: a success story for the last 20 years with no end in sight." Applied Physics B 100.1 (2010): 15-28.
- [180] L.R. Brovelli, I.D. Jung, D. Kopf, M. Kamp, M. Moser, F.X. Kärtner, U. Keller, Electron. Lett. 31, 287 (1995)
- [181] http://www.batop.com/information/SAM_infos.html
- [182] http://www.limo.de/fileadmin/PDF/Fasergekoppelte_Pumpmodule/LIMO32-F200-DL980-LM.pdf
- [183] http://www.lumics.com/fileadmin/user_upload/Datasheets_Lumics_Products/Multimode/TO_package/LU09xxT090.pdf
- [184] Joerg Koerner, Christian Vorholt, Hartmut Liebetrau, Martin Kahle, Diethard Kloepfel, Reinhard Seifert, Joachim Hein, and Malte C. Kaluza, "Measurement of temperature-dependent absorption and emission spectra of Yb:YAG,

Yb:LuAG, Yb:CaF₂ between 20 °C and 200 °C and predictions on their influence on laser performance,” J. Opt. Soc. Am. B **29**, 2493-2502 (2012)

[185] <http://www.batop.com/products/saturable-absorber/saturable-absorber-mirror/saturable-absorber-mirror-1040nm.html>

[186] Hönniger, Clemens, et al. “Q-switching stability limits of continuous-wave passive mode locking.” JOSA B 16.1 (1999): 46-56.

[187] Larotonda, M. A., A. A. Hnilo, and F. P. Diodati. “Diode-pumped self-starting Kerr-lens mode locking Nd: YAG laser.” Optics communications 183.5 (2000): 485-491.

[188] Träger, Frank, ed. Springer handbook of lasers and optics. Chapter5 Springer, 2007.

[189] Boudeile, Justine, et al. “Thermal behavior of ytterbium-doped fluorite crystals under high power pumping.” *Optics express* 16.14 (2008): 10098-10109.

[190] F. Friebel, F. Druon, J. Boudeile, D. N. Papadopoulos, M. Hanna, P. Georges, P. Camy, J. L. Doualan, A. Benayad, R. Moncorgé, C. Cassagne, and G. Boudebs, “Diode-pumped 99 fs Yb:CaF₂ oscillator,” Opt. Lett. **34**, 1474-1476 (2009).

[191] S. Ricaud, D. N. Papadopoulos, P. Camy, J. L. Doualan, R. Moncorgé, A. Courjaud, E. Mottay, P. Georges, and F. Druon, —Highly efficient, high-power, broadly tunable, cryogenically cooled and diode-pumped Yb:CaF₂,|| Opt. Lett. 35(22), 3757–3759 (2010).

- [192] J. L. Ladison, J. J. Price, J. D. Helfinstine, and W. R. Rosch, —Hardness, elastic modulus, and fracture toughness bulk properties in Corning calcium fluoride, Proc. SPIE 5754, 1329–1338 (2004).
- [193] Matthew J Bohn, R Jason Jones, Jean-Claude Diels, Mutual Kerr-lens mode-locking, Optics Communications, Volume 170, Issues 1–3, 15 October 1999, Pages 85-92,
- [194] Janice E. Aber, Maurice C. Newstein, and Bruce A. Garetz, “Femtosecond optical Kerr effect measurements in silicate glasses,” J. Opt. Soc. Am. B **17**, 120-127 (2000)
- [195] http://fp.optics.arizona.edu/optomech/references/glass/Schott/tie-35_transmittance_us.pdf
- [196] Lai, Ming, Jeff Nicholson, and Wolfgang Rudolph. “Multiple pulse operation of a femtosecond Ti: sapphire laser.” Optics communications 142.1 (1997): 45-49.
- [197] Rothenberg, Joshua E. “Pulse splitting during self-focusing in normally dispersive media.” Optics letters 17.8 (1992): 583-585.
- [198] Rothenberg, Joshua E. “Space–time focusing: breakdown of the slowly varying envelope approximation in the self-focusing of femtosecond pulses.” Optics letters 17.19 (1992): 1340-1342.
- [199] Höninger, Clemens, et al. "Q-switching stability limits of continuous-wave passive mode locking." JOSA B 16.1 (1999): 46-56.

- [200] Bohn, Matthew J., R. Jason Jones, and Jean-Claude Diels. "Mutual Kerr-lens mode-locking." Optics communications 170.1 (1999): 85-92.
- [201] K. J. Weingarten et al., "In situ small-signal gain of solid-state lasers determined from relaxation oscillation frequency measurements", Opt. Lett. 19 (15), 1140 (1994)
- [202] A.Schlatter et al., "Pulse-energy dynamics of passively mode-locked solid-state lasers above the Q-switching threshold", J. Opt. Soc. Am. B 21 (8), 1469 (2004)
- [203] Wagner, Hans Peter, et al. "Dispersion of the second-order nonlinear susceptibility in ZnTe, ZnSe, and ZnS." Physical Review B 58.16 (1998): 10494.
- [204] Klein, Claude A., and James Pappis. "ZnS, ZnSe, and ZnS/ZnSe windows: their impact on FLIR system performance." Optical Engineering 25.4 (1986): 254519-254519.
- [205] Gu, Bing, et al. "Three-photon absorption saturation in ZnO and ZnS crystals." Journal of Applied Physics 103.7 (2008): 073105.
- [206] Lai, Ming, Jeff Nicholson, and Wolfgang Rudolph. "Multiple pulse operation of a femtosecond Ti: sapphire laser." Optics communications 142.1 (1997): 45-49.J.-C. Diels, W. Rudolph, Ultrashort Laser Pulse Phenomena (Academic Press, San Diego, 1996).
- [207] Joshua E. Rothenberg, "Pulse splitting during self-focusing in normally dispersive media," Opt. Lett. 17, 583-585 (1992)
- [208] Ranka, Jinendra K., and Alexander L. Gaeta. "Breakdown of the slowly varying

envelope approximation in the self-focusing of ultrashort pulses." Optics letters 23.7 (1998): 534-536.

[209] Major, Arkady, et al. "Dispersion of the nonlinear refractive index in sapphire." Optics letters 29.6 (2004): 602-604.

[210] Lai, Ming. "Self-starting, self-mode-locked Ti: sapphire laser." Optics letters 19.10 (1994): 722-724.

[211] Larotonda, Miguel A., Alejandro A. Hnilo, and Francisco P. Diodati. "Multipulse Nd: YAG Kerr lens mode-locked laser." Optics communications 221.4 (2003): 395-402.

[212] Hnilo, Alejandro A., and Miguel A. Larotonda. "Dynamics of the diode-pumped Kerr-lens mode-locked Nd: YAG laser." JOSA B 18.10 (2001): 1451-1455.

[213] M. Larotonda, Laser de Nd:YAG con mode-locking por lente de Kerr bombeado por diodos, Ph.D. Thesis, Facultad de Ciencias Exactas, Universidad de Buenos Aires (2002)

[214] Magni, Vittorio, Giulio Cerullo, and Sandro De Silvestri. "Closed form Gaussian beam analysis of resonators containing a Kerr medium for femtosecond lasers." Optics communications 101.5 (1993): 365-370.

[215] J. Boudeile, J. Didierjean, P. Camy, J. L. Doualan, A. Benayad, V. Ménard, R. Moncorgé, F. Druon, F. Balembois, and P. Georges, "Thermal behaviour of ytterbium-doped fluorite crystals under high power pumping," Opt. Express 16, 10098-10109 (2008)

- [216] J.-C. Diels, W. Rudolph, *Ultrashort Laser Pulse Phenomena* (Academic Press, San Diego, 1996).
- [217] G. Cerullo, S. De Silvestri, and V. Magni, "Self-starting Kerr-lens mode locking of a Ti:sapphire laser," *Opt. Lett.* 19, 1040-1042 (1994)
- [218] D. C. Hutchings et al., "Kramers–Kronig relations in nonlinear optics", *Opt. Quantum Electron.* 24, 1 (1992)
- [219] Radzewicz, Czeslaw, Gary W. Pearson, and Jerzy S. Krasinski. "Use of ZnS as an additional highly nonlinear intracavity self-focusing element in a Ti: sapphire self-modelocked laser." *Optics communications* 102.5 (1993): 464-468.
- [220] M. Lai, "Exploiting the optical Kerr effect as a passive mode locker for ultrashort pulse generation," research proposal submitted for Newport Research Award, February 1989.
- [221] U. Keller, G. W. 'tHooft, W. H. Knox, and J. E. Cunningham, "Femtosecond pulses from a continuously self-starting passively mode-locked Ti:sapphire laser," *Opt. Lett.* 16, 1022-1024 (1991)
- [222] Michel Piché and François Salin, "Self-mode locking of solid-state lasers without apertures," *Opt. Lett.* 18, 1041-1043 (1993)
- [223] Larotonda, M. A., A. A. Hnilo, and F. P. Diodati. "Diode-pumped self-starting Kerr-lens mode locking Nd: YAG laser." *Optics communications* 183.5 (2000): 485-491.

- [224] Martínez, Oscar E., and Juan LA Chilla. "Self-mode-locking of Ti:sapphire lasers: a matrix formalism." *Optics letters* 17.17 (1992): 1210-1212.
- [225] Diels, J. C., and W. Rudolph. "Ultrashort Laser Pulse Phenomena Academic." San Diego, Calif (1996)
- [226] A. Lucca, G. Debourg, M. Jacquemet, F. Druon, F. Balembois, P. Georges, P. Camy, J. L. Doualan, and R. Moncorgé, "High-power diode-pumped Yb³⁺:CaF₂ femtosecond laser," *Opt. Lett.* 29, 2767-2769 (2004)
- [227] <http://www.batop.de/products/saturable-absorber/saturable-absorber-mirror/saturable-absorber-mirror-1040nm.html>
- [228] F. Friebel, F. Druon, J. Boudeile, D. N. Papadopoulos, M. Hanna, P. Georges, P. Camy, J. L. Doualan, A. Benayad, R. Moncorgé, C. Cassagne, and G. Boudebs, "Diode-pumped 99 fs Yb:CaF₂ oscillator," *Opt. Lett.* 34, 1474-1476 (2009)
- [229] Machinet, Guillaume, et al. "Kerr lens mode-locking of Yb: CaF₂." *Advanced Solid-State Photonics*. Optical Society of America, 2012.
- [230] Machinet, Guillaume, et al. "High-brightness fiber laser-pumped 68 fs–2.3 W Kerr-lens mode-locked Yb:CaF₂ oscillator." *Optics letters* 38.20 (2013): 4008-4010.
- [231] Radzewicz, Czeslaw, Gary W. Pearson, and Jerzy S. Krasinski. "Use of ZnS as an additional highly nonlinear intracavity self-focusing element in a Ti: sapphire self-modelocked laser." *Optics communications* 102.5 (1993): 464-468.

- [232] Larotonda, M. A., A. A. Hnilo, and F. P. Diodati. "Diode-pumped self-starting Kerr-lens mode locking Nd: YAG laser." *Optics communications* 183.5 (2000): 485-491.
- [233] Larotonda, Miguel A., Alejandro A. Hnilo, and Francisco P. Diodati. "Multipulse Nd: YAG Kerr lens mode-locked laser." *Optics communications* 221.4 (2003): 395-402.
- [234] <http://www.batop.de/products/saturable-absorber/saturable-absorber-mirror/data-sheet/saturable-absorber-mirror-1040nm/saturable-absorber-mirror-SAM-1040-0.5-1ps.pdf>
- [235] A. Lucca, G. Debourg, M. Jacquemet, F. Druon, F. Balembois, P. Georges, P. Camy, J. L. Doualan, and R. Moncorgé, "High-power diode-pumped Yb³⁺:CaF₂ femtosecond laser," *Opt. Lett.* 29, 2767-2769 (2004)
- [236] N. V. Kuleshov, A. A. Lagatsky, A. V. Podlipensky, V. P. Mikhailov, and G. Huber, "Pulsed laser operation of Yb-dope KY(WO₄)₂ and KGd(WO₄)₂," *Opt. Lett.* 22(17), 1317–1319 (1997).
- [237] Zhao, Haitao, and Arkady Major. "Powerful 67 fs Kerr-lens mode-locked prismless Yb: KGW oscillator." *Optics express* 21.26 (2013): 31846-31851.
- [238] Giesen, Adolf, and Jochen Speiser. "Fifteen years of work on thin-disk lasers: results and scaling laws." *Selected Topics in Quantum Electronics, IEEE Journal of* 13.3 (2007): 598-609.